

Density Model for Blue Whale (*Balaenoptera musculus*) for the U.S. East Coast: Supplementary Report

Model Version 2.1

Duke University Marine Geospatial Ecology Laboratory*

2023-05-27


Citation

When citing our methodology or results generally, please cite Roberts et al. (2016, 2023). The complete references appear at the end of this document. We are preparing a new article for a peer-reviewed journal that will eventually replace those. Until that is published, those are the best general citations.

When citing this model specifically, please use this reference:

Roberts JJ, Yack TM, Cañadas A, Fujioka E, Halpin PN, Barco SG, Boisseau O, Chavez-Rosales S, Cole TVN, Cotter MP, Cummings EW, Davis GE, DiGiovanni Jr. RA, Garrison LP, Gowan TA, Jackson KA, Kenney RD, Khan CB, Lockhart GG, Lomac-MacNair KS, McAlarney RJ, McLellan WA, Mullin KD, Nowacek DP, O'Brien O, Pabst DA, Palka DL, Quintana-Rizzo E, Redfern JV, Rickard ME, White M, Whitt AD, Zoidis AM (2022) Density Model for Blue Whale (*Balaenoptera musculus*) for the U.S. East Coast, Version 2.1, 2023-05-27, and Supplementary Report. Marine Geospatial Ecology Laboratory, Duke University, Durham, North Carolina.

Copyright and License

 This document and the accompanying results are © 2023 by the Duke University Marine Geospatial Ecology Laboratory and are licensed under a [Creative Commons Attribution 4.0 International License](https://creativecommons.org/licenses/by/4.0/).

Model Version History

Version	Date	Description
1	2015-01-06	Initial version.
1.1	2015-03-06	Updated the documentation. No changes to the model.
1.2	2015-05-14	Updated calculation of CVs. Switched density rasters to logarithmic breaks. No changes to the model.
1.3	2015-09-26	Updated the documentation. No changes to the model. Model files released as supplementary information to Roberts et al. (2016).

*For questions or to offer feedback please contact Jason Roberts (jason.roberts@duke.edu) and Tina Yack (tina.yack@duke.edu)

(continued)

Version	Date	Description
2	2022-06-20	This model is a major update over the prior version, with substantial additional data, improved statistical methods, and an increased spatial resolution. It was released as part of the final delivery of the U.S. Navy Marine Species Density Database (NMSDD) for the Atlantic Fleet Testing and Training (AFTT) Phase IV Environmental Impact Statement. Several new collaborators joined and contributed survey data: New York State Department of Environmental Conservation, TetraTech, HDR, and Marine Conservation Research. We incorporated additional surveys from all continuing and new collaborators through the end of 2020. (Because some environmental covariates were only available through 2019, certain models only extend through 2019.) We increased the spatial resolution to 5 km and, at NOAA's request, we extended the model further inshore from New York through Maine. We reformulated and refitted all detection functions and spatial models. We updated all environmental covariates to newer products, when available, and added several covariates to the set of candidates. For models that incorporated dynamic covariates, we estimated model uncertainty using a new method that accounts for both model parameter error and temporal variability.
2.1	2023-05-27	Completed the supplementary report documenting the details of this model. Corrected the 5 and 95 percent rasters so that they contain the value 0 where the taxon was assumed absent, rather than NoData. Nothing else was changed.

1 Survey Data

We built this model from data collected between 1998-2020 (Table 1, Figure 1). In keeping with our primary strategy for the 2022 modeling cycle, we excluded data prior to 1998 in order to utilize biological covariates derived from satellite ocean color observations, which were only available for a few months before 1998. We excluded the North Atlantic right whale Early Warning System (EWS) surveys of the southeast calving grounds (conducted by FWRI, CMARI/SSA/WLT, and New England Aquarium) because they reported no sightings of blue whales over the 17 years of surveys contributed by those programs. We restricted the model to aerial survey transects collected in sea states of Beaufort 5 or less or 4 or less, depending on the program and the sightings it collected. We restricted the model to shipboard transects collected in Beaufort 5 or less if high-power pedestal-mounted binoculars were used, or 4 or less if naked eyes were used. For surveys of all types, we also excluded transects with poor weather or visibility for surveys that reported those conditions.

Table 1: Survey effort and observations considered for this model. Effort is tallied as the cumulative length of on-effort transects. Observations are the number of groups and individuals encountered while on effort. Off effort observations and those lacking an estimate of group size or distance to the group were excluded.

Institution	Program	Period	Effort	Observations		
			1000s km	Groups	Individuals	Mean Group Size
Aerial Surveys						
HDR	Navy Norfolk Canyon	2018-2019	11	1	1	1
NEAq	CNM	2017-2020	2	2	2	1
NEAq	MMS-WEA	2017-2020	37	0	0	
NEAq	NLPSC	2011-2015	43	0	0	
NEFSC	AMAPPS	2010-2019	89	1	1	1
NEFSC	NARWSS	2003-2020	484	8	8	1
NEFSC	Pre-AMAPPS	1999-2008	46	0	0	
NJDEP	NJEBS	2008-2009	11	0	0	
NYS-DEC/TT	NYBWM	2017-2020	77	2	2	1
SEFSC	AMAPPS	2010-2020	114	0	0	
SEFSC	MATS	2002-2005	27	0	0	
UNCW	MidA Bottlenose	2002-2002	17	0	0	
UNCW	Navy Cape Hatteras	2011-2017	34	0	0	
UNCW	Navy Jacksonville	2009-2017	92	0	0	
UNCW	Navy Norfolk Canyon	2015-2017	14	0	0	
UNCW	Navy Onslow Bay	2007-2011	49	0	0	
UNCW	SEUS NARW EWS	2005-2008	114	0	0	
VAMSC	MD DNR WEA	2013-2015	16	0	0	
VAMSC	Navy VACAPES	2016-2017	19	0	0	
VAMSC	VA CZM WEA	2012-2015	21	0	0	
		Total	1,319	14	14	1
Shipboard Surveys						
MCR	SOTW Visual	2012-2019	9	2	2	1
NEFSC	AMAPPS	2011-2016	16	7	7	1
NEFSC	Pre-AMAPPS	1998-2007	11	0	0	
NJDEP	NJEBS	2008-2009	14	0	0	
SEFSC	AMAPPS	2011-2016	17	0	0	
SEFSC	Pre-AMAPPS	1998-2006	30	0	0	
		Total	96	9	9	1
		Grand Total	1,415	23	23	1

Table 2: Institutions that contributed surveys used in this model.

Institution	Full Name
HDR	HDR, Inc.
MCR	Marine Conservation Research

Table 2: Institutions that contributed surveys used in this model. *(continued)*

Institution	Full Name
NEAq	New England Aquarium
NEFSC	NOAA Northeast Fisheries Science Center
NJDEP	New Jersey Department of Environmental Protection
NYS-DEC/TT	New York State Department of Environmental Conservation and Tetra Tech, Inc.
SEFSC	NOAA Southeast Fisheries Science Center
UNCW	University of North Carolina Wilmington
VAMSC	Virginia Aquarium & Marine Science Center

Table 3: Descriptions and references for survey programs used in this model.

Program	Description	References
AMAPPS	Atlantic Marine Assessment Program for Protected Species	Palka et al. (2017), Palka et al. (2021)
CNM	Northeast Canyons Marine National Monument Aerial Surveys	Redfern et al. (2021)
MATS	Mid-Atlantic Tursiops Surveys	
MD DNR WEA	Aerial Surveys of the Maryland Wind Energy Area	Barco et al. (2015)
MidA Bottlenose	Mid-Atlantic Onshore/Offshore Bottlenose Dolphin Surveys	Torres et al. (2005)
MMS-WEA	Marine Mammal Surveys of the MA and RI Wind Energy Areas	Quintana-Rizzo et al. (2021), O'Brien et al. (2022)
NARWSS	North Atlantic Right Whale Sighting Surveys	Cole et al. (2007)
Navy Cape Hatteras	Aerial Surveys of the Navy's Cape Hatteras Study Area	McLellan et al. (2018)
Navy Jacksonville	Aerial Surveys of the Navy's Jacksonville Study Area	Foley et al. (2019)
Navy Norfolk Canyon	Aerial Surveys of the Navy's Norfolk Canyon Study Area	Cotter (2019), McAlarney et al. (2018)
Navy Onslow Bay	Aerial Surveys of the Navy's Onslow Bay Study Area	Read et al. (2014)
Navy VACAPES	Aerial Survey Baseline Monitoring in the Continental Shelf Region of the VACAPES OPAREA	Mallette et al. (2017)
NJEBS	New Jersey Ecological Baseline Study	Geo-Marine, Inc. (2010), Whitt et al. (2015)
NLPSC	Northeast Large Pelagic Survey Collaborative Aerial Surveys	Leiter et al. (2017), Stone et al. (2017)
NYBWM	New York Bight Whale Monitoring Surveys	Zoidis et al. (2021)
Pre-AMAPPS	Pre-AMAPPS Marine Mammal Abundance Surveys	Mullin and Fulling (2003), Garrison et al. (2010), Palka (2006)
SEUS NARW EWS	Southeast U.S. Right Whale Early Warning System Surveys	
SOTW Visual	R/V Song of the Whale Visual Surveys	Ryan et al. (2013)
VA CZM WEA	Virginia CZM Wind Energy Area Surveys	Mallette et al. (2014), Mallette et al. (2015)

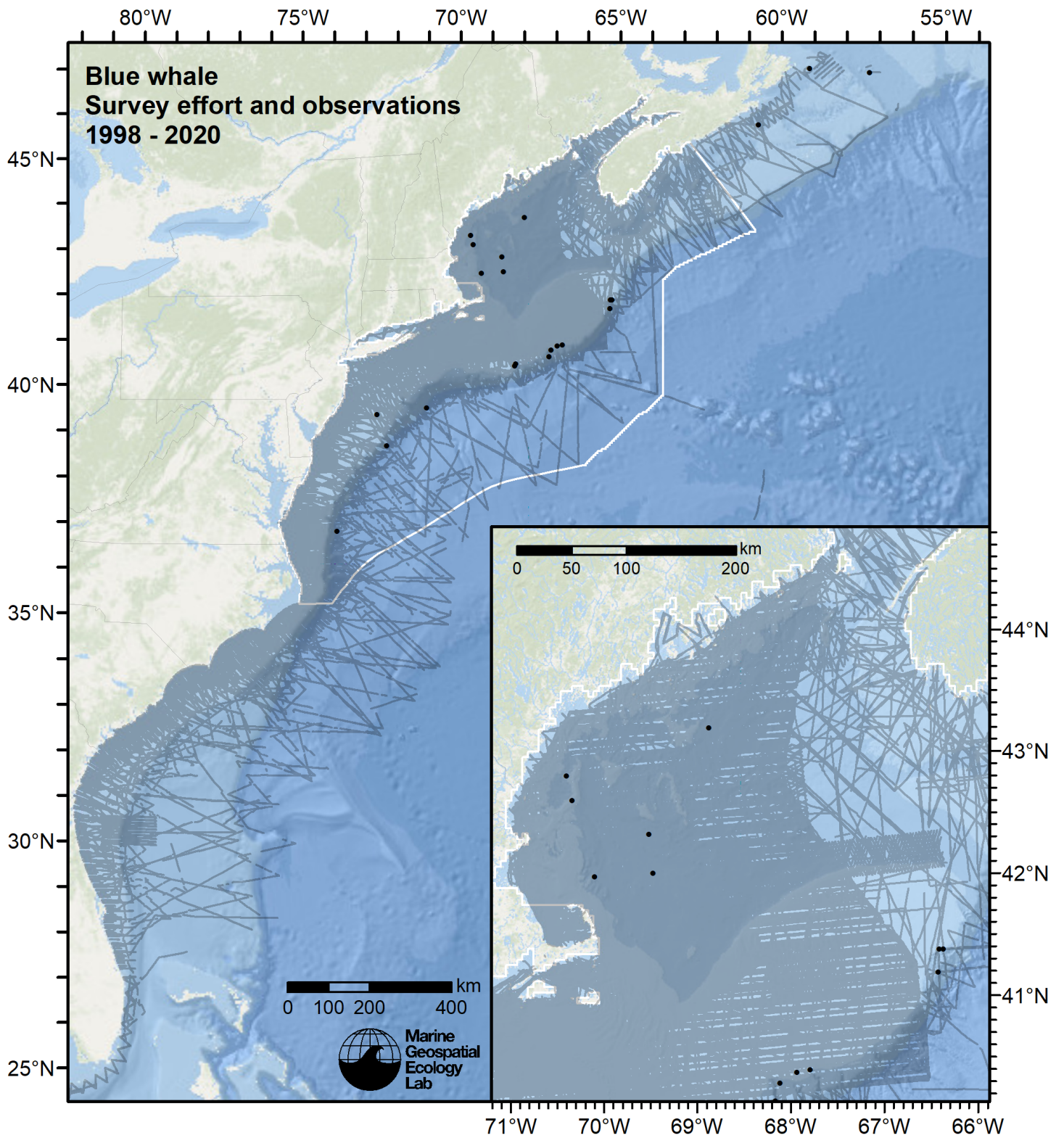


Figure 1: Survey effort and blue whale observations available for density modeling, after detection functions were applied, and excluded segments and truncated observations were removed.

2 Detection Functions

2.1 With a Taxonomic Covariate

We fitted the detection functions in this section to pools of species with similar detectability characteristics and used the taxonomic identification as a covariate (ScientificName) to account for differences between them. We consulted the literature and observer teams to determine appropriate poolings. We usually employed this approach to boost the counts of observations in the detection functions, which increased the chance that other covariates such as Beaufort sea state could be used to account for differences in observing conditions. When defining the taxonomic covariate, we sometimes had too few observations of species to allocate each of them their own level of the covariate and had to group them together, again consulting the literature and observers for advice on species similarity. Also, when species were observed frequently enough to be allocated their own levels but statistical tests indicated no significant difference between the levels, we usually grouped them together into a single level.

2.1.1 Aerial Surveys

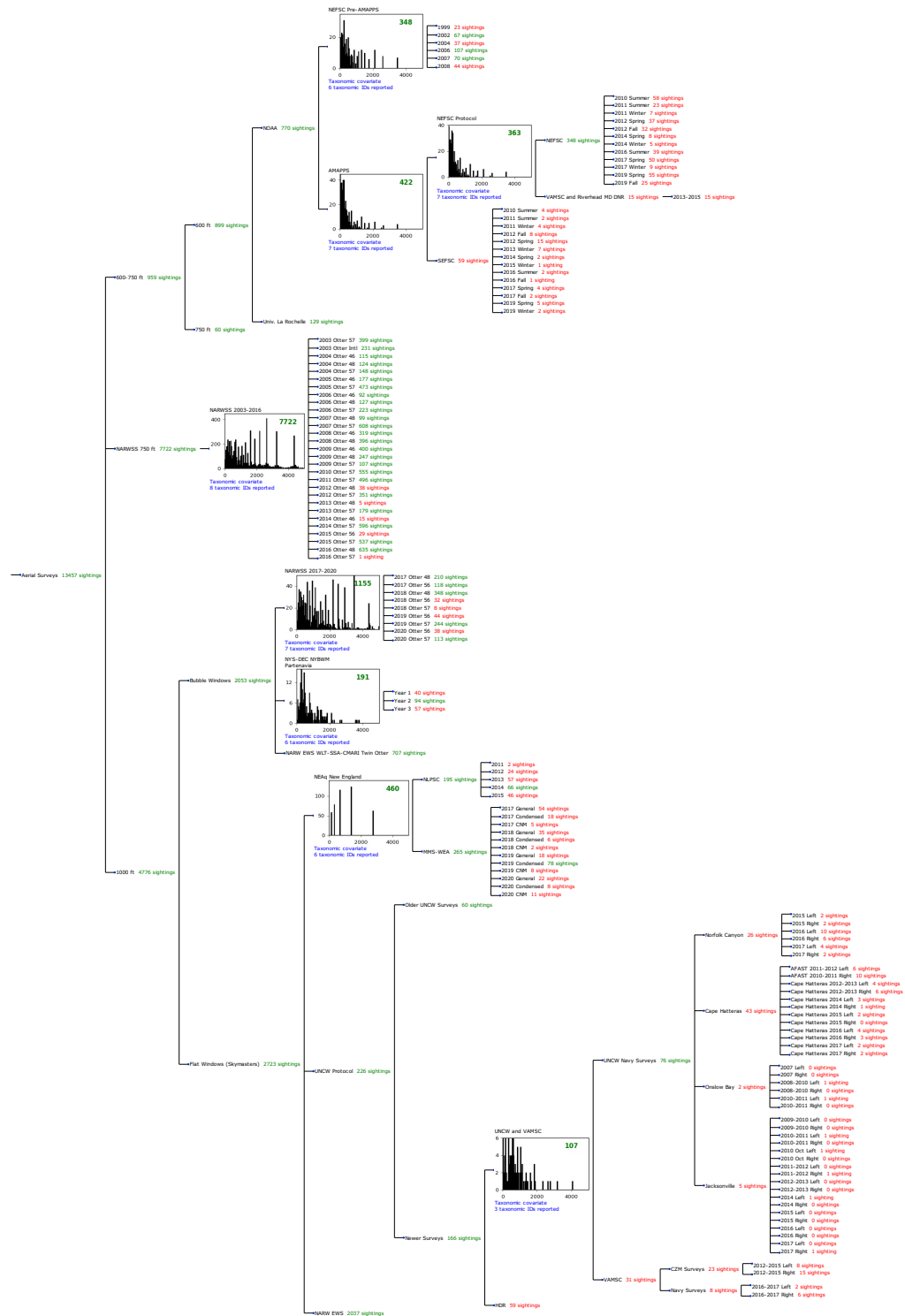


Figure 2: Detection hierarchy for aerial surveys, showing how they were pooled during detectability modeling, for detection functions that pooled multiple taxa and used a taxonomic covariate to account for differences between them. Each histogram represents a detection function and summarizes the perpendicular distances of observations that were pooled to fit it, prior to truncation. Observation counts, also prior to truncation, are shown in green when they met the recommendation of Buckland et al. (2001) that detection functions utilize at least 60 sightings, and red otherwise. For rare taxa, it was not always possible to meet this recommendation, yielding higher statistical uncertainty. During the spatial modeling stage of the analysis, effective strip widths were computed for each survey using the closest detection function above it in the hierarchy (i.e. moving from right to left in the figure). Surveys that do not have a detection function above them in this figure were either addressed by a detection function presented in a different section of this report, or were omitted from the analysis.

2.1.1.1 NEFSC Pre-AMAPPS

After right-truncating observations greater than 1500 m, we fitted the detection function to the 312 observations that remained (Table 4). The selected detection function (Figure 3) used a hazard rate key function with Beaufort (Figure 4) and OriginalScientificName (Figure 5) as covariates.

Table 4: Observations used to fit the NEFSC Pre-AMAPPS detection function.

ScientificName	n
Balaenoptera borealis	7
Balaenoptera borealis/physalus	29
Balaenoptera physalus	117
Eubalaena glacialis	29
Megaptera novaeangliae	113
Physeter macrocephalus	17
Total	312

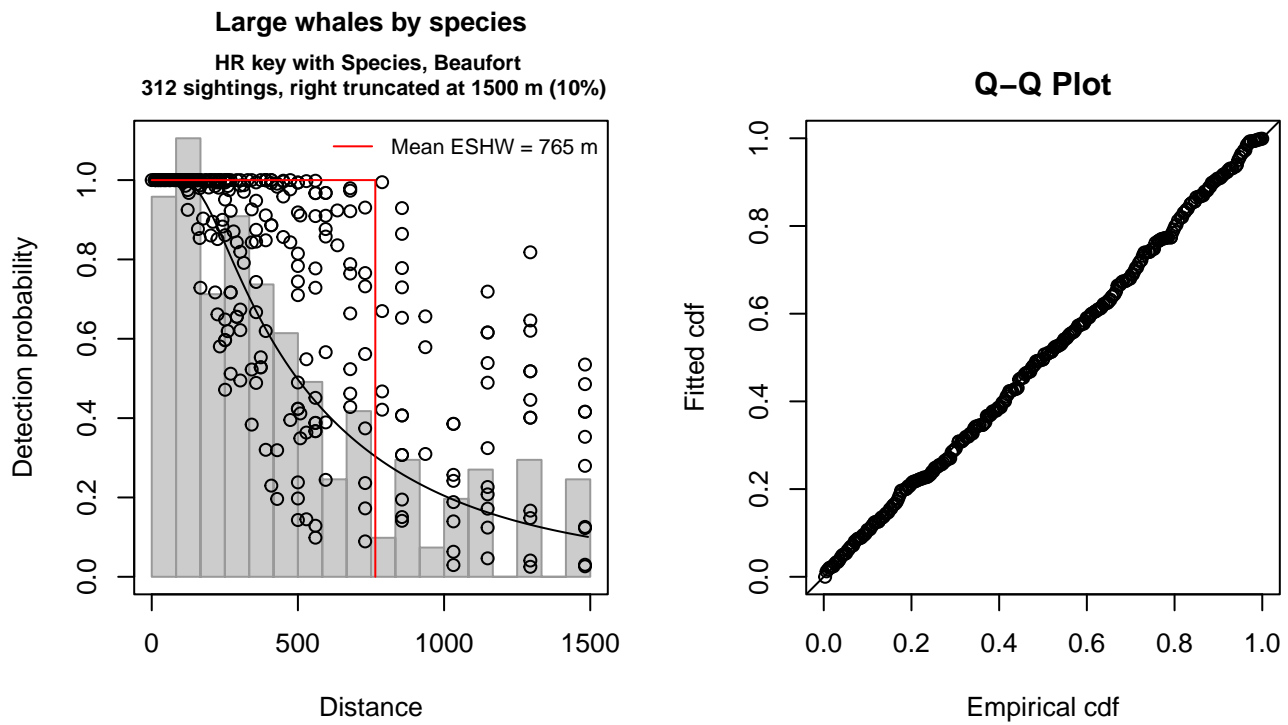


Figure 3: NEFSC Pre-AMAPPS detection function and Q-Q plot showing its goodness of fit.

Statistical output for this detection function:

Summary for ds object

Number of observations : 312
Distance range : 0 - 1500
AIC : 4374.841

Detection function:

Hazard-rate key function

Detection function parameters

Scale coefficient(s):

	estimate	se
(Intercept)	5.0768091	0.24837645

OriginalScientificNameHumpback, Right	0.9199384	0.16439351
OriginalScientificNameUnid. fin or sei	0.4943579	0.25189646
Beaufort	0.3122214	0.08477314

Shape coefficient(s):

	estimate	se
(Intercept)	0.8162868	0.1272435

	Estimate	SE	CV
Average p	0.4257901	0.03176212	0.07459573
N in covered region	732.7553573	64.19166079	0.08760313

Distance sampling Cramer-von Mises test (unweighted)

Test statistic = 0.028690 p = 0.980269

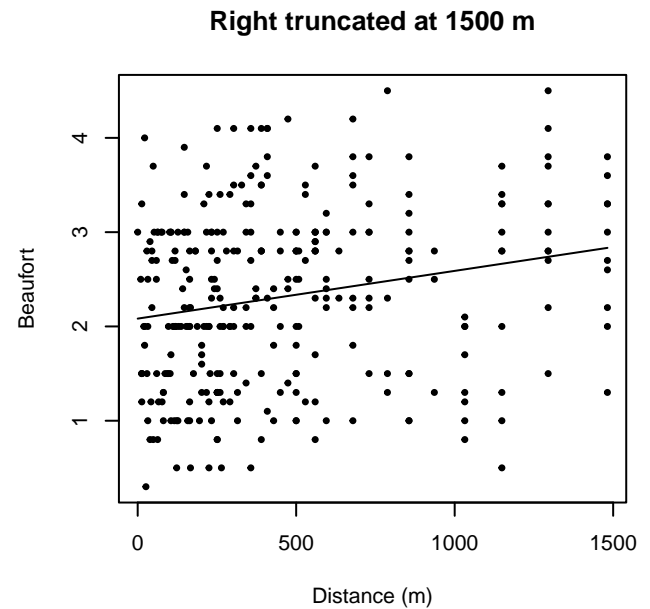
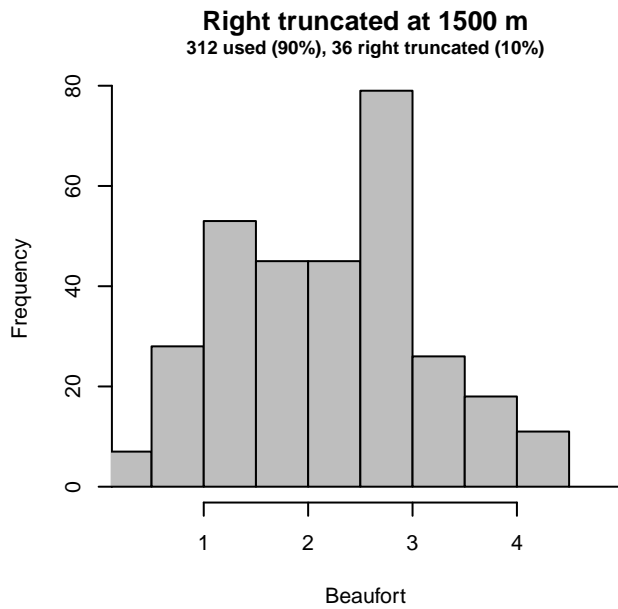
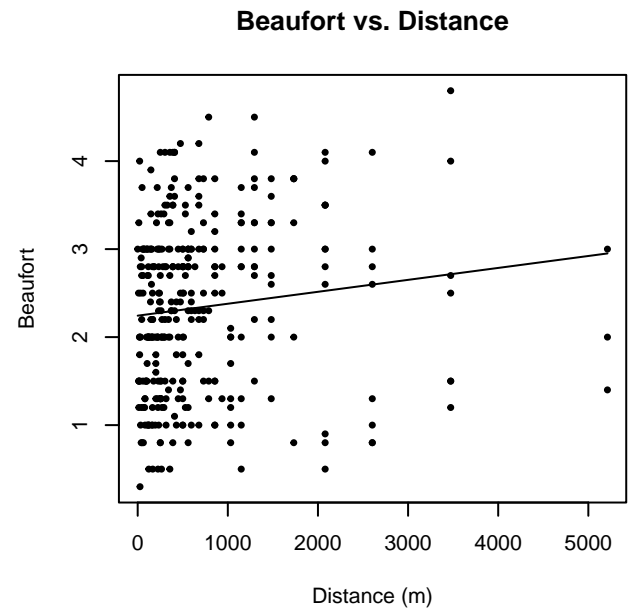
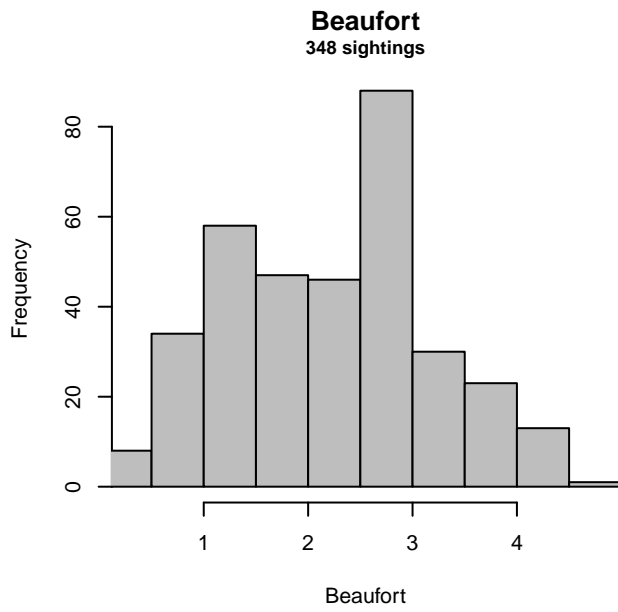


Figure 4: Distribution of the Beaufort covariate before (top row) and after (bottom row) observations were truncated to fit the NEFSC Pre-AMAPPS detection function.

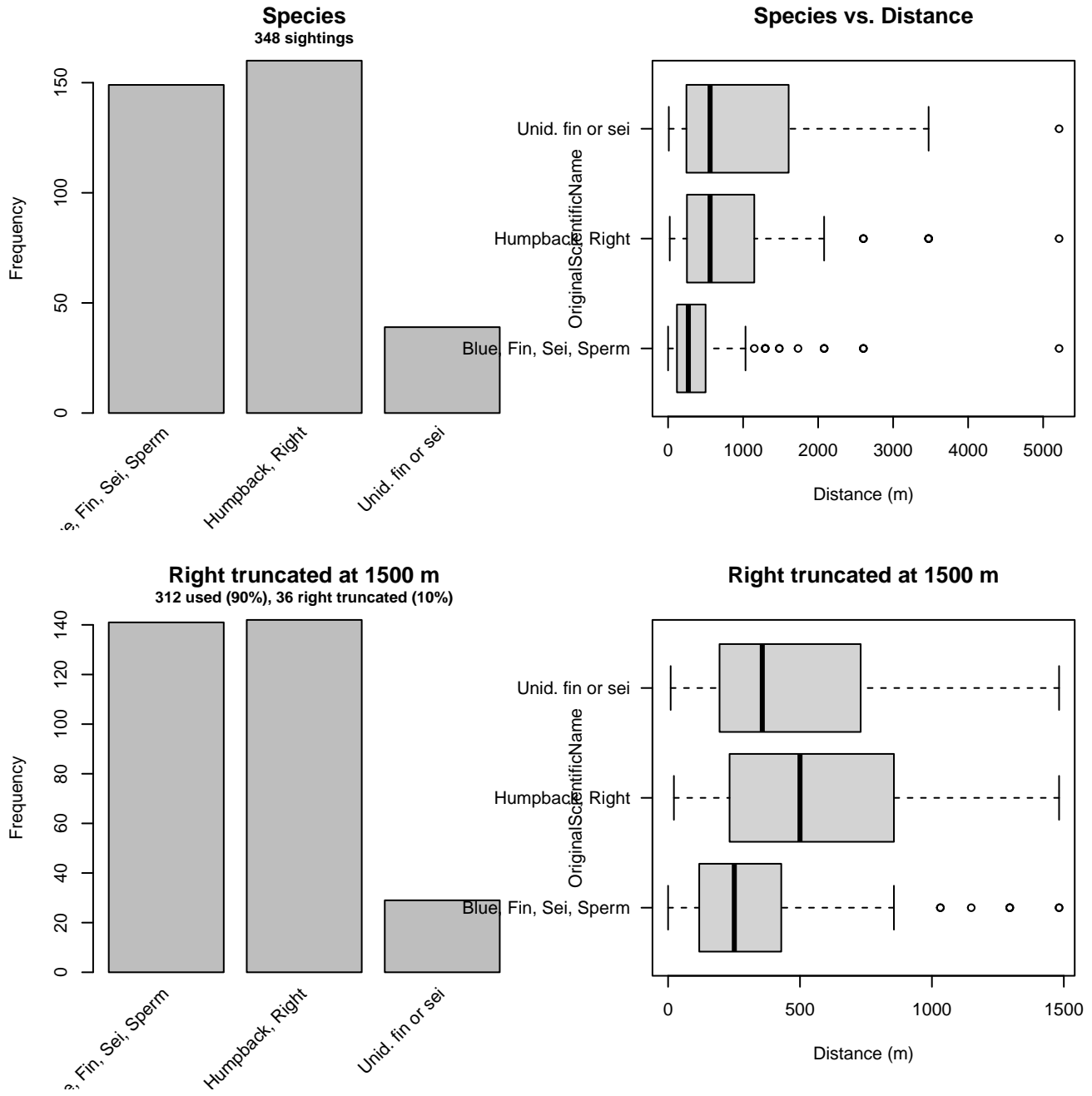


Figure 5: Distribution of the OriginalScientificName covariate before (top row) and after (bottom row) observations were truncated to fit the NEFSC Pre-AMAPPS detection function.

2.1.1.2 NEFSC AMAPPS Protocol

After right-truncating observations greater than 1500 m, we fitted the detection function to the 342 observations that remained (Table 5). The selected detection function (Figure 6) used a hazard rate key function with Beaufort (Figure 7), OriginalScientificName (Figure 8) and Season (Figure 9) as covariates.

Table 5: Observations used to fit the NEFSC AMAPPS Protocol detection function.

ScientificName	n
Balaenoptera borealis	14
Balaenoptera borealis/physalus	26
Balaenoptera musculus	1
Balaenoptera physalus	116
Eubalaena glacialis	23
Megaptera novaeangliae	150
Physeter macrocephalus	12
Total	342

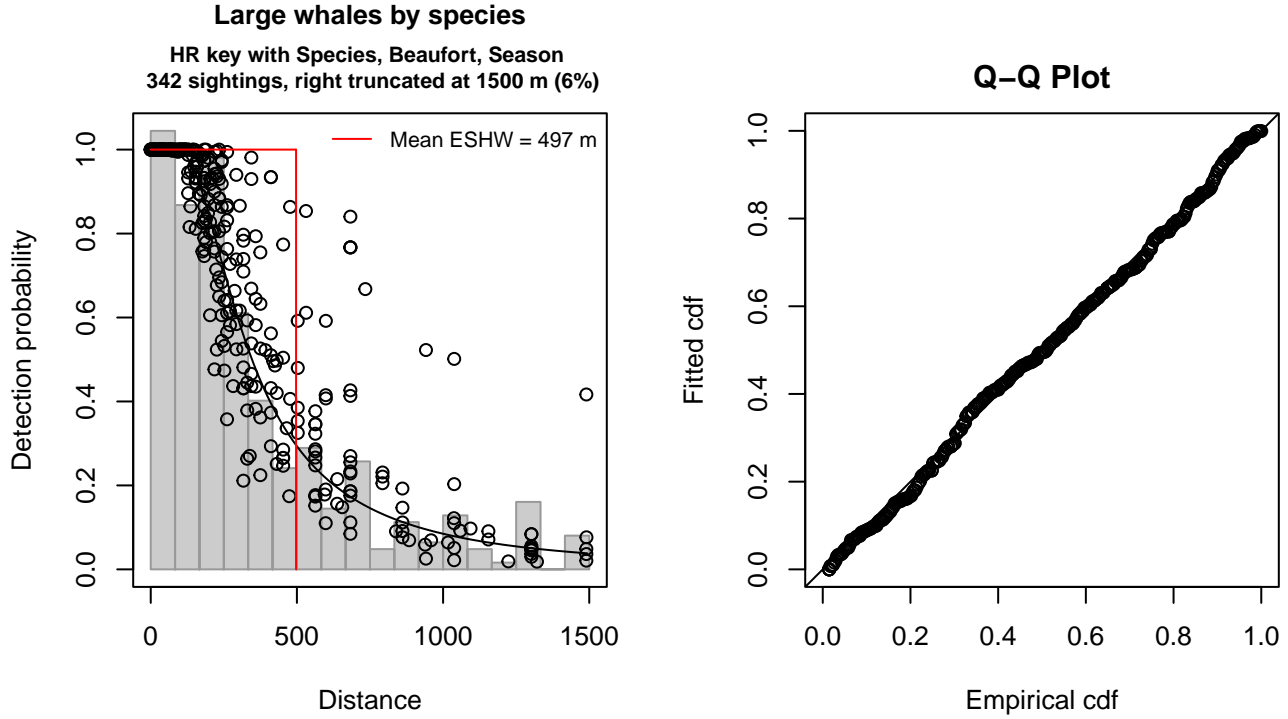


Figure 6: NEFSC AMAPPS Protocol detection function and Q-Q plot showing its goodness of fit.

Statistical output for this detection function:

Summary for ds object

Number of observations : 342
Distance range : 0 - 1500
AIC : 4666.929

Detection function:

Hazard-rate key function

Detection function parameters

Scale coefficient(s):

	estimate	se
(Intercept)	5.1473984	0.28568102
OriginalScientificNameHumpback, Right	0.3396040	0.14675903
OriginalScientificNameUnid. fin or sei	1.0647525	0.34041574
Beaufort	0.2004836	0.08188346
SeasonSummer, Fall, Winter	-0.2694922	0.15571712

Shape coefficient(s):

	estimate	se
(Intercept)	0.748414	0.08996968

	Estimate	SE	CV
Average p	0.3053758	0.02225385	0.07287364
N in covered region	1119.9314103	96.45660426	0.08612724

Distance sampling Cramer-von Mises test (unweighted)

Test statistic = 0.064193 p = 0.787617

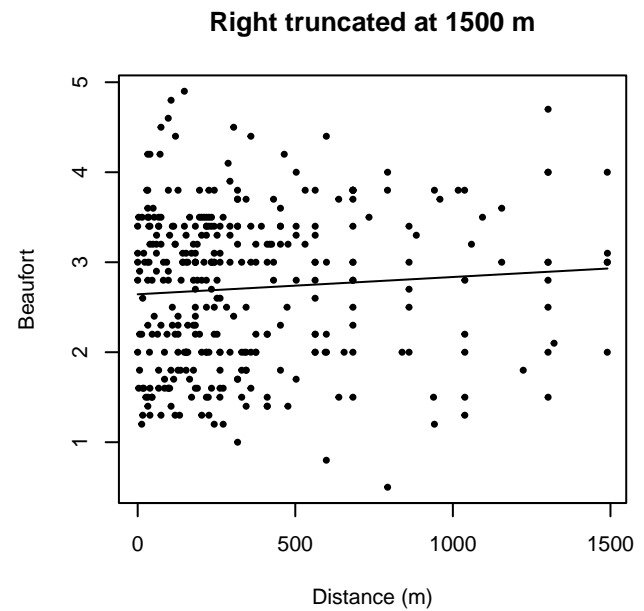
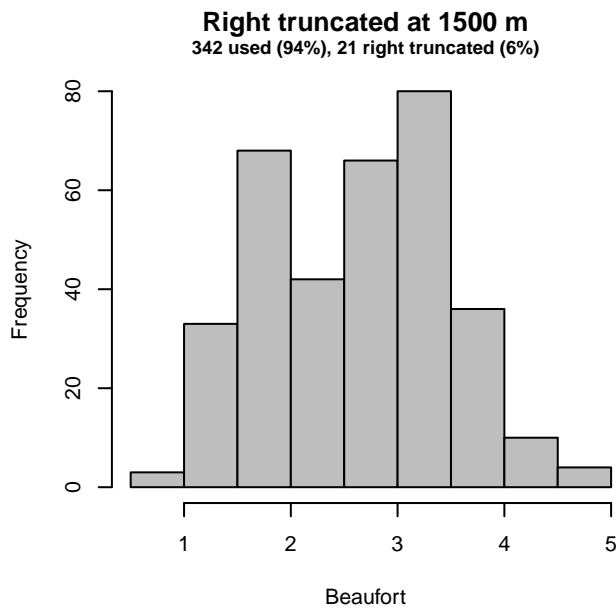
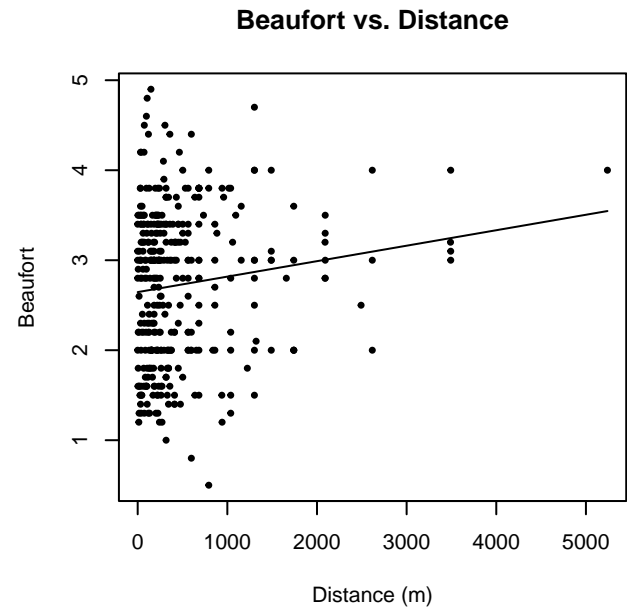
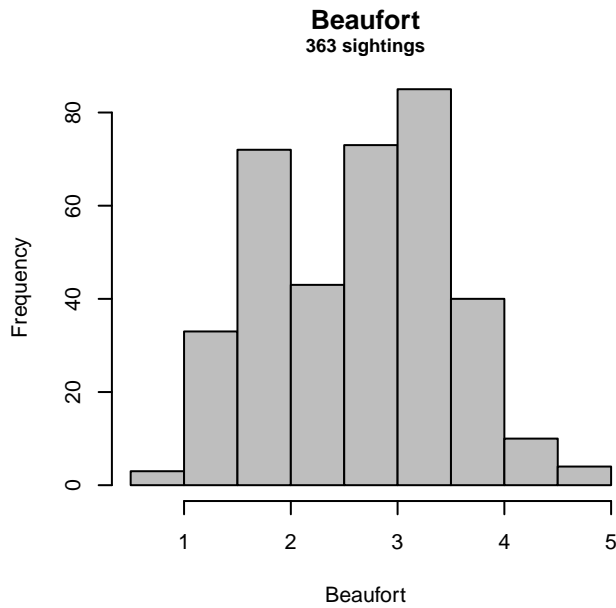


Figure 7: Distribution of the Beaufort covariate before (top row) and after (bottom row) observations were truncated to fit the NEFSC AMAPPS Protocol detection function.

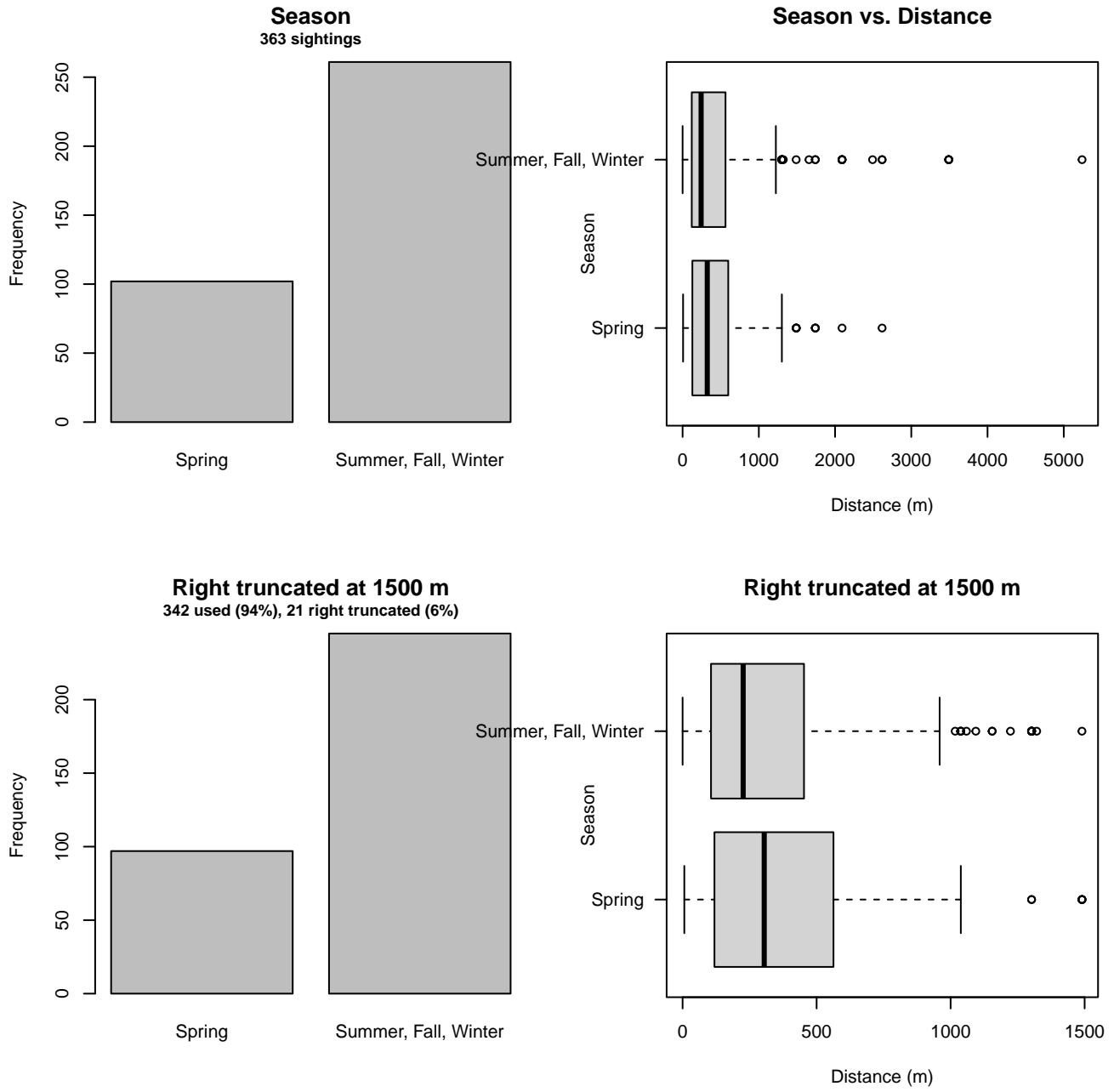


Figure 9: Distribution of the Season covariate before (top row) and after (bottom row) observations were truncated to fit the NEFSC AMAPPS Protocol detection function.

2.1.1.3 AMAPPS

After right-truncating observations greater than 600 m, we fitted the detection function to the 341 observations that remained (Table 6). The selected detection function (Figure 10) used a hazard rate key function with OriginalScientificName (Figure 11) as a covariate.

Table 6: Observations used to fit the AMAPPS detection function.

ScientificName	n
Balaenoptera borealis	11
Balaenoptera borealis/physalus	16
Balaenoptera musculus	1
Balaenoptera physalus	132
Eubalaena glacialis	26
Megaptera novaeangliae	137
Physeter macrocephalus	18
Total	341

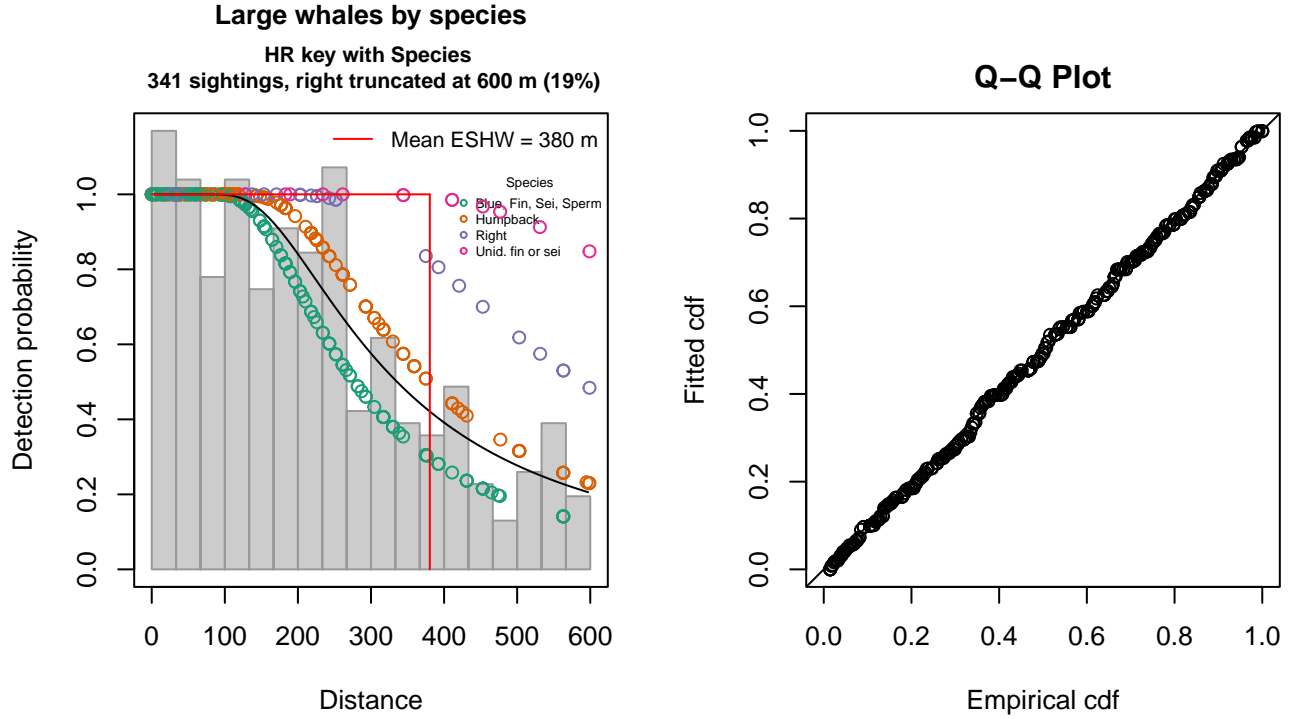


Figure 10: AMAPPS detection function and Q-Q plot showing its goodness of fit.

Statistical output for this detection function:

Summary for ds object

Number of observations : 341
Distance range : 0 - 600
AIC : 4279.869

Detection function:

Hazard-rate key function

Detection function parameters

Scale coefficient(s):

	estimate	se
(Intercept)	5.4543823	0.1418158
OriginalScientificNameHumpback	0.3133386	0.1690242
OriginalScientificNameRight	0.7482762	0.3681078
OriginalScientificNameUnid. fin or sei	1.2365031	1.2174894

Shape coefficient(s):

	estimate	se
(Intercept)	0.7615805	0.1934441

	Estimate	SE	CV
Average p	0.615325	0.03870801	0.06290662
N in covered region	554.178703	39.73247609	0.07169614

Distance sampling Cramer-von Mises test (unweighted)
 Test statistic = 0.031782 p = 0.969954

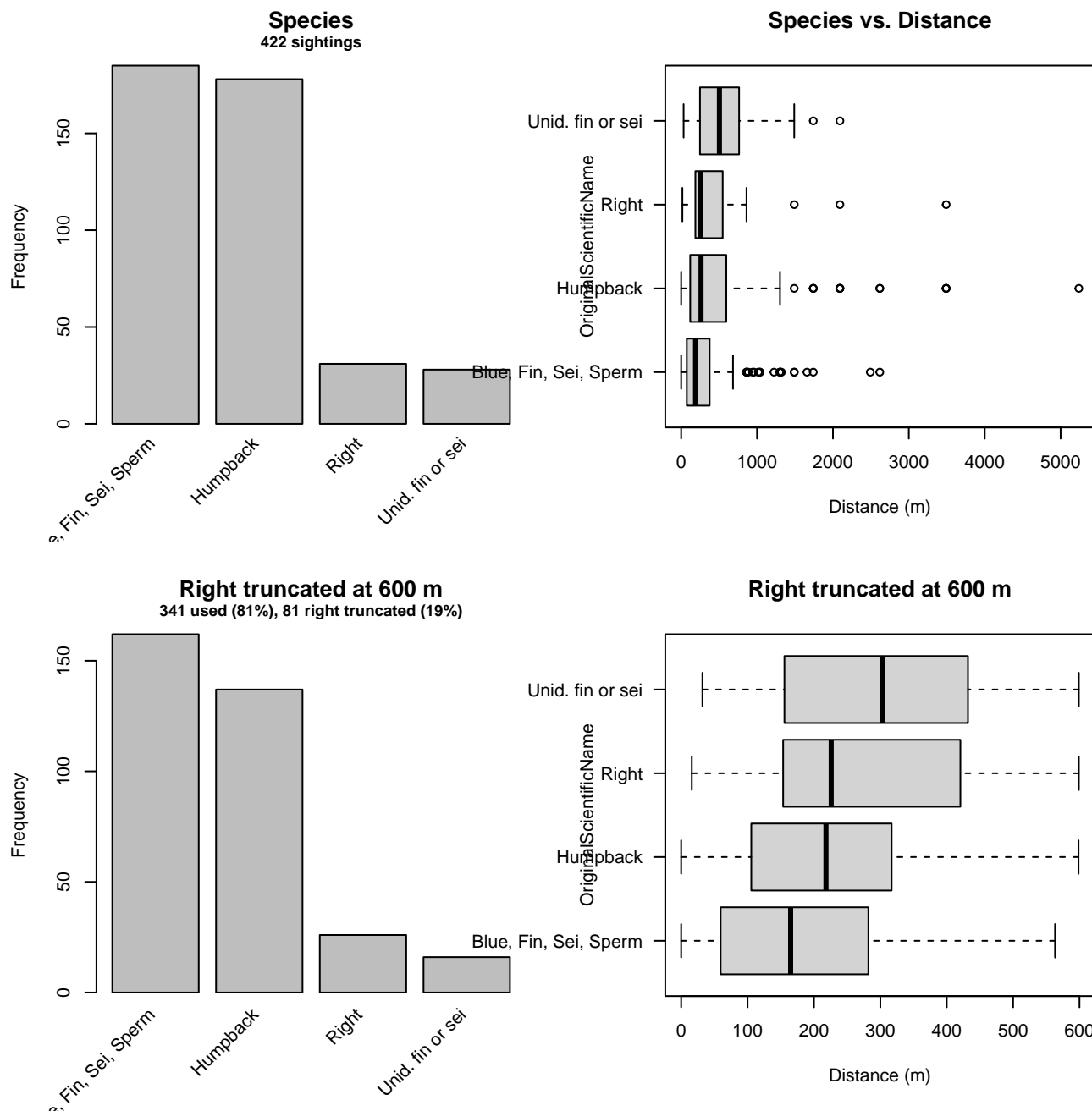


Figure 11: Distribution of the OriginalScientificName covariate before (top row) and after (bottom row) observations were truncated to fit the AMAPPS detection function.

2.1.1.4 NARWSS 2003-2016

After right-truncating observations greater than 5236 m, we fitted the detection function to the 7315 observations that remained (Table 7). The selected detection function (Figure 12) used a hazard rate key function with Beaufort (Figure 13), Glare (Figure 14), OriginalScientificName (Figure 15) and Visibility (Figure 16) as covariates.

Table 7: Observations used to fit the NARWSS 2003-2016 detection function.

ScientificName	n
Balaena mysticetus	1
Balaenoptera borealis	849
Balaenoptera borealis/physalus	550
Balaenoptera musculus	8
Balaenoptera physalus	1605
Eubalaena glacialis	1340
Megaptera novaeangliae	2890
Physeter macrocephalus	72
Total	7315

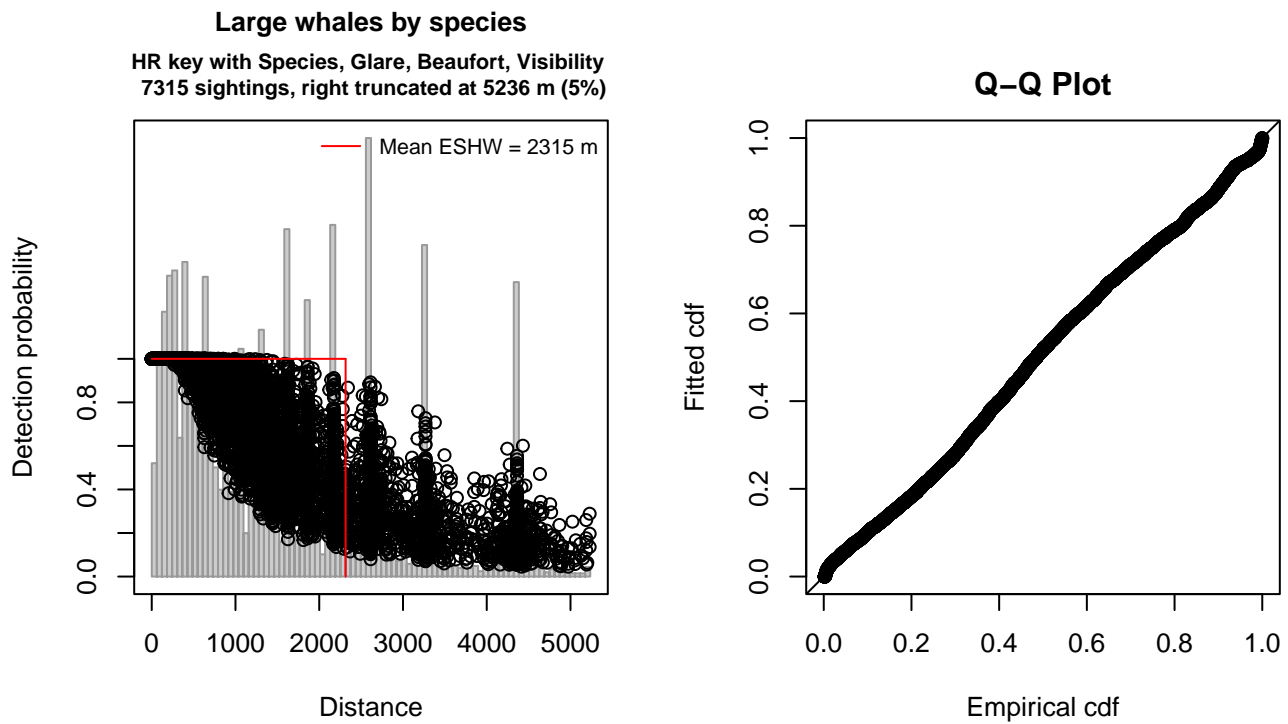


Figure 12: NARWSS 2003-2016 detection function and Q-Q plot showing its goodness of fit.

Statistical output for this detection function:

```
Summary for ds object
Number of observations : 7315
Distance range       : 0 - 5236
AIC                  : 121443.8
```

```
Detection function:
Hazard-rate key function
```

```
Detection function parameters
Scale coefficient(s):
```

	estimate	se
(Intercept)	6.441965720	0.099786764
OriginalScientificNameHumpback	0.514291401	0.053837700
OriginalScientificNameRight, Bowhead	0.246897383	0.063136414
OriginalScientificNameSei, Bryde's	-0.161553308	0.069396712
OriginalScientificNameSperm	0.319075357	0.224385467
OriginalScientificNameUnid. fin or sei	0.829751791	0.098643556
GlareSevere	0.362397475	0.058132933
Beaufort	0.093367857	0.021887375
Visibility	0.007771288	0.002225131

Shape coefficient(s):

	estimate	se
(Intercept)	0.4992226	0.03060822

	Estimate	SE	CV
Average p	4.138072e-01	7.450829e-03	0.01800555
N in covered region	1.767731e+04	3.571549e+02	0.02020414

Distance sampling Cramer-von Mises test (unweighted)

Test statistic = 1.329669 p = 0.000424

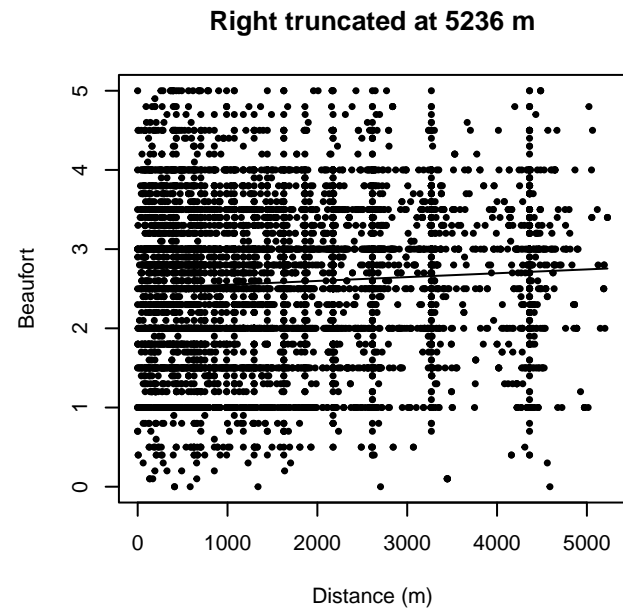
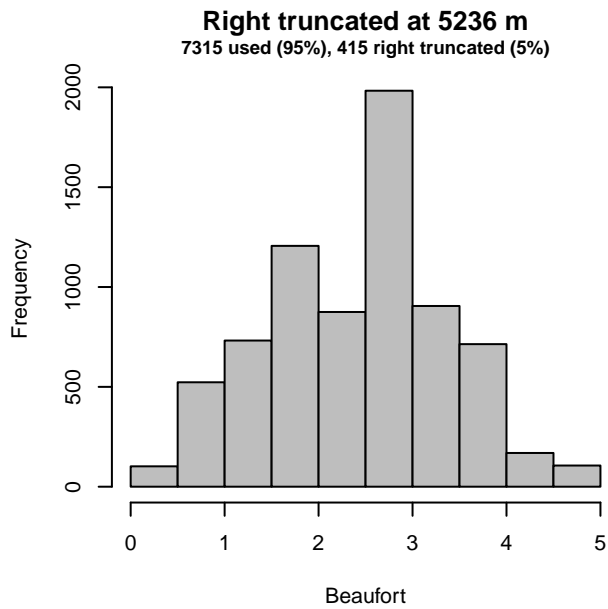
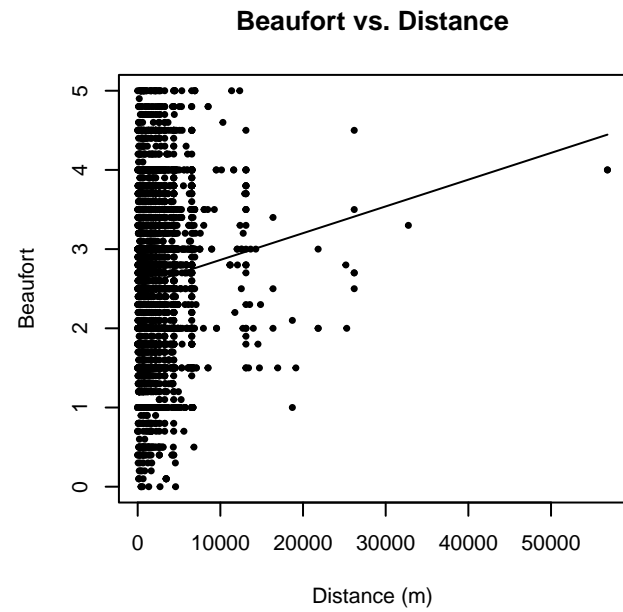
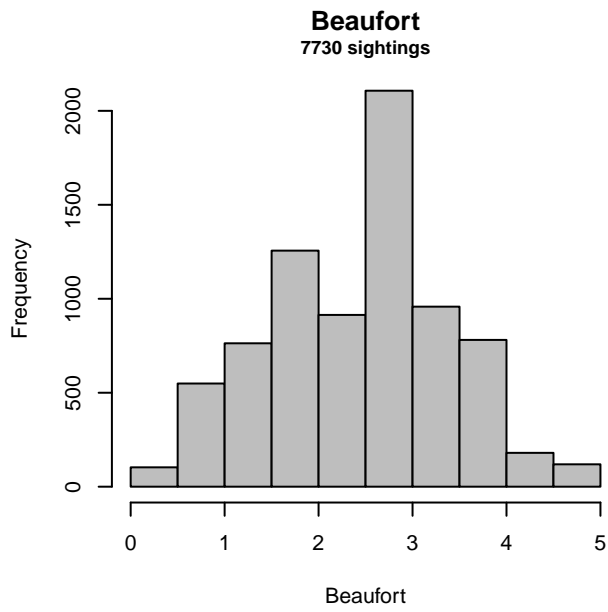


Figure 13: Distribution of the Beaufort covariate before (top row) and after (bottom row) observations were truncated to fit the NARWSS 2003-2016 detection function.

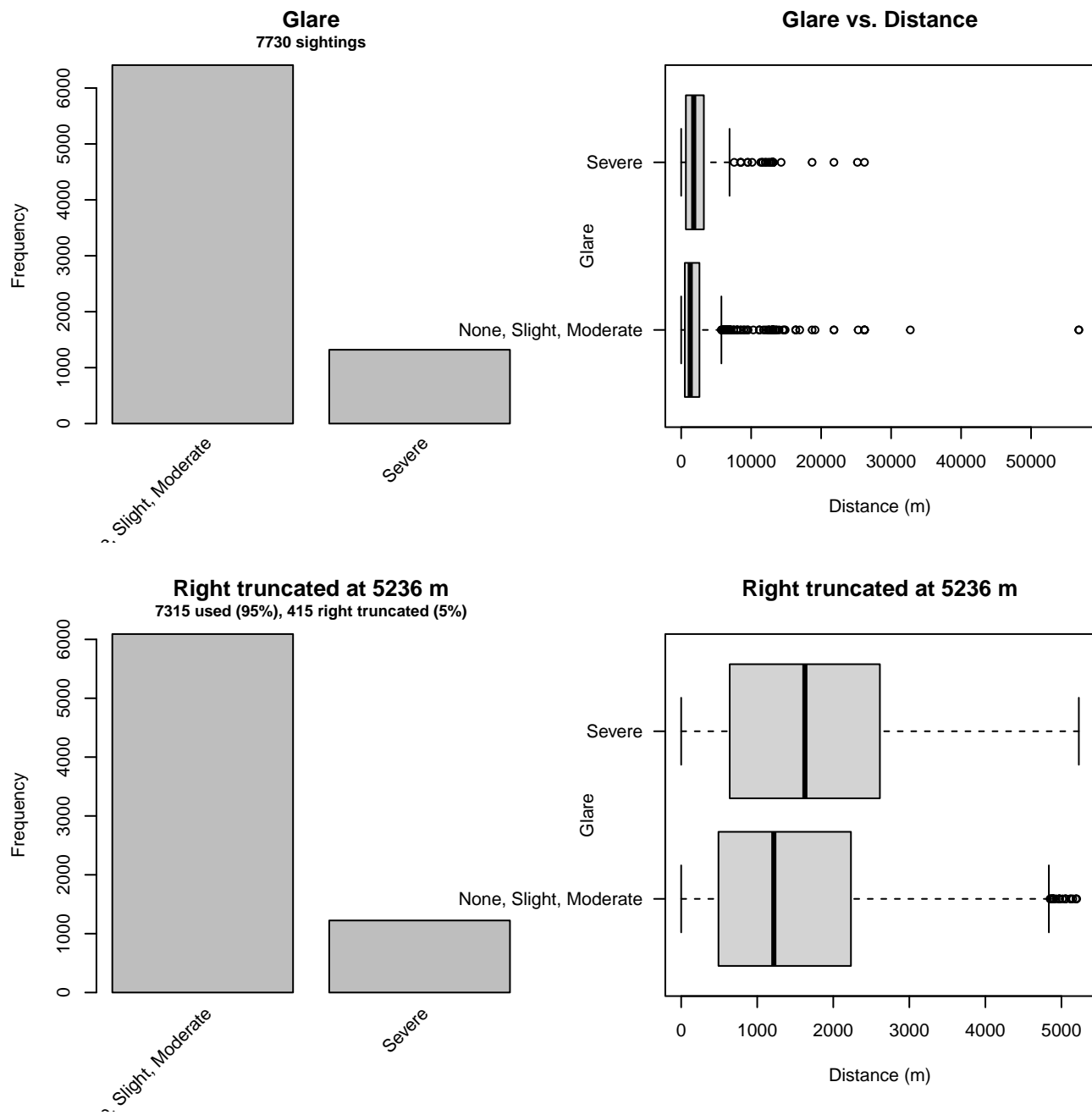


Figure 14: Distribution of the Glare covariate before (top row) and after (bottom row) observations were truncated to fit the NARWSS 2003-2016 detection function.

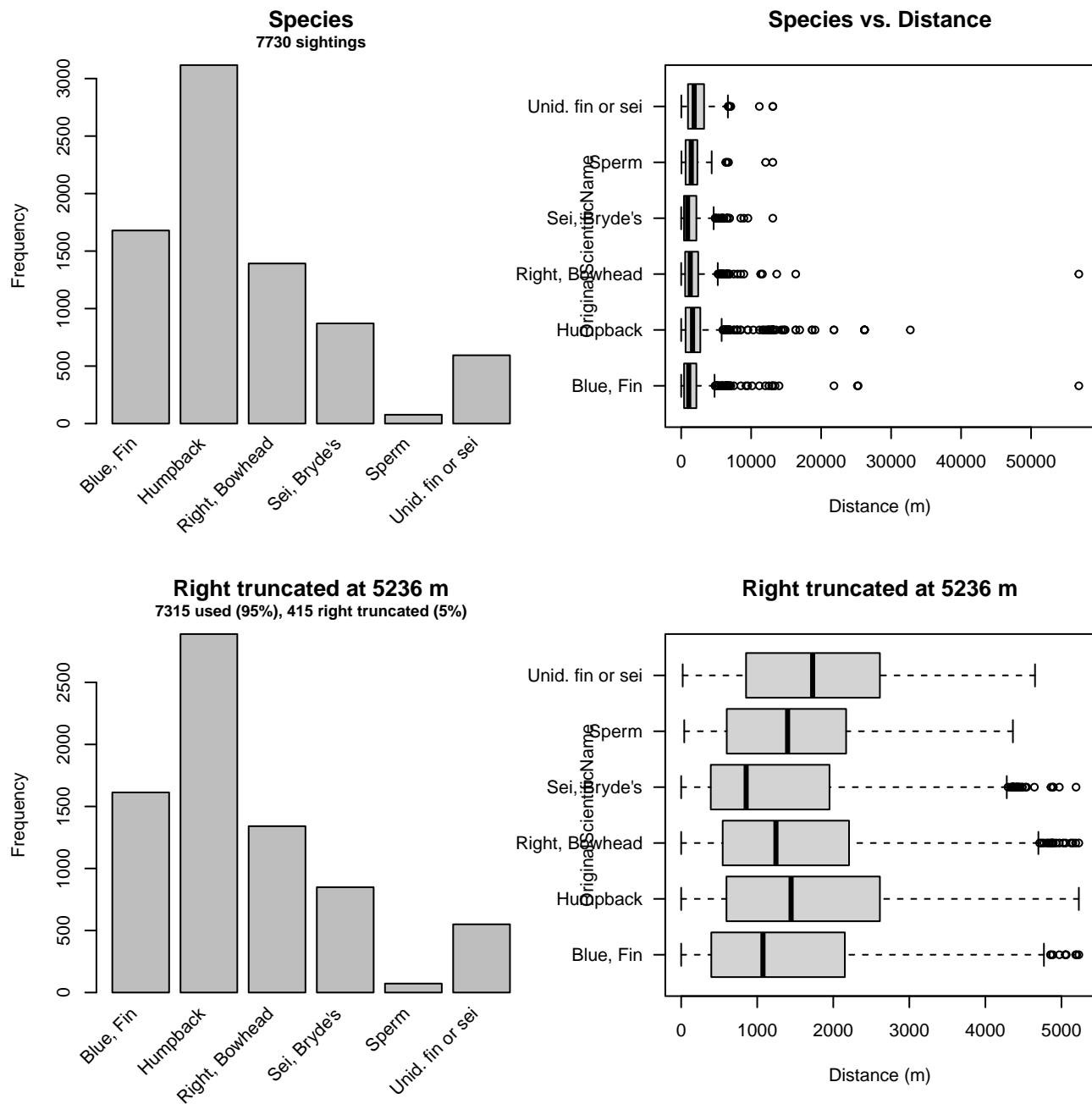


Figure 15: Distribution of the OriginalScientificName covariate before (top row) and after (bottom row) observations were truncated to fit the NARWSS 2003-2016 detection function.

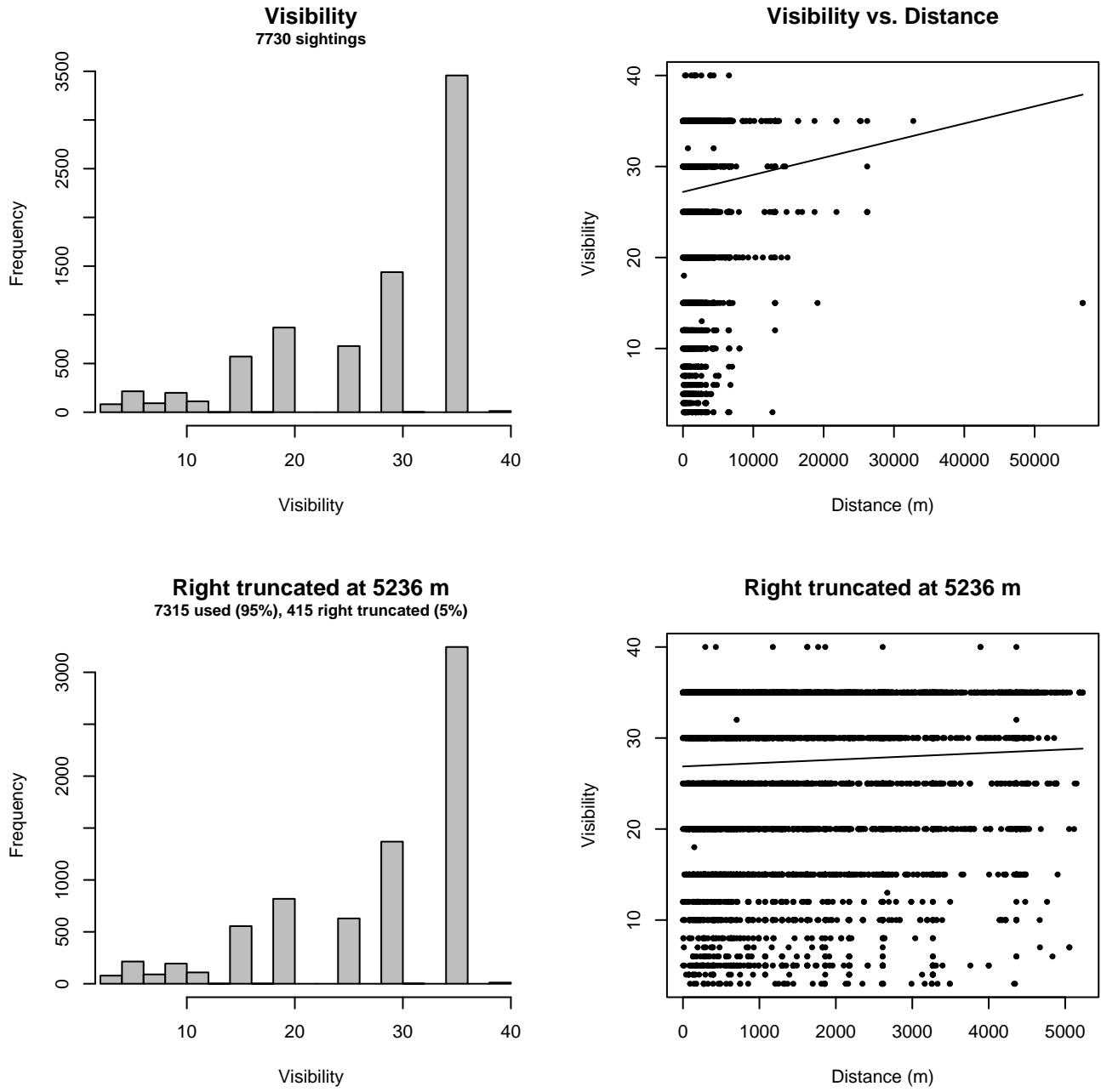


Figure 16: Distribution of the Visibility covariate before (top row) and after (bottom row) observations were truncated to fit the NARWSS 2003-2016 detection function.

2.1.1.5 NARWSS 2017-2020

After right-truncating observations greater than 5236 m, we fitted the detection function to the 1088 observations that remained (Table 8). The selected detection function (Figure 17) used a hazard rate key function with OriginalScientificName (Figure 18) and QualityCode (Figure 19) as covariates.

Table 8: Observations used to fit the NARWSS 2017-2020 detection function.

ScientificName	n
Balaena mysticetus	2
Balaenoptera borealis	163
Balaenoptera borealis/physalus	39
Balaenoptera physalus	242
Eubalaena glacialis	233
Megaptera novaeangliae	402
Physeter macrocephalus	7
Total	1088

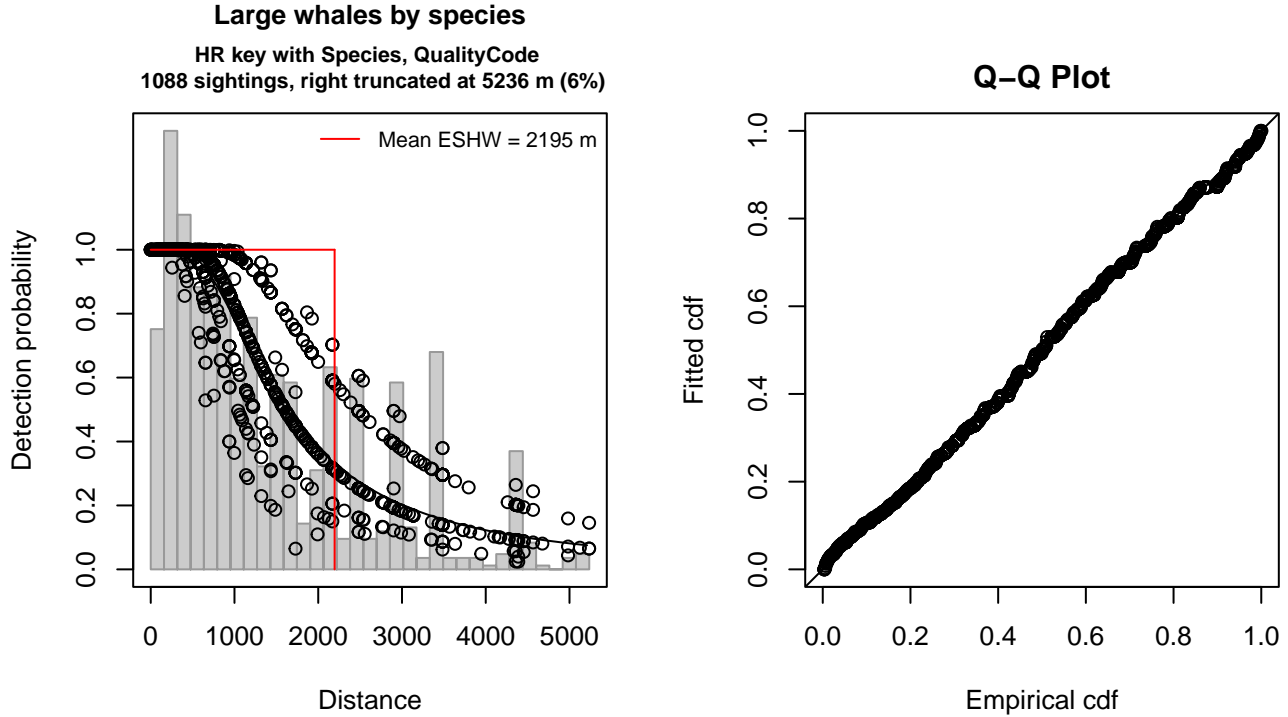


Figure 17: NARWSS 2017-2020 detection function and Q-Q plot showing its goodness of fit.

Statistical output for this detection function:

Summary for ds object

Number of observations : 1088
 Distance range : 0 - 5236
 AIC : 17913.86

Detection function:

Hazard-rate key function

Detection function parameters

Scale coefficient(s):

	estimate	se
(Intercept)	7.1921029	0.08301497
OriginalScientificNameHumpback	0.4314943	0.09757578
OriginalScientificNameSei, Bryde's	-0.2566332	0.12547460
OriginalScientificNameUnid. fin or sei	0.5879315	0.27089226
QualityCodeGood	-0.4330452	0.11641444
QualityCodeModerate	-0.8540468	0.46513807

Shape coefficient(s):

	estimate	se
(Intercept)	0.6773699	0.07059228

	Estimate	SE	CV
Average p	0.3933208	0.01632601	0.04150813
N in covered region	2766.1897508	132.78849331	0.04800412

Distance sampling Cramer-von Mises test (unweighted)

Test statistic = 0.142983 p = 0.411684

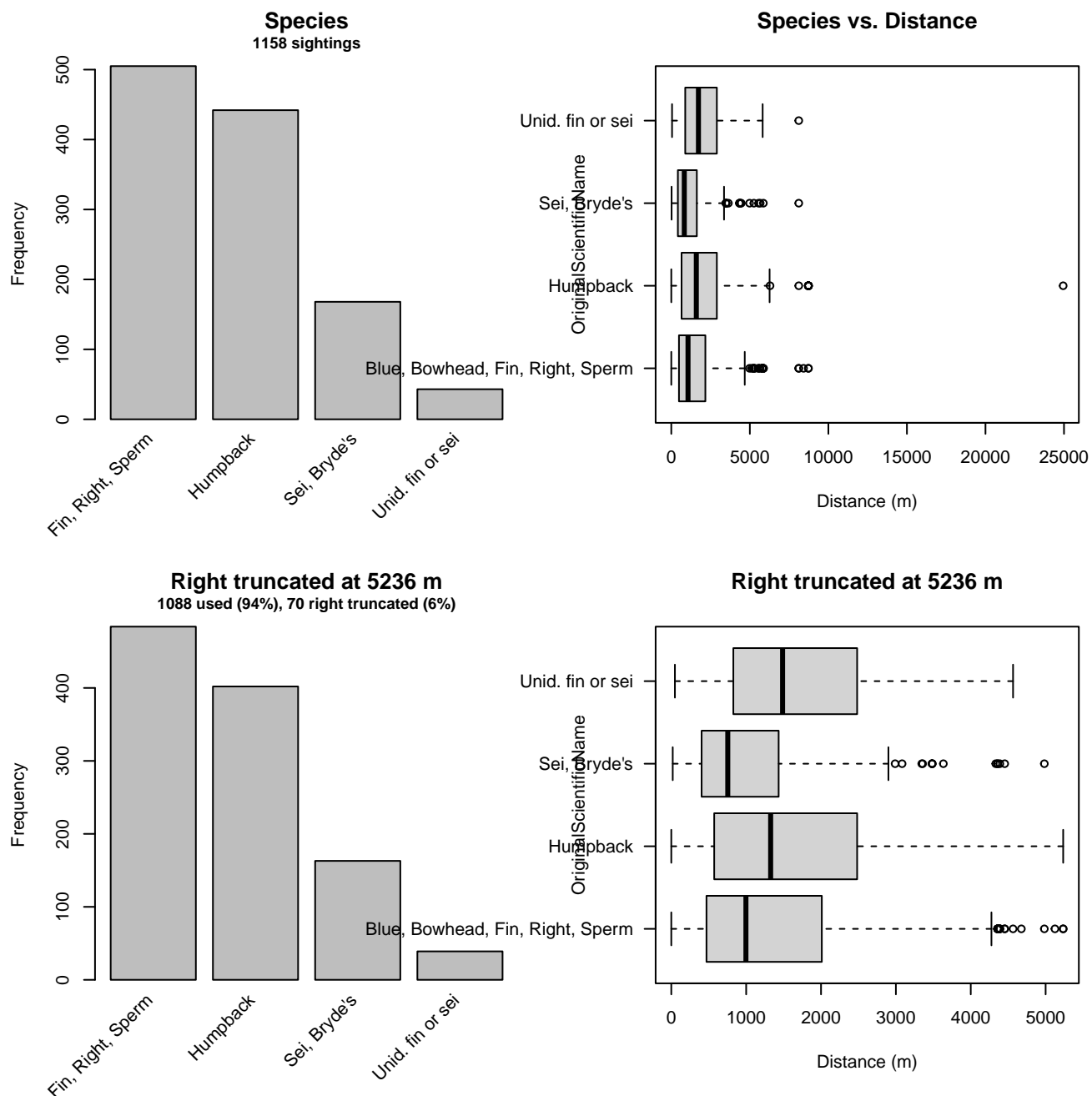


Figure 18: Distribution of the OriginalScientificName covariate before (top row) and after (bottom row) observations were truncated to fit the NARWSS 2017-2020 detection function.

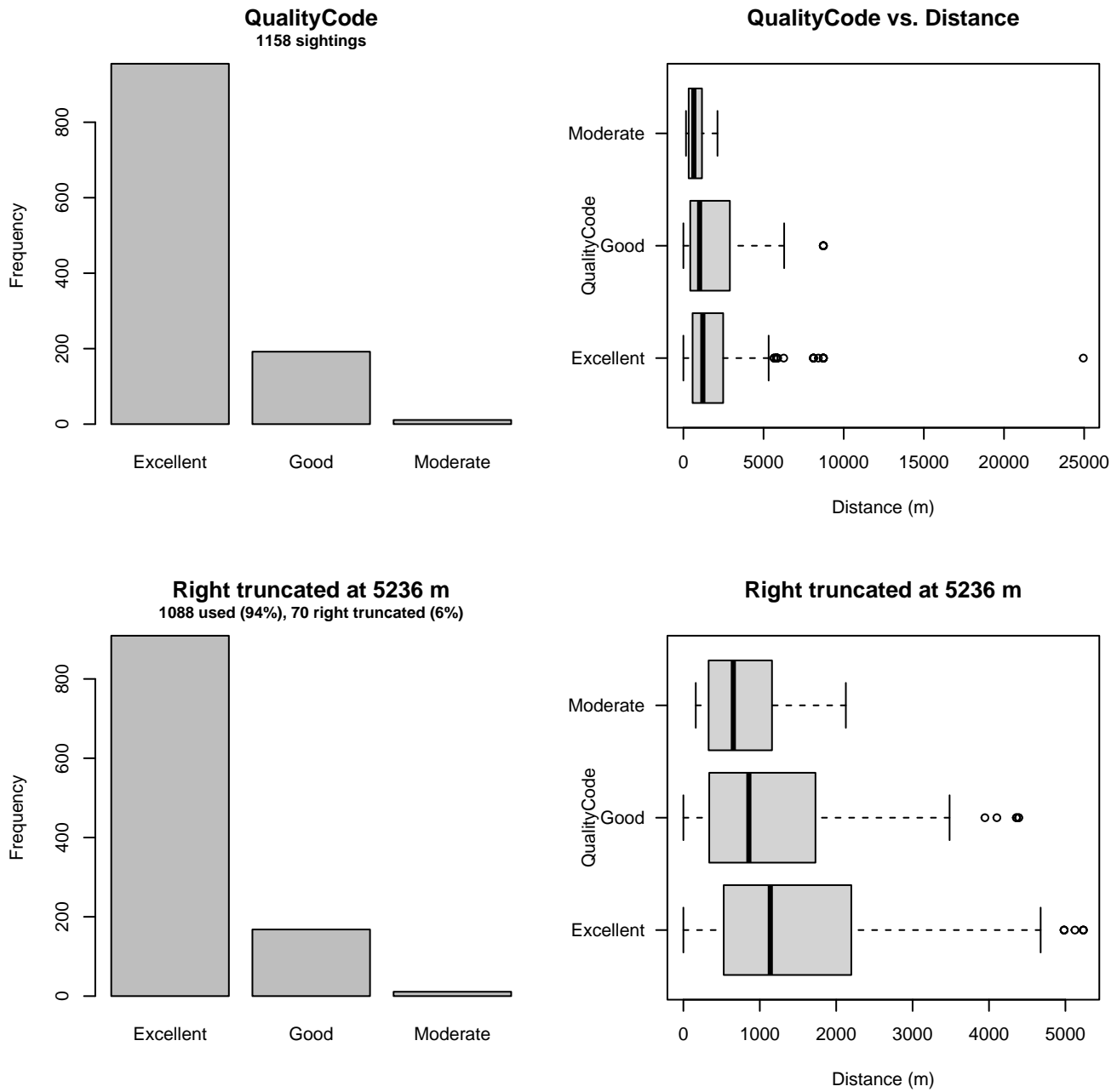


Figure 19: Distribution of the QualityCode covariate before (top row) and after (bottom row) observations were truncated to fit the NARWSS 2017-2020 detection function.

2.1.1.6 NYS-DEC NYBWM Partenavia

After right-truncating observations greater than 2100 m and left-truncating observations less than 125 m (Figure 21), we fitted the detection function to the 172 observations that remained (Table 9). The selected detection function (Figure 20) used a hazard rate key function with OriginalScientificName (Figure 22), Season (Figure 23) and SurveyID (Figure 24) as covariates.

Table 9: Observations used to fit the NYS-DEC NYBWM Partenavia detection function.

ScientificName	n
Balaenoptera borealis	2
Balaenoptera musculus	2
Balaenoptera physalus	82
Eubalaena glacialis	12
Megaptera novaeangliae	57
Physeter macrocephalus	17
Total	172

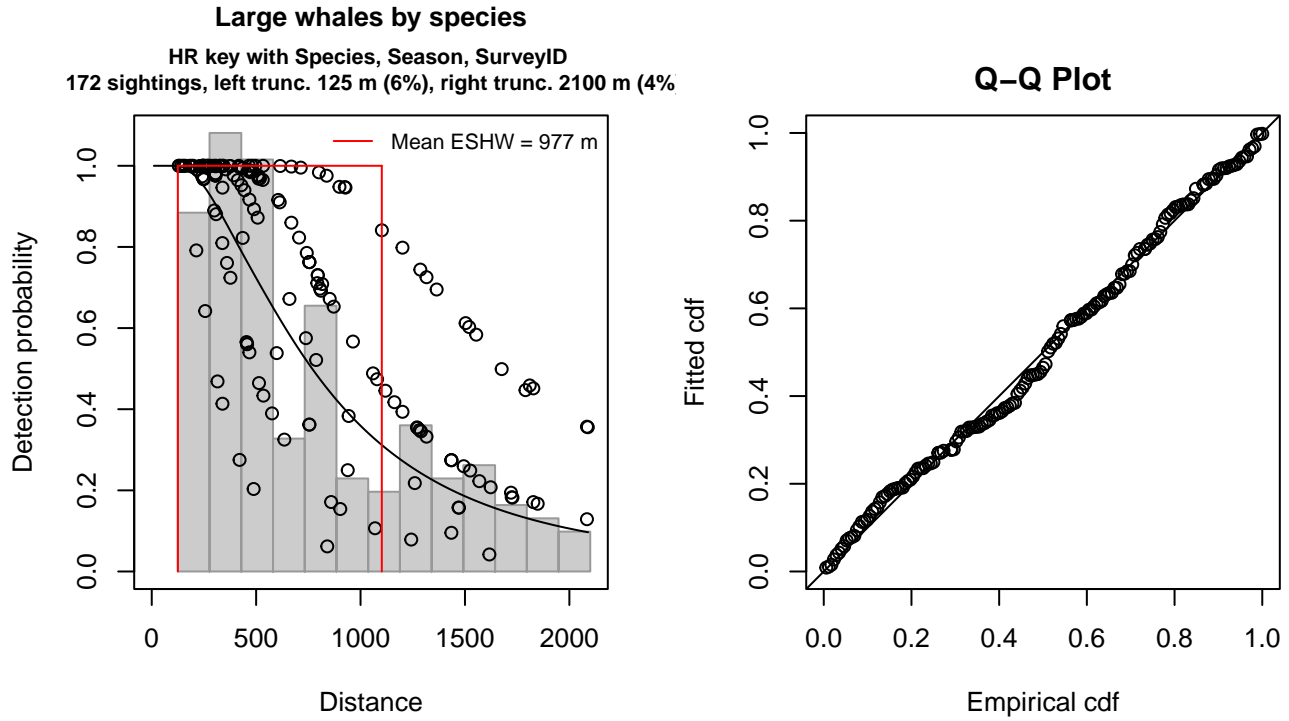


Figure 20: NYS-DEC NYBWM Partenavia detection function and Q-Q plot showing its goodness of fit.

Statistical output for this detection function:

```
Summary for ds object
Number of observations : 172
Distance range       : 125 - 2100
AIC                  : 2521.205
```

```
Detection function:
Hazard-rate key function
```

```
Detection function parameters
Scale coefficient(s):
```

	estimate	se
(Intercept)	5.5563867	0.3693793
OriginalScientificNameHumpback, Right	0.4977955	0.2125828
SeasonSpring	0.7279337	0.2896812
SeasonSummer	0.7542217	0.2477951
SurveyIDYears 2-3	0.4837030	0.2648931

```
Shape coefficient(s):
```

	estimate	se
(Intercept)	0.8485132	0.197714

	Estimate	SE	CV
Average p	0.4075964	0.06072428	0.1489814
N in covered region	421.9860458	68.23264910	0.1616941

Distance sampling Cramer-von Mises test (unweighted)
 Test statistic = 0.068137 p = 0.763045

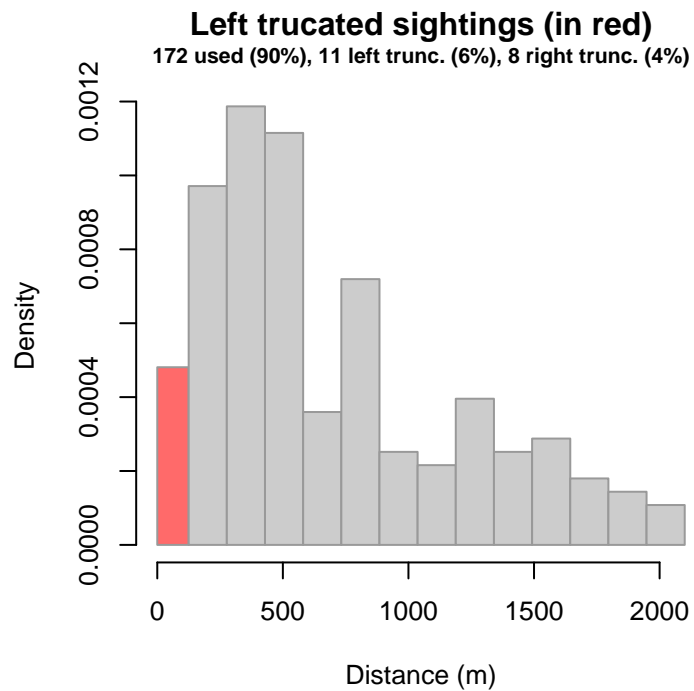


Figure 21: Density histogram of observations used to fit the NYS-DEC NYBWM Partenavia detection function, with the left-most bar showing observations at distances less than 125 m, which were left-truncated and excluded from the analysis [Buckland et al. (2001)]. (This bar may be very short if there were very few left-truncated sightings, or very narrow if the left truncation distance was very small; in either case it may not appear red.)

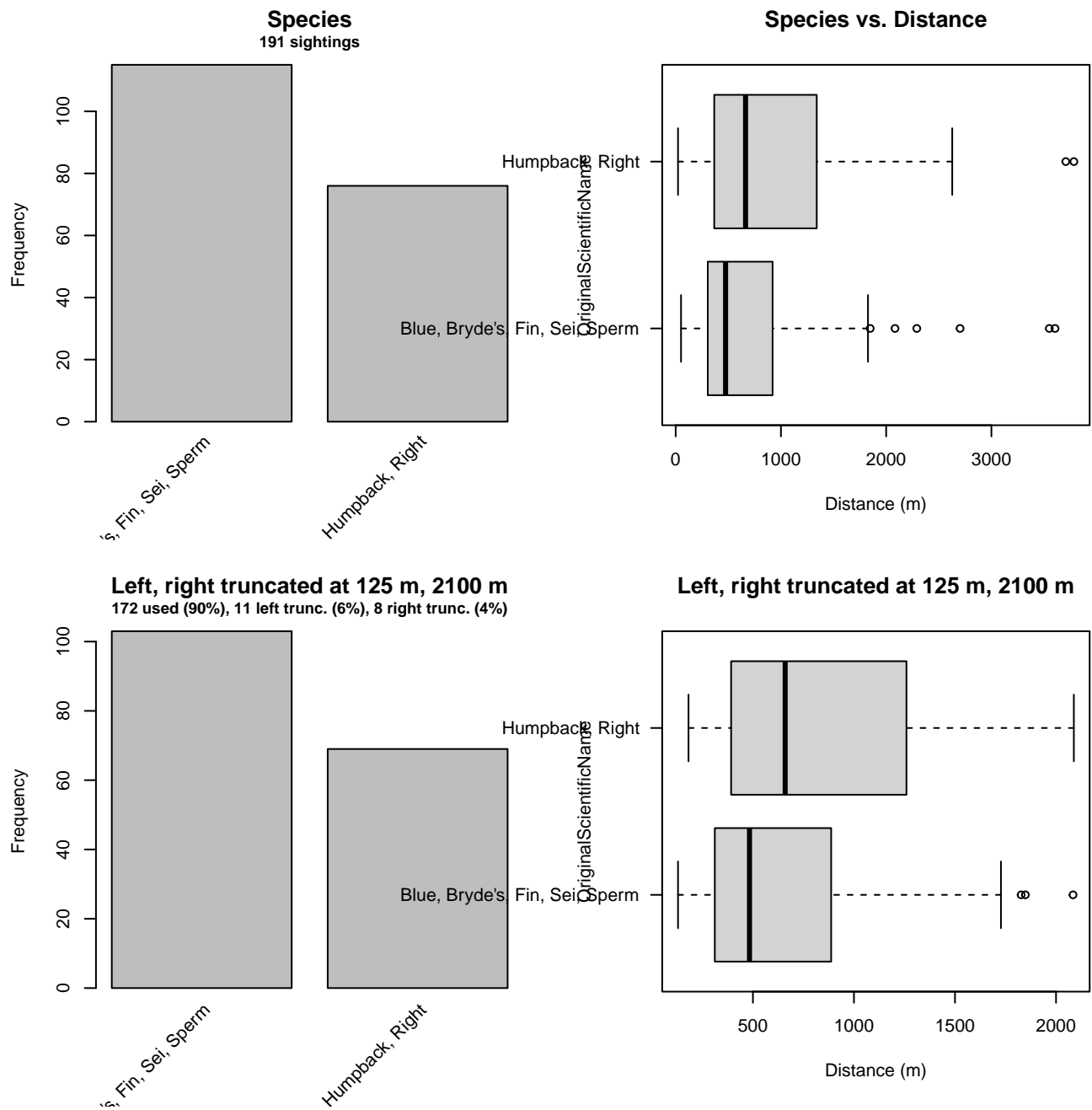


Figure 22: Distribution of the OriginalScientificName covariate before (top row) and after (bottom row) observations were truncated to fit the NYS-DEC NYBWM Partenavia detection function.

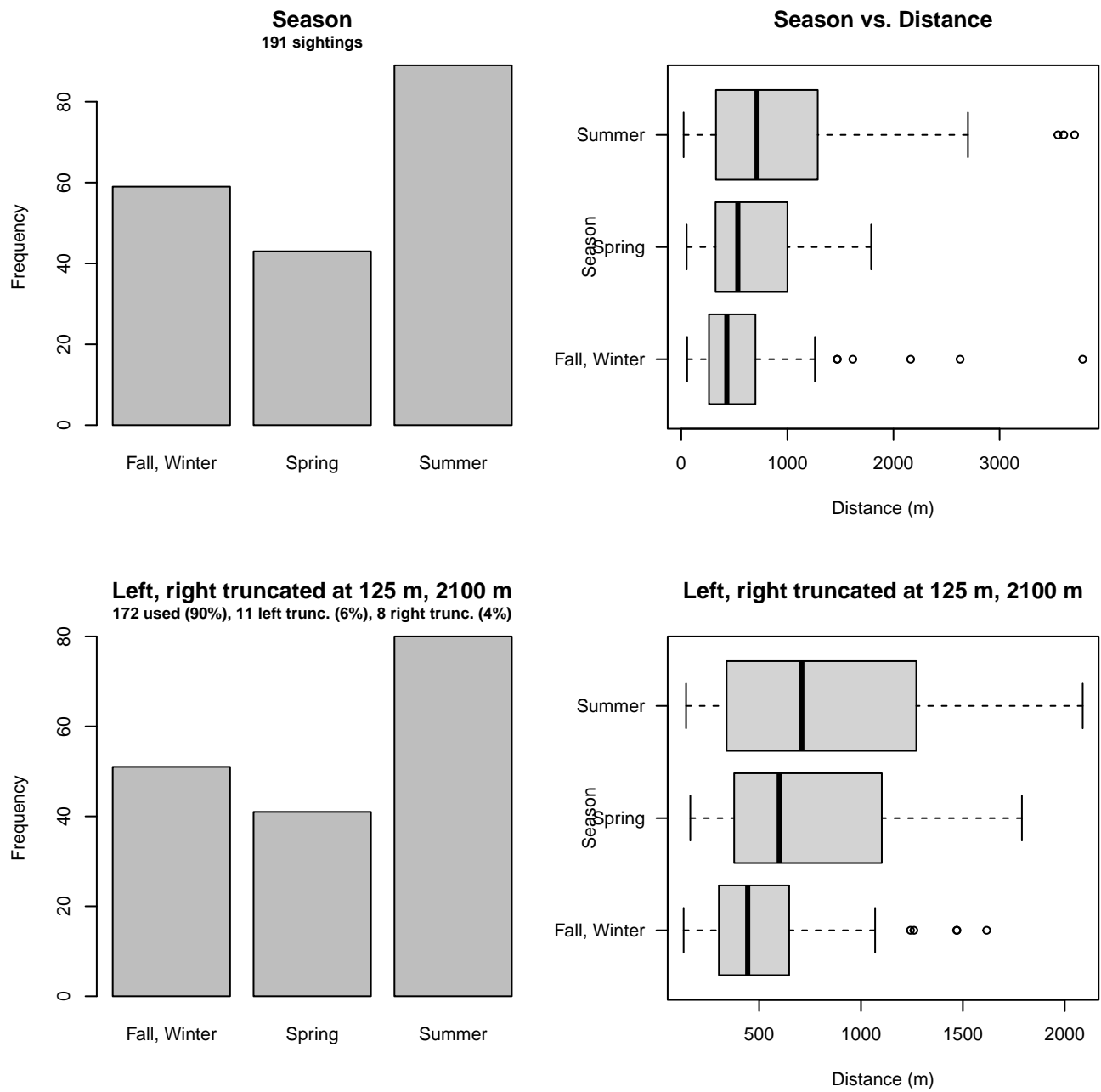


Figure 23: Distribution of the Season covariate before (top row) and after (bottom row) observations were truncated to fit the NYS-DEC NYBWM Partenavia detection function.

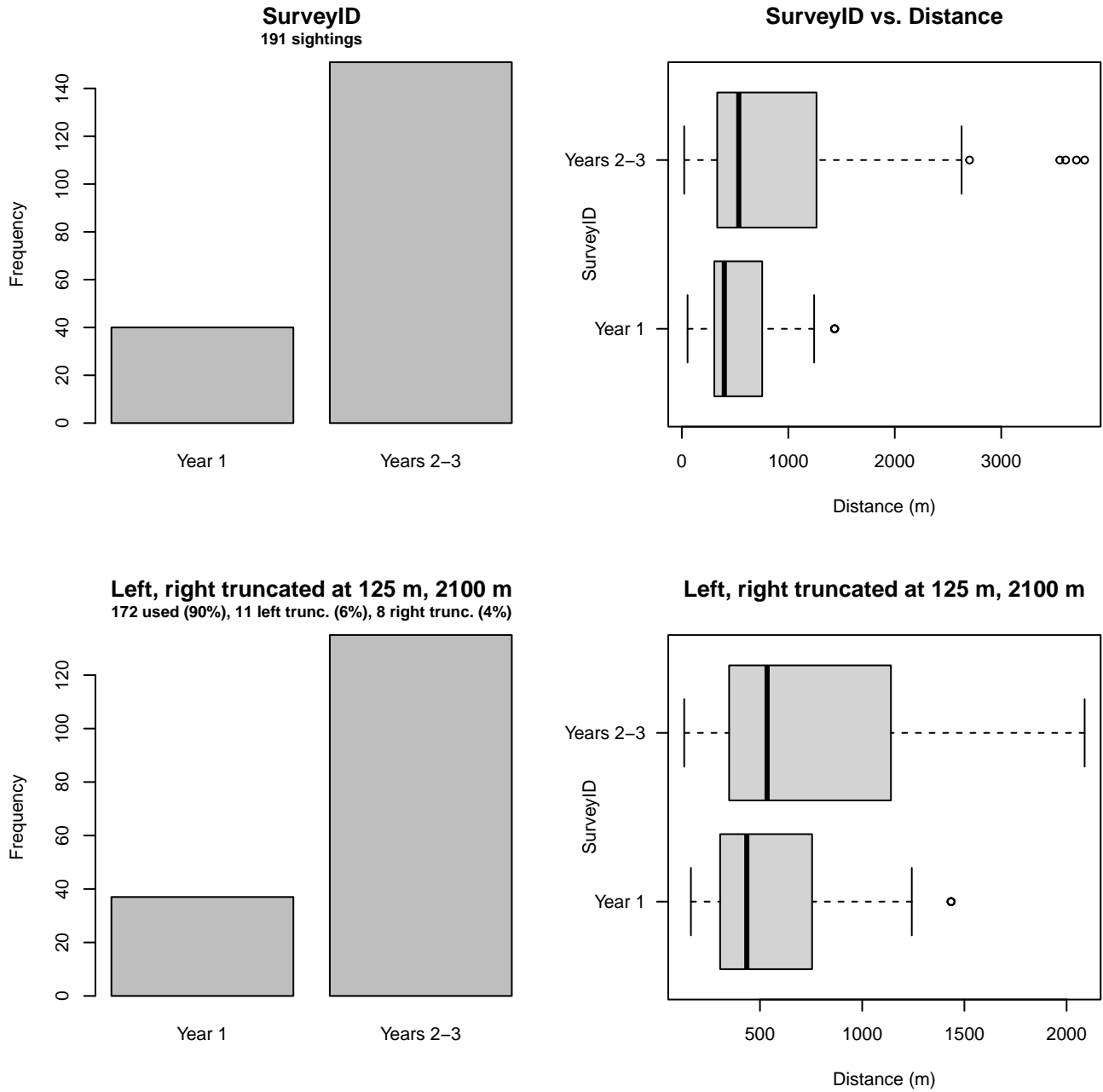


Figure 24: Distribution of the SurveyID covariate before (top row) and after (bottom row) observations were truncated to fit the NYS-DEC NYBWM Partenavia detection function.

2.1.1.7 NEAq New England

After right-truncating observations greater than 3704 m and left-truncating observations less than 71 m (Figure 26), we fitted the detection function to the 441 observations that remained (Table 10). The selected detection function (Figure 25) used a half normal key function with Beaufort (Figure 27), Glare (Figure 28) and OriginalScientificName (Figure 29) as covariates.

Table 10: Observations used to fit the NEAq New England detection function.

ScientificName	n
Balaenoptera borealis	44
Balaenoptera musculus	2
Balaenoptera physalus	128
Eubalaena glacialis	146
Megaptera novaeangliae	112
Physeter macrocephalus	9
Total	441

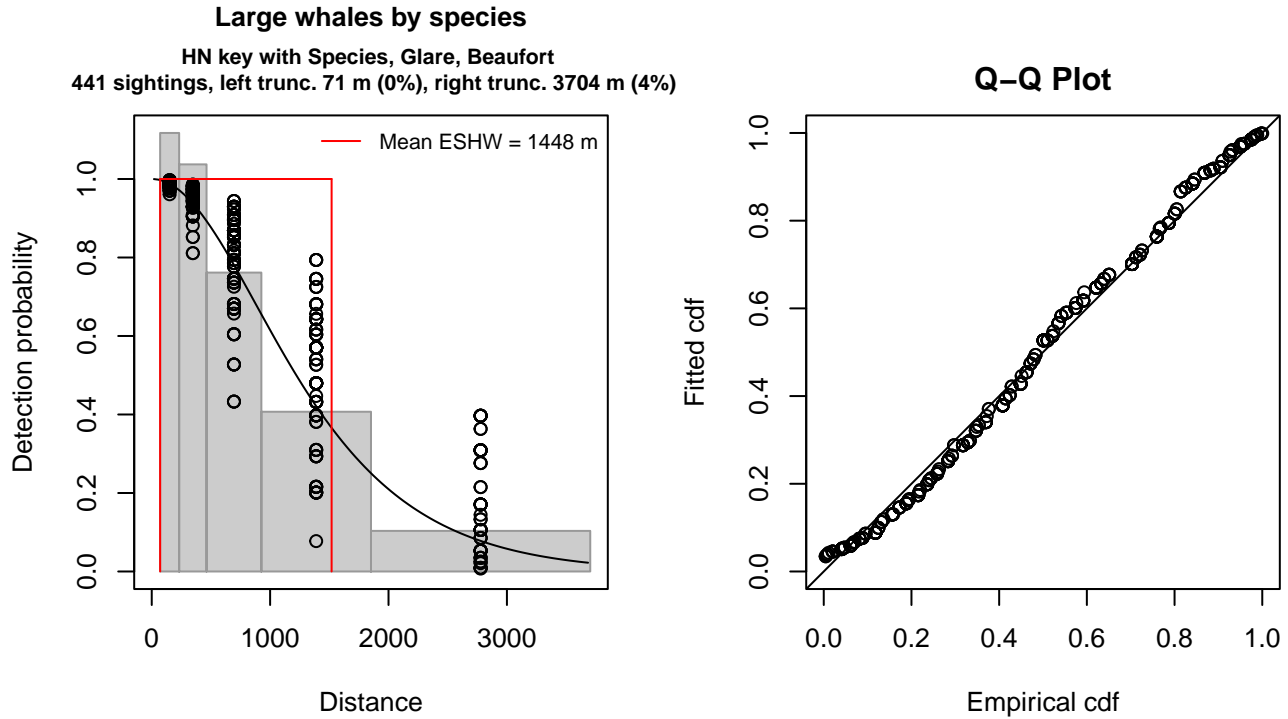


Figure 25: NEAq New England detection function and Q-Q plot showing its goodness of fit.

Statistical output for this detection function:

Summary for ds object

Number of observations : 441
 Distance range : 71 - 3704
 AIC : 1351.833

Detection function:

Half-normal key function

Detection function parameters

Scale coefficient(s):

	estimate	se
(Intercept)	6.4199373	0.11956192
OriginalScientificNameHumpback	0.1198260	0.10455078
OriginalScientificNameRight	-0.1344891	0.09839291
GlareSevere	0.3449677	0.16999750
GlareSlight, Moderate	0.3904627	0.09774396
Beaufort2	0.3680223	0.09867329
Beaufort3-4	0.6919932	0.12929768

	Estimate	SE	CV
Average p	0.3618698	0.01608762	0.04445694
N in covered region	1218.6704246	72.16746829	0.05921820

Distance sampling Cramer-von Mises test (unweighted)
Test statistic = 0.341945 p = 0.103421

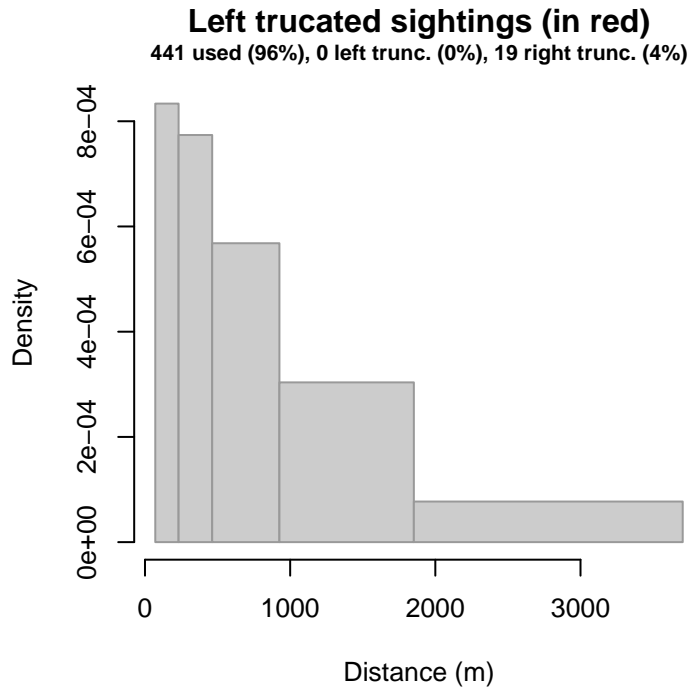


Figure 26: Density histogram of observations used to fit the NEAq New England detection function, with the left-most bar showing observations at distances less than 71 m, which were left-truncated and excluded from the analysis [Buckland et al. (2001)]. (This bar may be very short if there were very few left-truncated sightings, or very narrow if the left truncation distance was very small; in either case it may not appear red.)

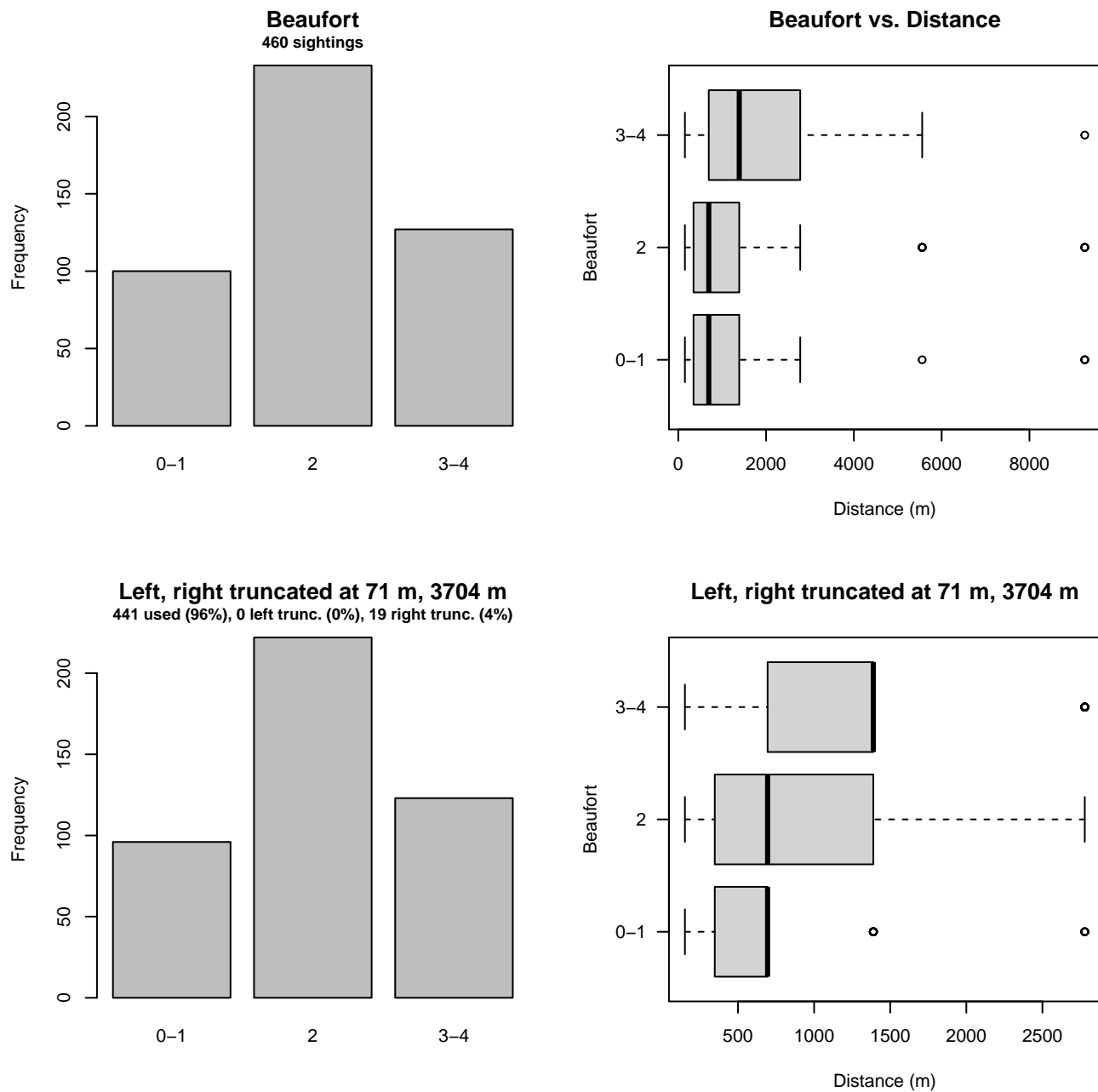


Figure 27: Distribution of the Beaufort covariate before (top row) and after (bottom row) observations were truncated to fit the NEAq New England detection function.

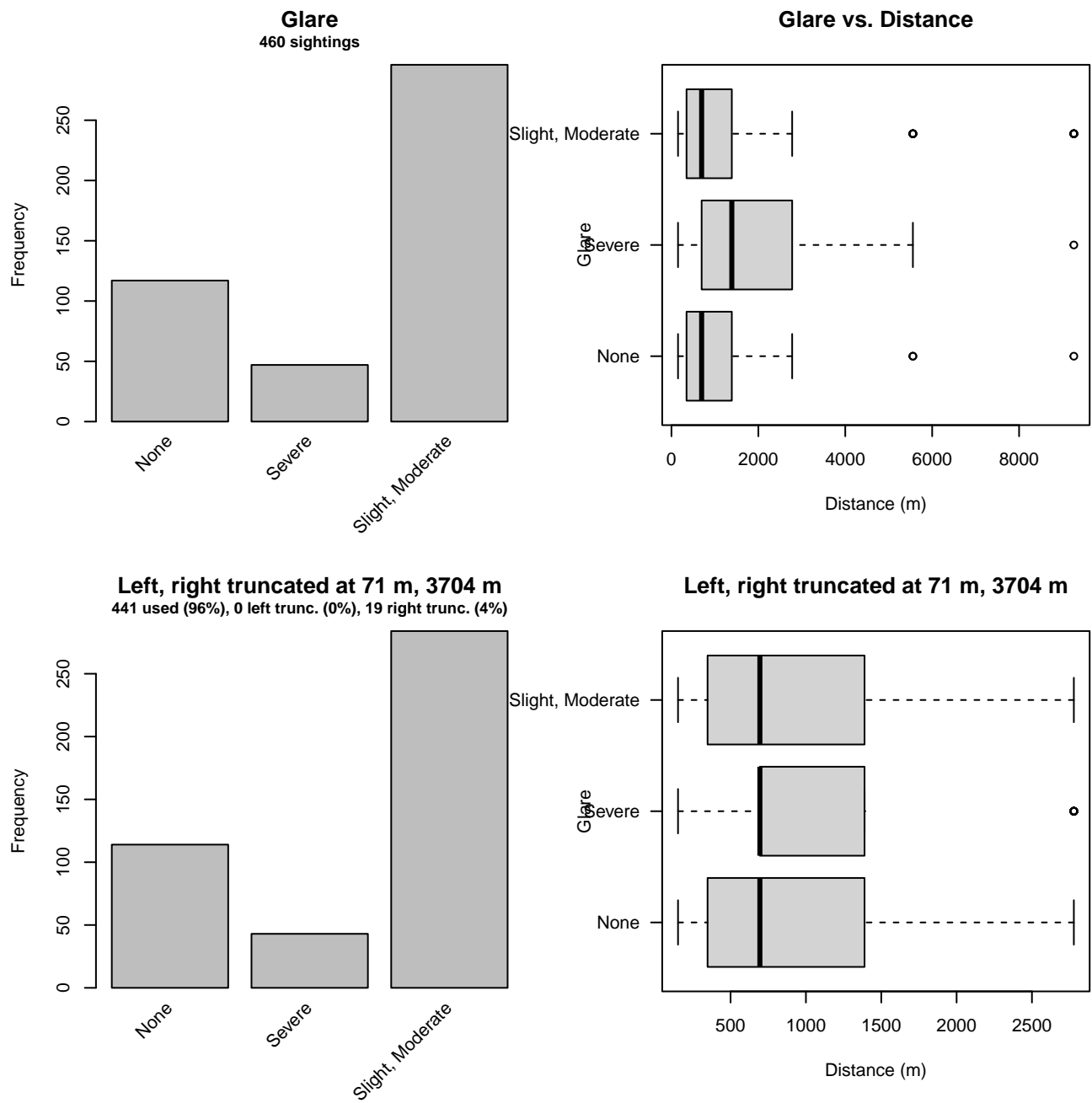


Figure 28: Distribution of the Glare covariate before (top row) and after (bottom row) observations were truncated to fit the NEAq New England detection function.

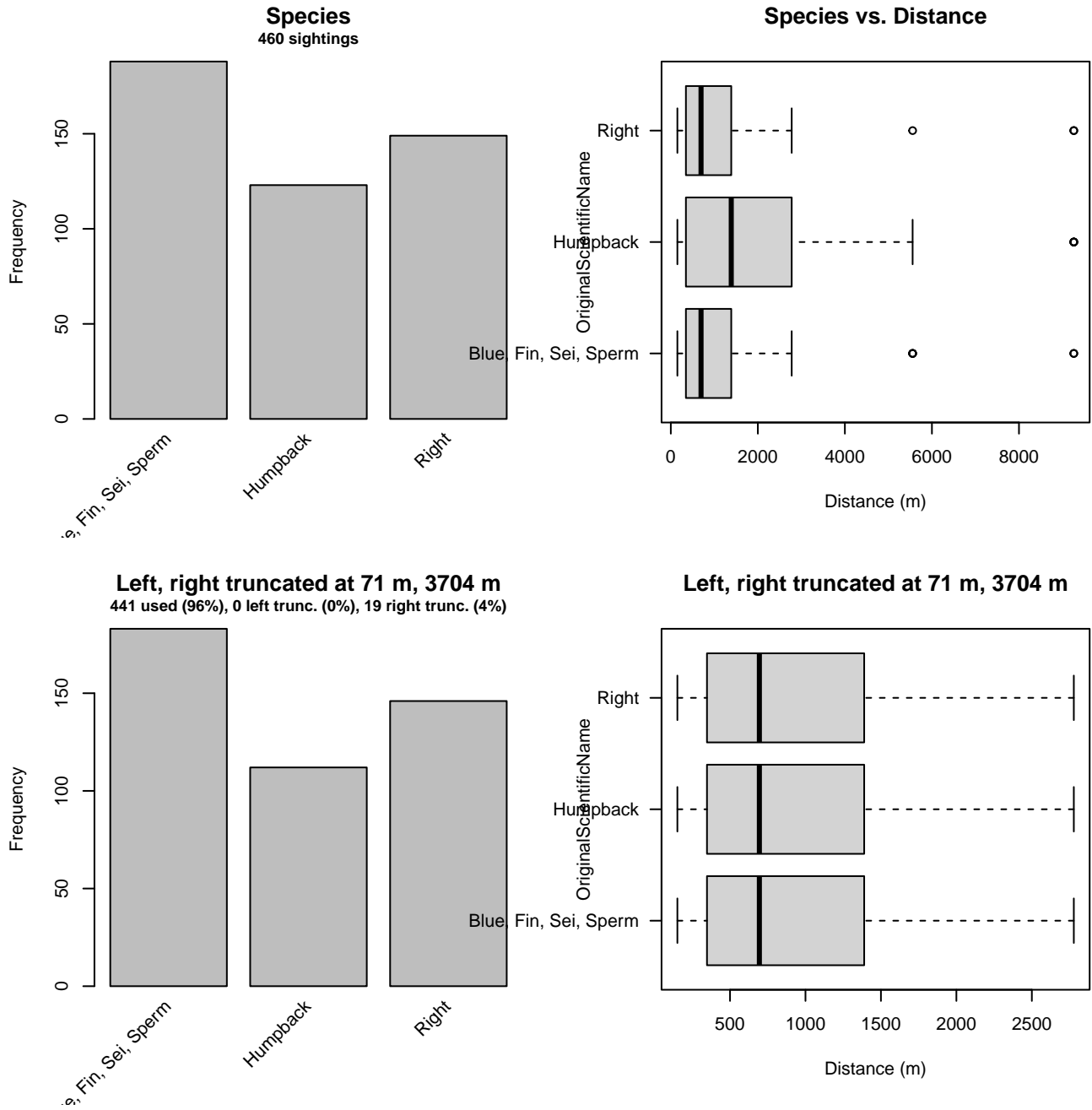


Figure 29: Distribution of the OriginalScientificName covariate before (top row) and after (bottom row) observations were truncated to fit the NEAq New England detection function.

2.1.1.8 UNCW and VAMSC

After right-truncating observations greater than 2000 m, we fitted the detection function to the 100 observations that remained (Table 11). The selected detection function (Figure 30) used a hazard rate key function with OriginalScientificName (Figure 31) as a covariate.

Table 11: Observations used to fit the UNCW and VAMSC detection function.

ScientificName	n
Balaenoptera physalus	27
Megaptera novaeangliae	31
Physeter macrocephalus	42
Total	100

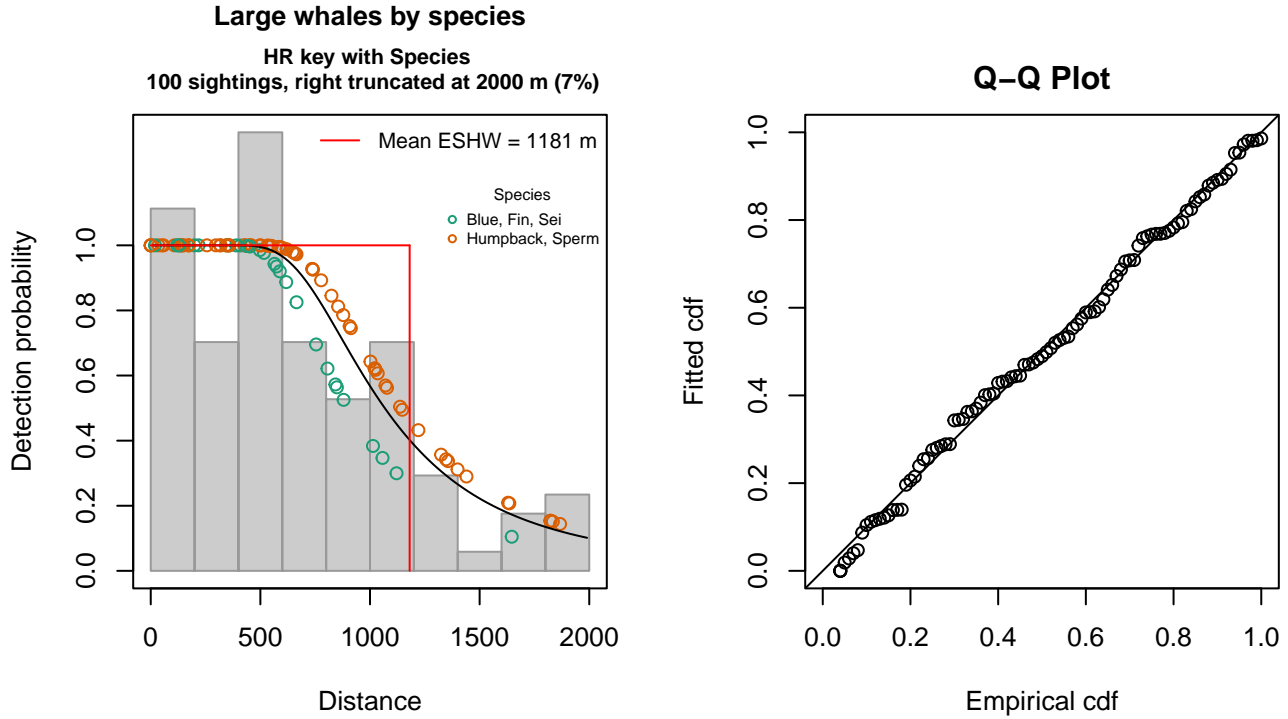


Figure 30: UNCW and VAMSC detection function and Q-Q plot showing its goodness of fit.

Statistical output for this detection function:

Summary for ds object

Number of observations : 100
Distance range : 0 - 2000
AIC : 1484.772

Detection function:

Hazard-rate key function

Detection function parameters

Scale coefficient(s):

	estimate	se
(Intercept)	6.6826489	0.2197841
OriginalScientificNameHumpback, Sperm	0.2371163	0.2278764

Shape coefficient(s):

	estimate	se
(Intercept)	1.11195	0.3071042

	Estimate	SE	CV
Average p	0.5857436	0.05399642	0.0921844
N in covered region	170.7231622	19.23003142	0.1126387

Distance sampling Cramer-von Mises test (unweighted)
 Test statistic = 0.036117 p = 0.952042

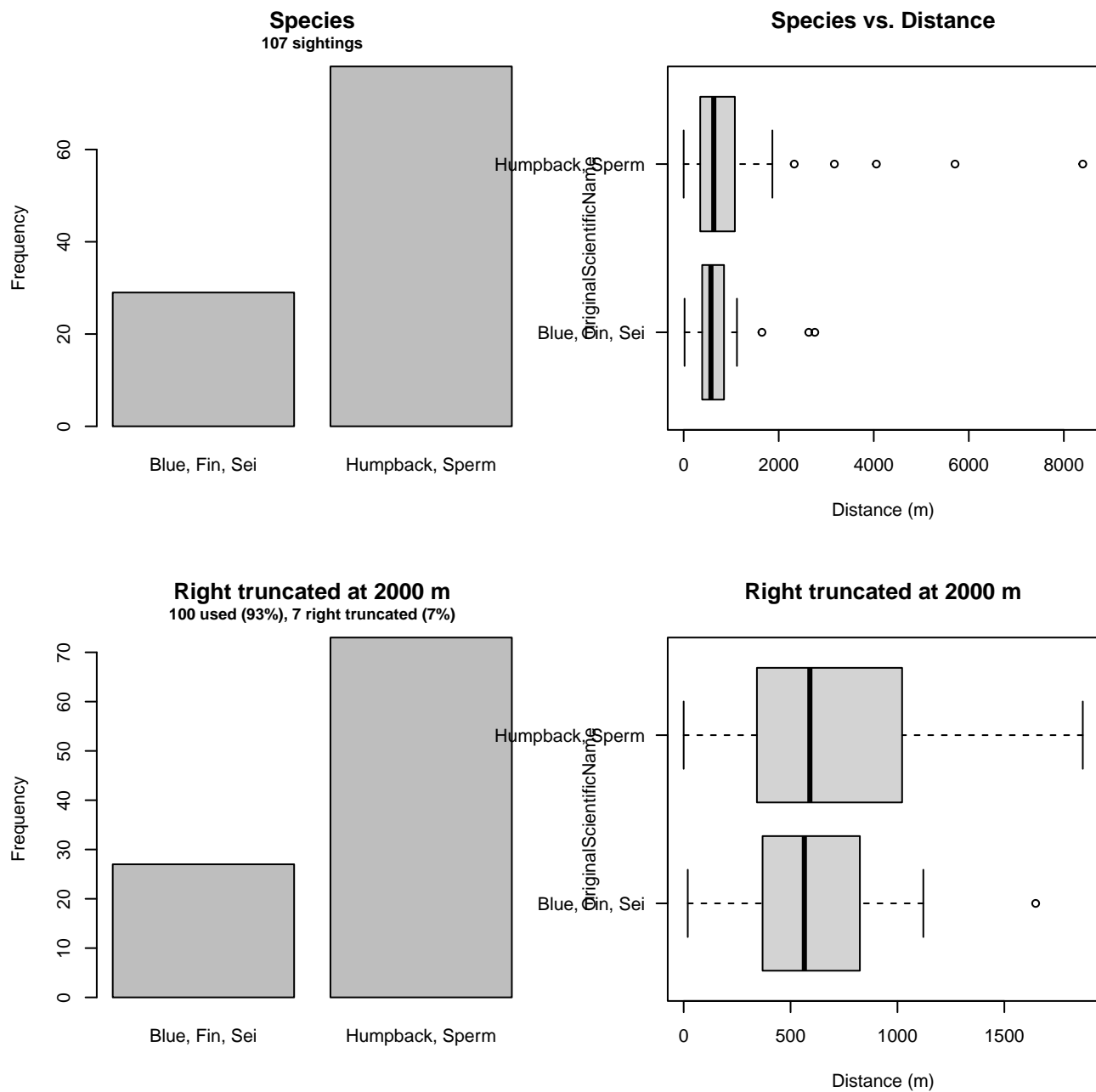


Figure 31: Distribution of the OriginalScientificName covariate before (top row) and after (bottom row) observations were truncated to fit the UNCW and VAMSC detection function.

2.1.2 Shipboard Surveys

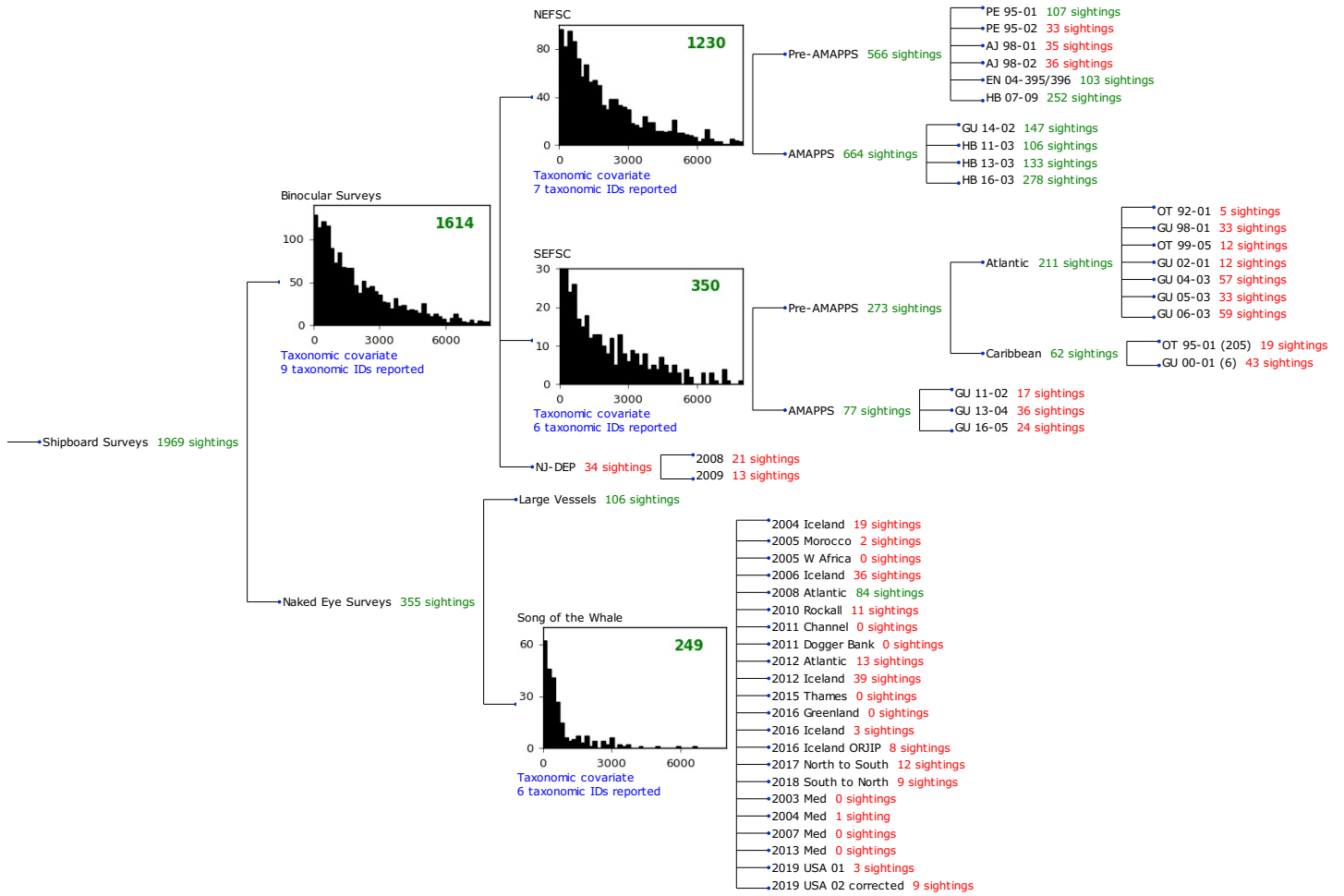


Figure 32: Detection hierarchy for shipboard surveys, showing how they were pooled during detectability modeling, for detection functions that pooled multiple taxa and used a taxonomic covariate to account for differences between them. Each histogram represents a detection function and summarizes the perpendicular distances of observations that were pooled to fit it, prior to truncation. Observation counts, also prior to truncation, are shown in green when they met the recommendation of Buckland et al. (2001) that detection functions utilize at least 60 sightings, and red otherwise. For rare taxa, it was not always possible to meet this recommendation, yielding higher statistical uncertainty. During the spatial modeling stage of the analysis, effective strip widths were computed for each survey using the closest detection function above it in the hierarchy (i.e. moving from right to left in the figure). Surveys that do not have a detection function above them in this figure were either addressed by a detection function presented in a different section of this report, or were omitted from the analysis.

2.1.2.1 NEFSC

After right-truncating observations greater than 7000 m, we fitted the detection function to the 1201 observations that remained (Table 12). The selected detection function (Figure 33) used a hazard rate key function with OriginalScientificName (Figure 34) and Program (Figure 35) as covariates.

Table 12: Observations used to fit the NEFSC detection function.

ScientificName	n
Balaenoptera borealis	24
Balaenoptera borealis/physalus	88
Balaenoptera musculus	7
Balaenoptera physalus	280
Eubalaena glacialis	53
Megaptera novaeangliae	289
Physeter macrocephalus	460
Total	1201

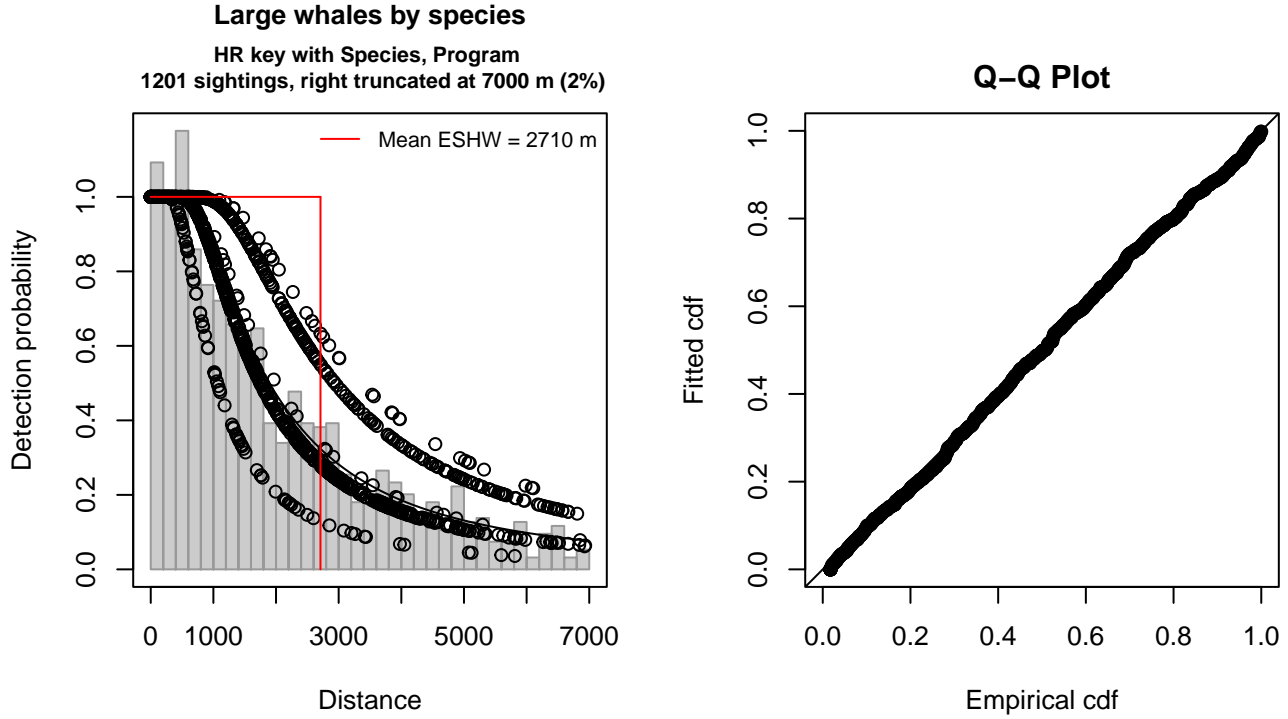


Figure 33: NEFSC detection function and Q-Q plot showing its goodness of fit.

Statistical output for this detection function:

Summary for ds object

Number of observations : 1201
Distance range : 0 - 7000
AIC : 20458.33

Detection function:

Hazard-rate key function

Detection function parameters

Scale coefficient(s):

	estimate	se
(Intercept)	7.2780926	0.1052538
OriginalScientificNameHumpback, Sperm	0.4967174	0.1052988
OriginalScientificNameUnid. fin or sei	0.6284650	0.1945392
ProgramMarine Mammal Abundance Surveys	-0.5195829	0.0968891

Shape coefficient(s):

	estimate	se
(Intercept)	0.5494314	0.0661582

	Estimate	SE	CV
Average p	0.3639429	0.01592018	0.04374363
N in covered region	3299.9683075	163.75203637	0.04962231

Distance sampling Cramer-von Mises test (unweighted)
 Test statistic = 0.126712 p = 0.469029

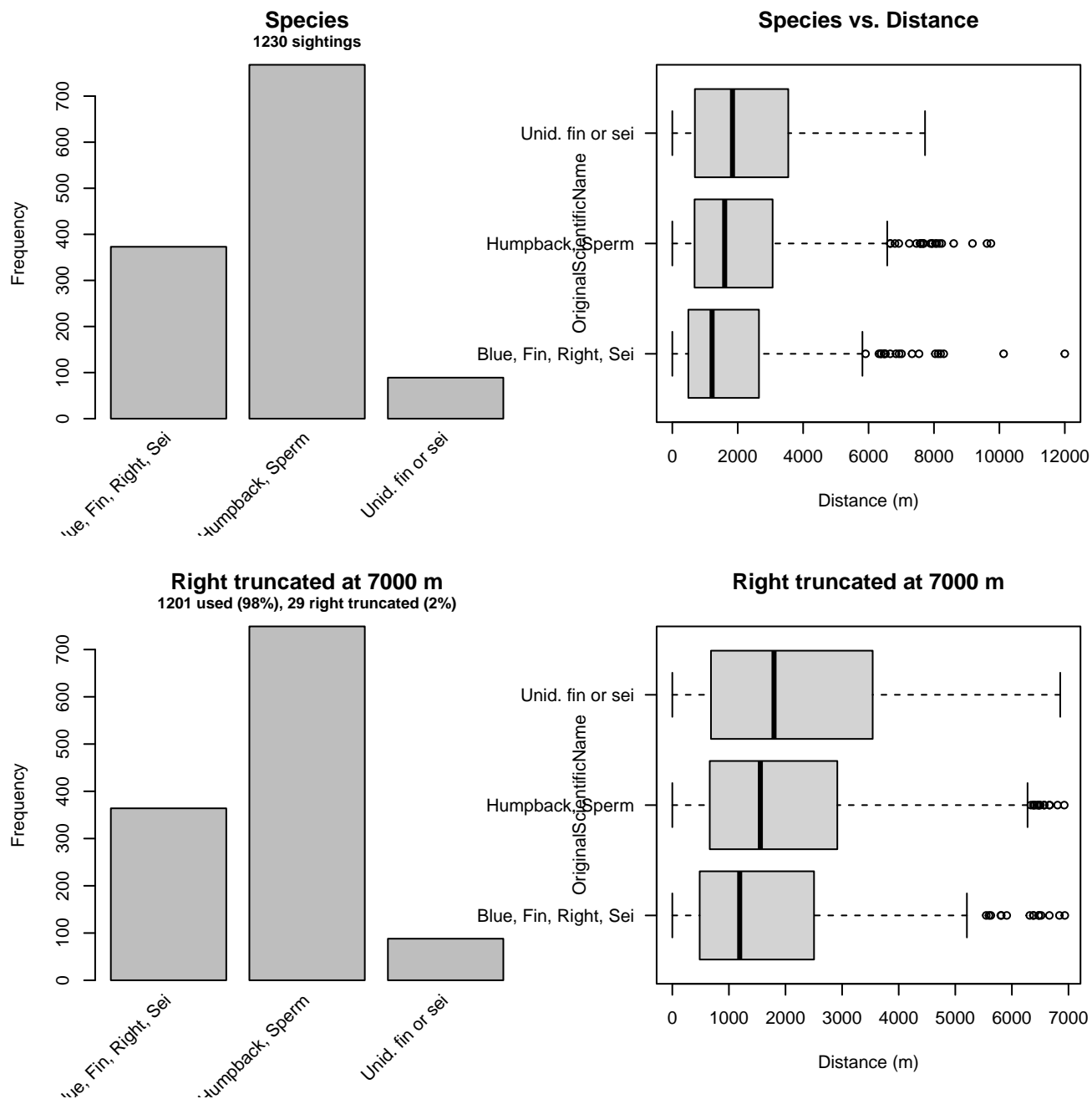


Figure 34: Distribution of the OriginalScientificName covariate before (top row) and after (bottom row) observations were truncated to fit the NEFSC detection function.

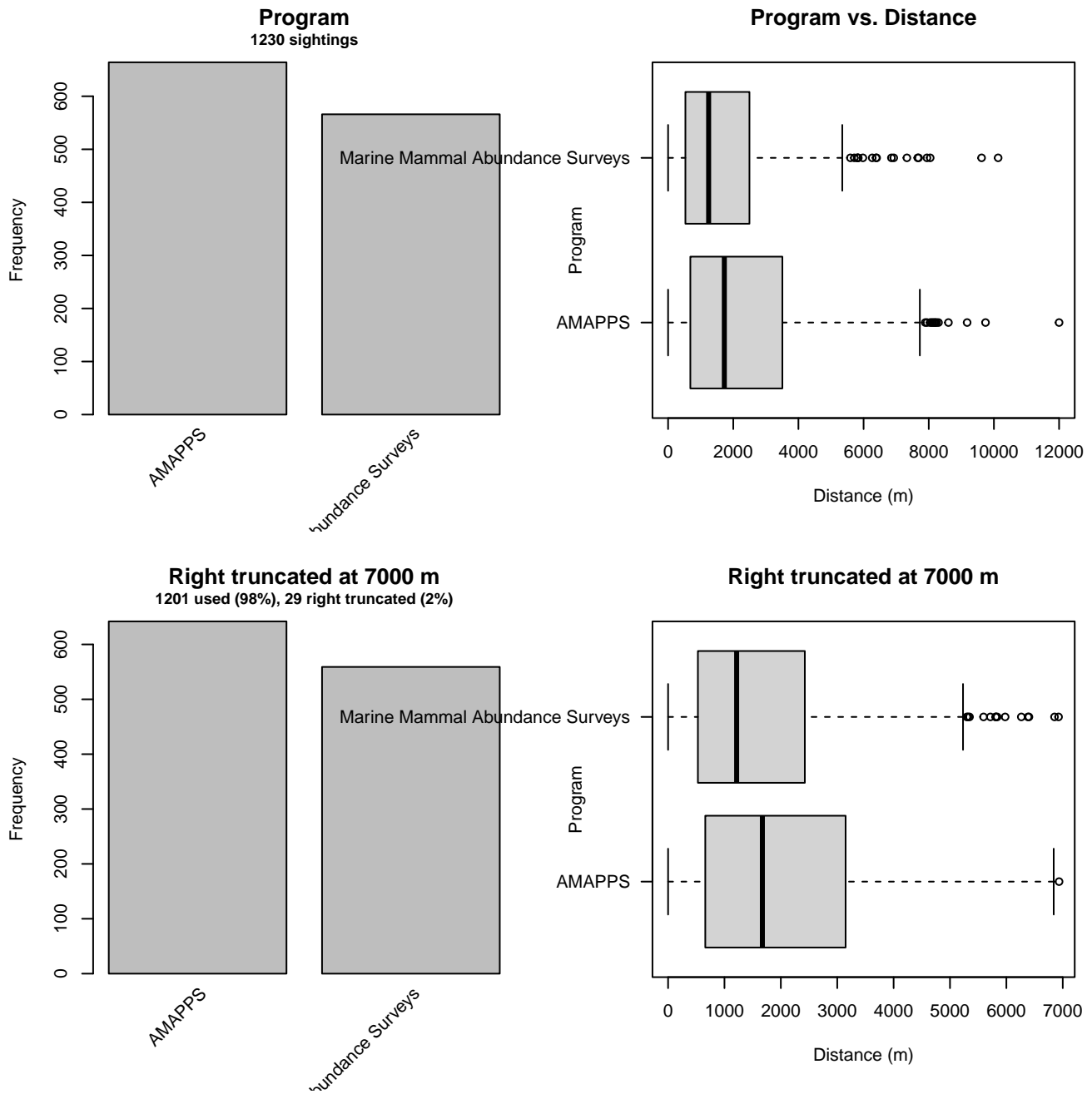


Figure 35: Distribution of the Program covariate before (top row) and after (bottom row) observations were truncated to fit the NEFSC detection function.

2.1.2.2 SEFSC

After right-truncating observations greater than 6000 m, we fitted the detection function to the 332 observations that remained (Table 13). The selected detection function (Figure 36) used a hazard rate key function with Beaufort (Figure 37), OriginalScientificName (Figure 38) and Program (Figure 39) as covariates.

Table 13: Observations used to fit the SEFSC detection function.

ScientificName	n
Balaenoptera borealis/edeni	3
Balaenoptera edeni	10
Balaenoptera physalus	17
Eubalaena glacialis	2
Megaptera novaeangliae	32
Physeter macrocephalus	268
Total	332

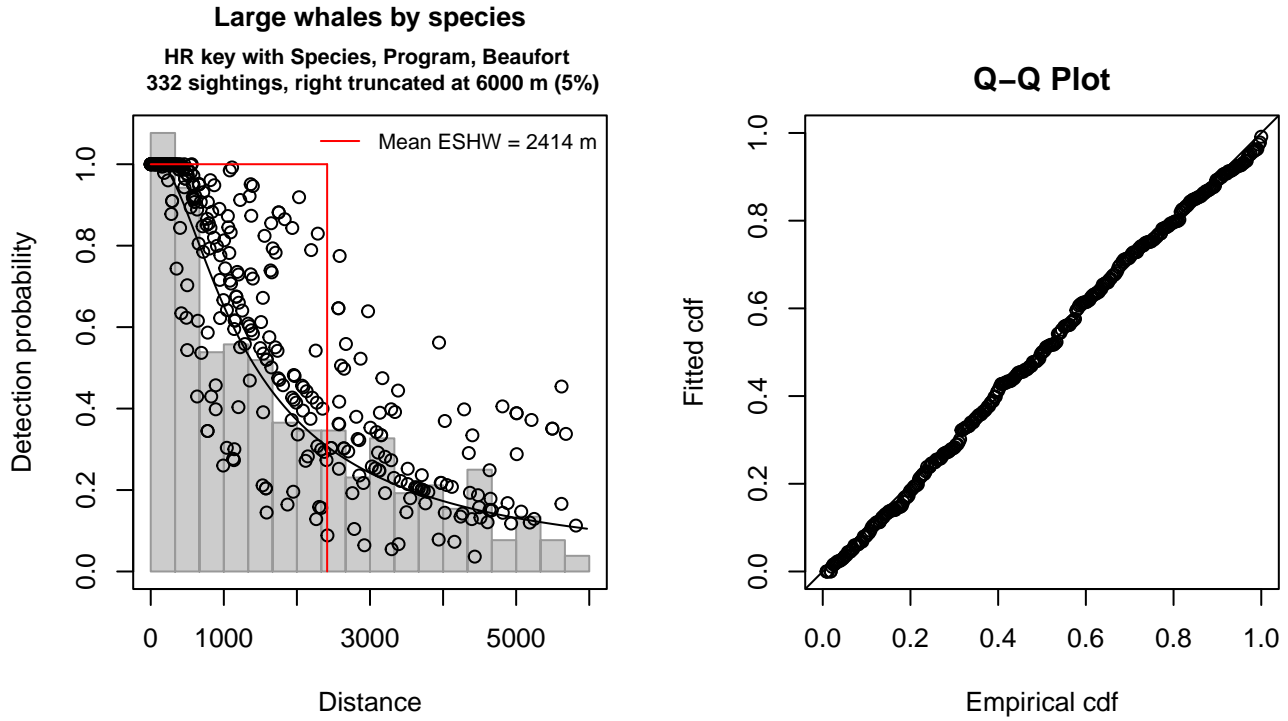


Figure 36: SEFSC detection function and Q-Q plot showing its goodness of fit.

Statistical output for this detection function:

Summary for ds object

Number of observations : 332
Distance range : 0 - 6000
AIC : 5604.674

Detection function:

Hazard-rate key function

Detection function parameters

Scale coefficient(s):

	estimate	se
(Intercept)	7.4794246	0.4929618
OriginalScientificNameSperm	0.7957413	0.3448895
ProgramAtlantic Pre-AMAPPS	-0.7295682	0.3154763
ProgramCaribbean	-0.7773443	0.4064337
Beaufort	-0.1322436	0.1039800

Shape coefficient(s):

	estimate	se
(Intercept)	0.3345999	0.1370809

	Estimate	SE	CV
Average p	0.3546416	0.03786854	0.1067797
N in covered region	936.1563072	108.72789053	0.1161429

Distance sampling Cramer-von Mises test (unweighted)
 Test statistic = 0.055285 p = 0.843624

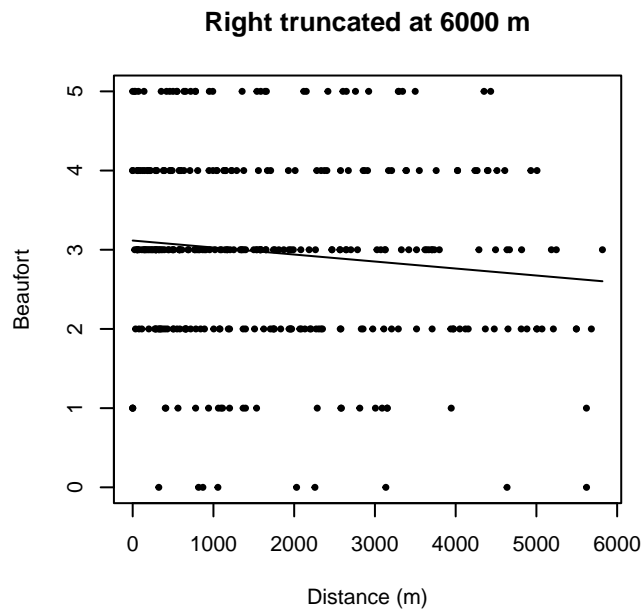
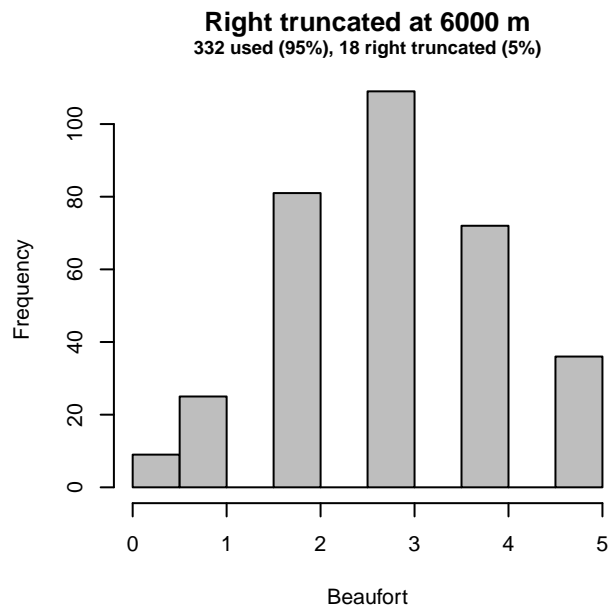
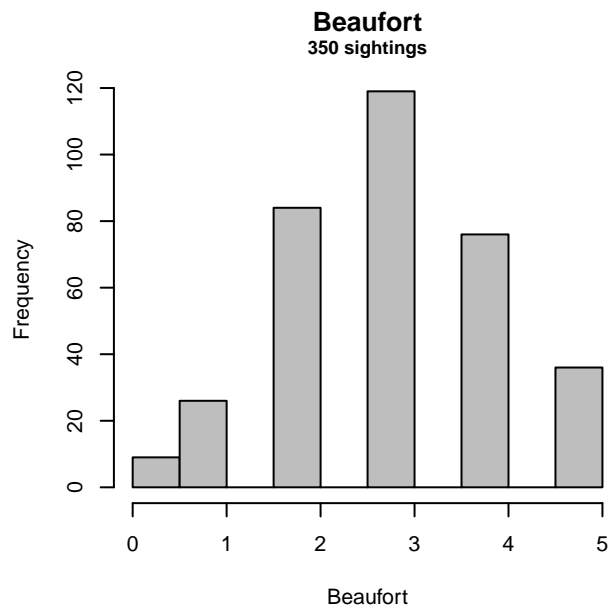


Figure 37: Distribution of the Beaufort covariate before (top row) and after (bottom row) observations were truncated to fit the SEFSC detection function.

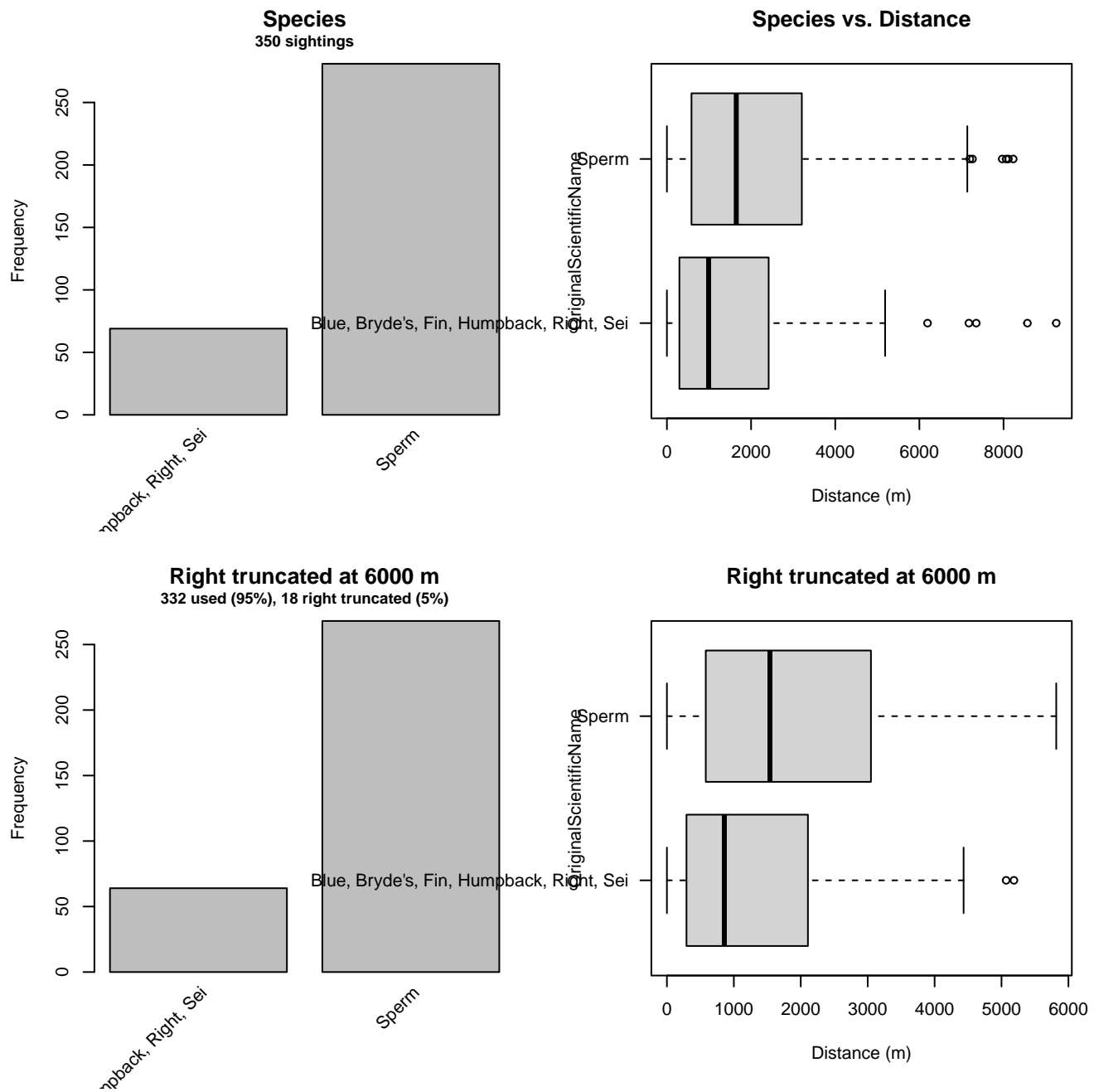


Figure 38: Distribution of the OriginalScientificName covariate before (top row) and after (bottom row) observations were truncated to fit the SEFSC detection function.

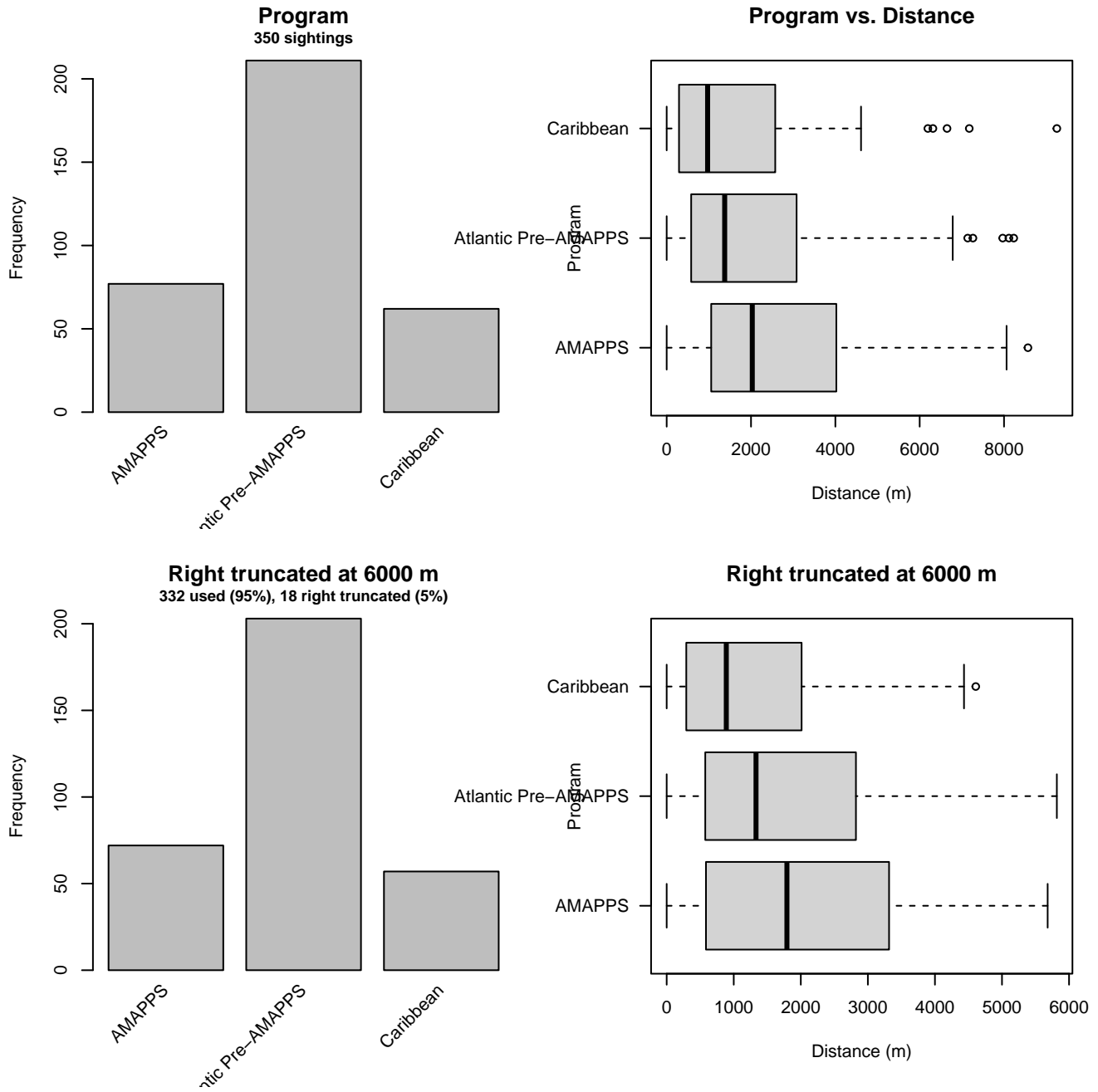


Figure 39: Distribution of the Program covariate before (top row) and after (bottom row) observations were truncated to fit the SEFSC detection function.

2.1.2.3 Binocular Surveys

After right-truncating observations greater than 5000 m, we fitted the detection function to the 1471 observations that remained (Table 14). The selected detection function (Figure 40) used a hazard rate key function with OriginalScientificName (Figure 41) and Program (Figure 42) as covariates.

Table 14: Observations used to fit the Binocular Surveys detection function.

ScientificName	n
Balaenoptera borealis	22
Balaenoptera borealis/edeni	3
Balaenoptera borealis/physalus	79
Balaenoptera edeni	8
Balaenoptera musculus	6
Balaenoptera physalus	308
Eubalaena glacialis	55
Megaptera novaeangliae	307
Physeter macrocephalus	683
Total	1471

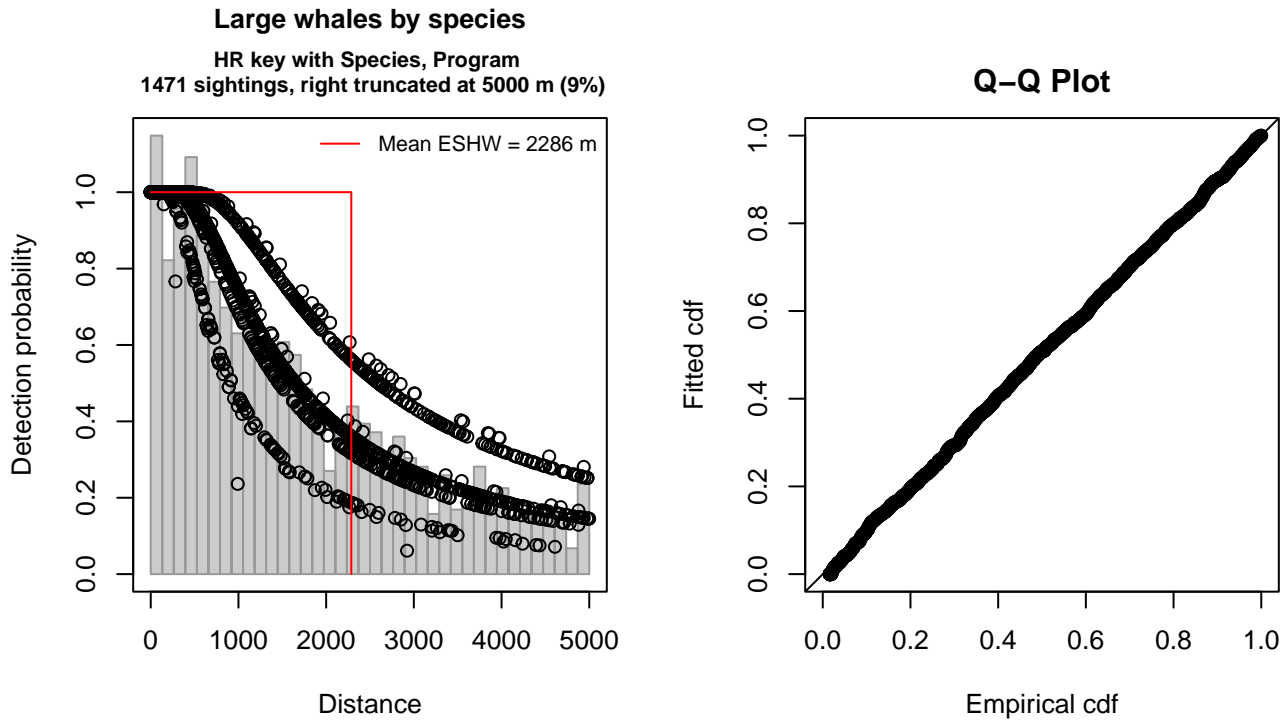


Figure 40: Binocular Surveys detection function and Q-Q plot showing its goodness of fit.

Statistical output for this detection function:

Summary for ds object

Number of observations : 1471
Distance range : 0 - 5000
AIC : 24498.15

Detection function:

Hazard-rate key function

Detection function parameters

Scale coefficient(s):

	estimate	se
(Intercept)	7.0154074	0.1387774
OriginalScientificNameHumpback, Sperm	0.5736762	0.1427682
OriginalScientificNameUnid. Bryde's, fin, or sei	0.6607853	0.2833819
ProgramAtlantic Pre-AMAPPS	-0.4551133	0.1309943

Shape coefficient(s):

	estimate	se
(Intercept)	0.2925203	0.0742023

	Estimate	SE	CV
Average p	0.4357633	0.02101424	0.04822398
N in covered region	3375.6858719	176.17568539	0.05218960

Distance sampling Cramer-von Mises test (unweighted)

Test statistic = 0.043159 p = 0.916226

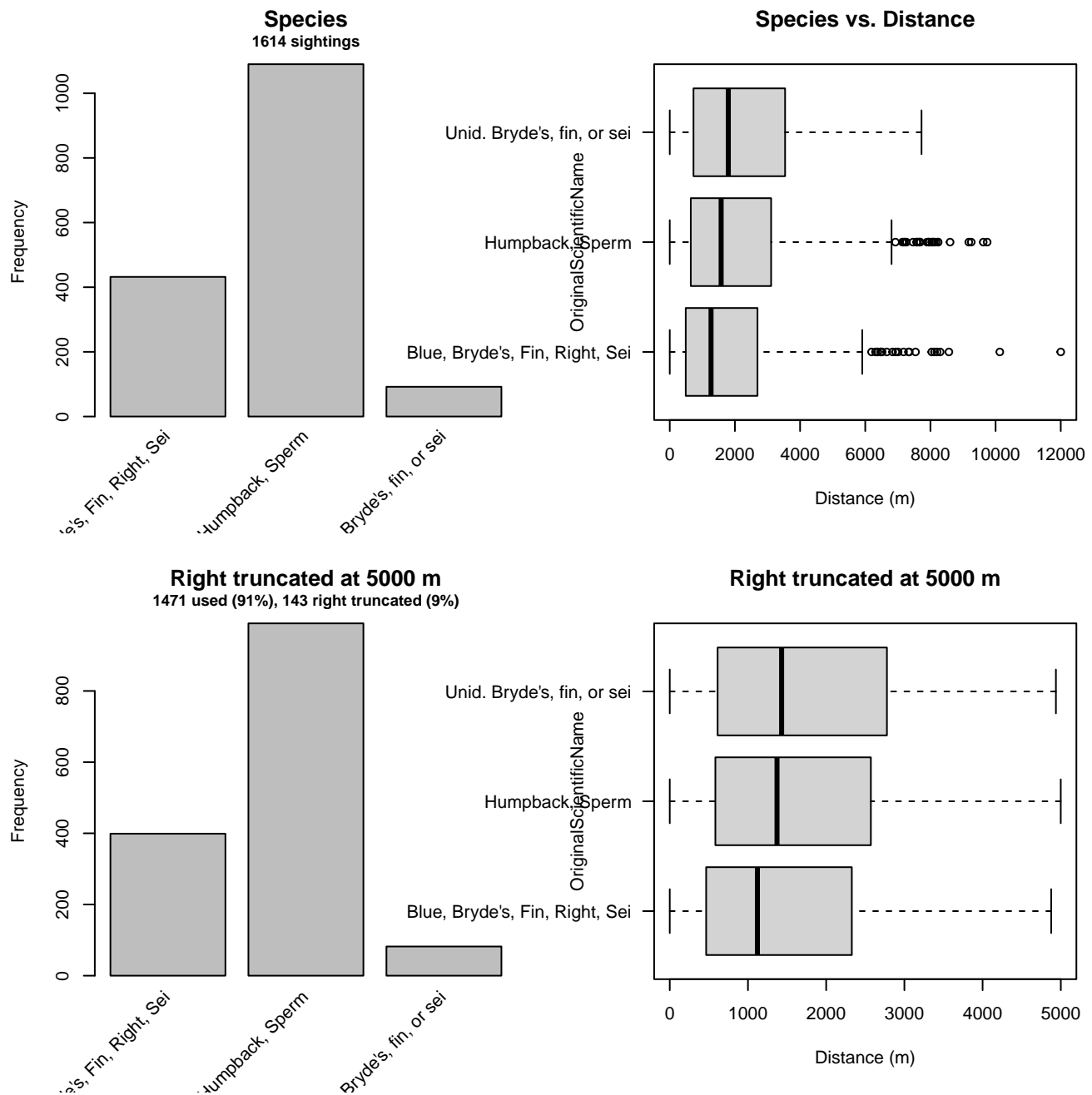


Figure 41: Distribution of the OriginalScientificName covariate before (top row) and after (bottom row) observations were truncated to fit the Binocular Surveys detection function.

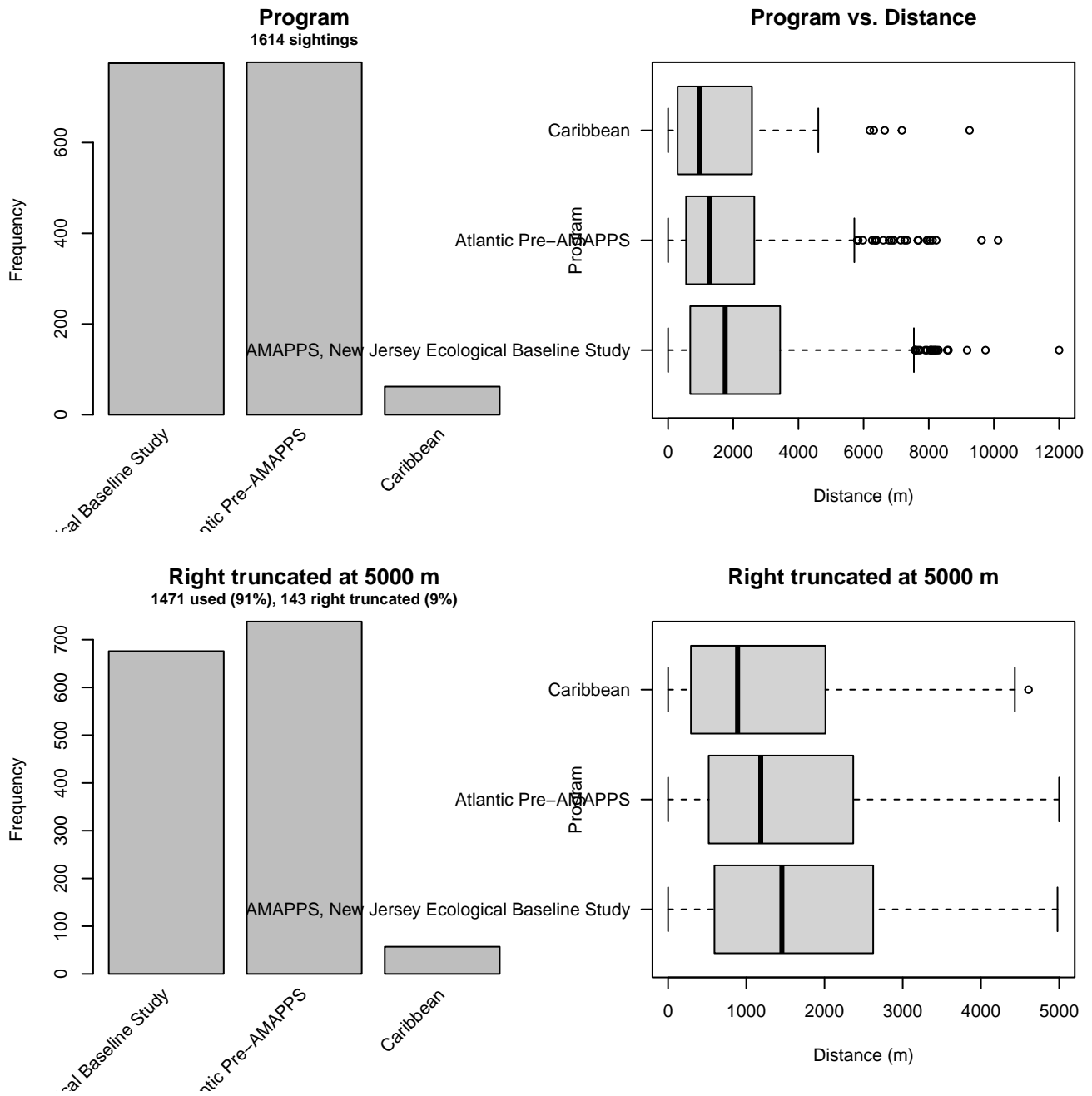


Figure 42: Distribution of the Program covariate before (top row) and after (bottom row) observations were truncated to fit the Binocular Surveys detection function.

2.1.2.4 Song of the Whale

After right-truncating observations greater than 3000 m, we fitted the detection function to the 239 observations that remained (Table 15). The selected detection function (Figure 43) used a hazard rate key function with Glare (Figure 44), OriginalScientificName (Figure 45) and WeatherCode (Figure 46) as covariates.

Table 15: Observations used to fit the Song of the Whale detection function.

ScientificName	n
Balaenoptera borealis	13
Balaenoptera edeni	7
Balaenoptera musculus	8
Balaenoptera physalus	27
Megaptera novaeangliae	69
Physeter macrocephalus	115
Total	239

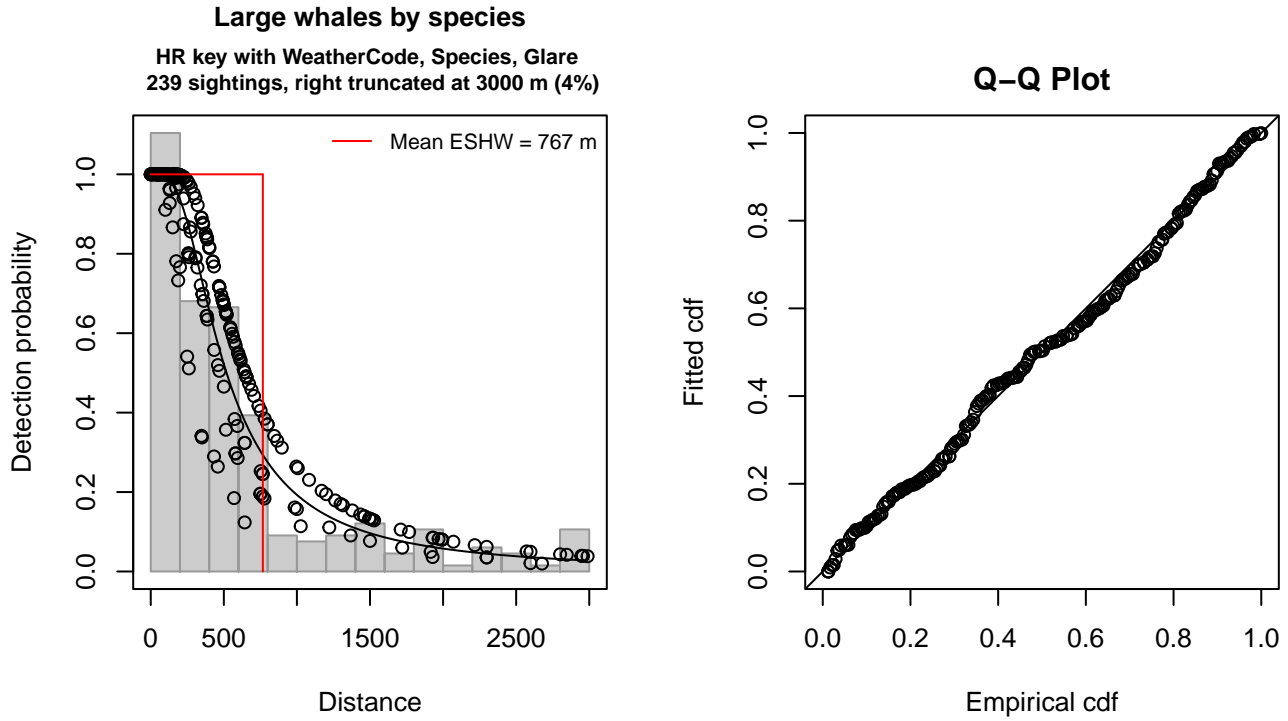


Figure 43: Song of the Whale detection function and Q-Q plot showing its goodness of fit.

Statistical output for this detection function:

Summary for ds object

Number of observations : 239
 Distance range : 0 - 3000
 AIC : 3547.931

Detection function:

Hazard-rate key function

Detection function parameters

Scale coefficient(s):

	estimate	se
(Intercept)	5.9647631	0.2274130
WeatherCodeHaze	-0.8889445	0.5747918
OriginalScientificNameHumpback, Sperm	0.3084029	0.2238350
GlareSevere	-0.4670165	0.2579856

Shape coefficient(s):

estimate	se
----------	----

(Intercept) 0.6276528 0.09675212

	Estimate	SE	CV
Average p	0.2409962	0.02414927	0.100206
N in covered region	991.7170380	114.27753421	0.115232

Distance sampling Cramer-von Mises test (unweighted)
 Test statistic = 0.073160 p = 0.732317

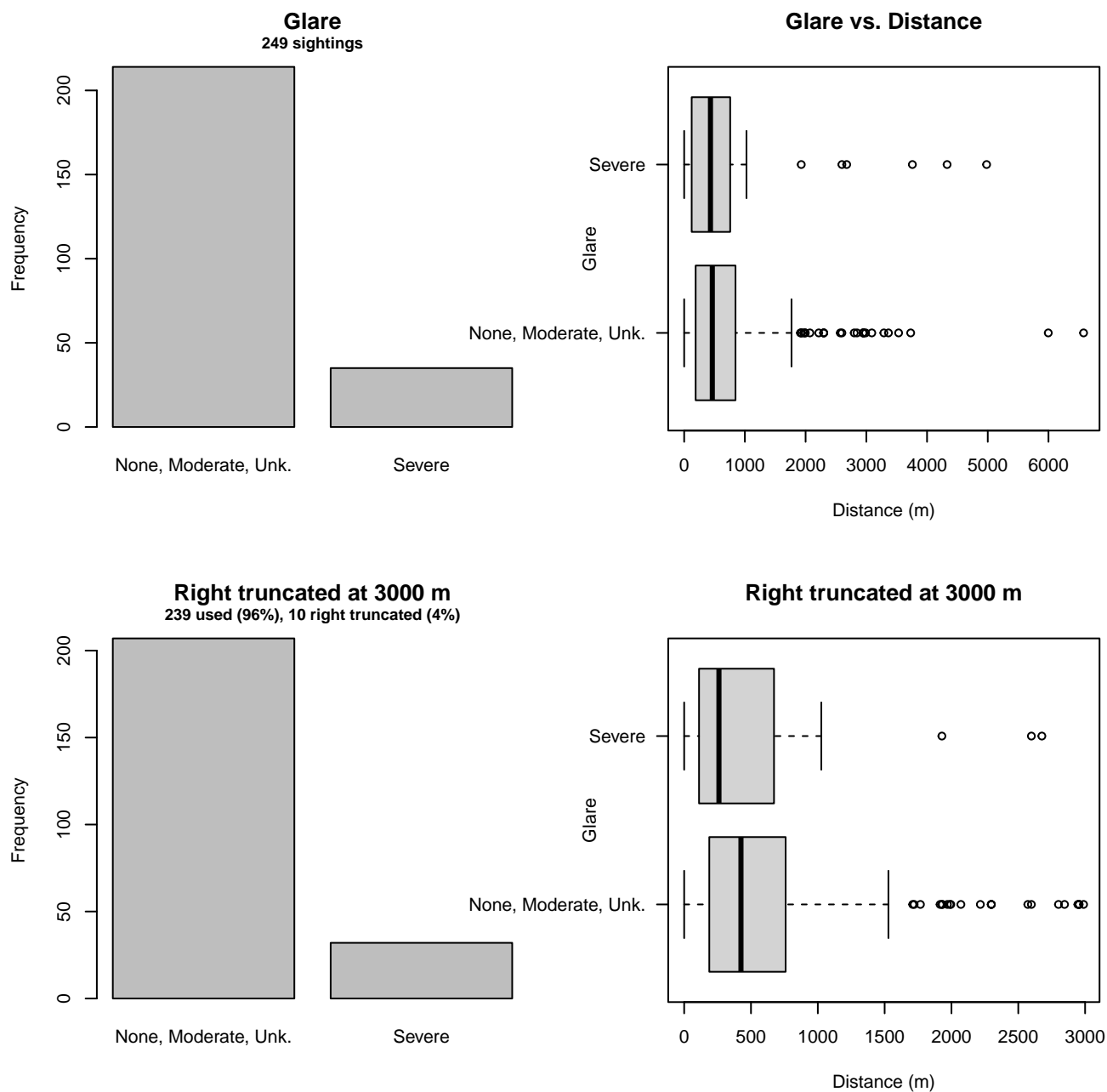


Figure 44: Distribution of the Glare covariate before (top row) and after (bottom row) observations were truncated to fit the Song of the Whale detection function.

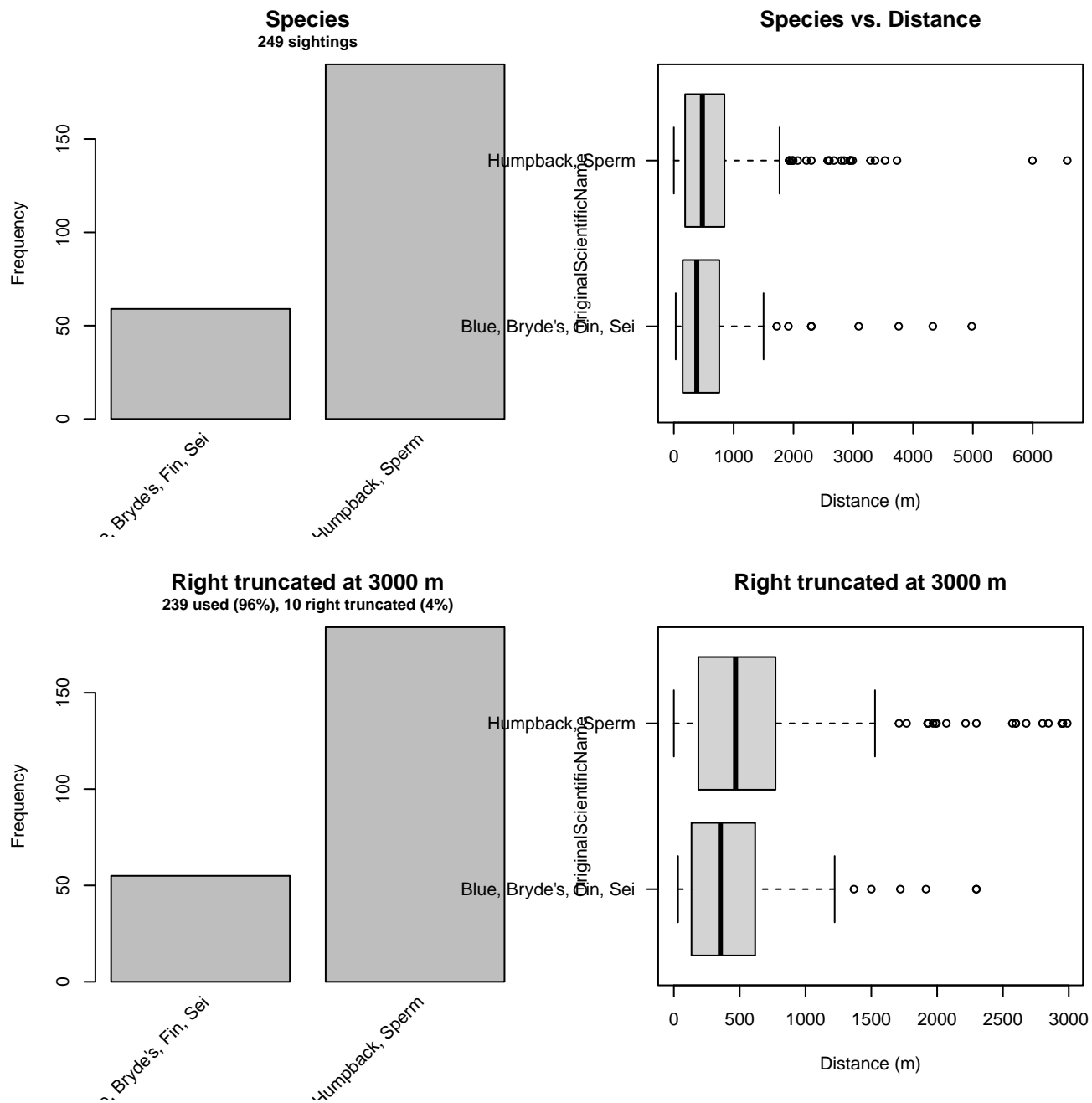


Figure 45: Distribution of the OriginalScientificName covariate before (top row) and after (bottom row) observations were truncated to fit the Song of the Whale detection function.

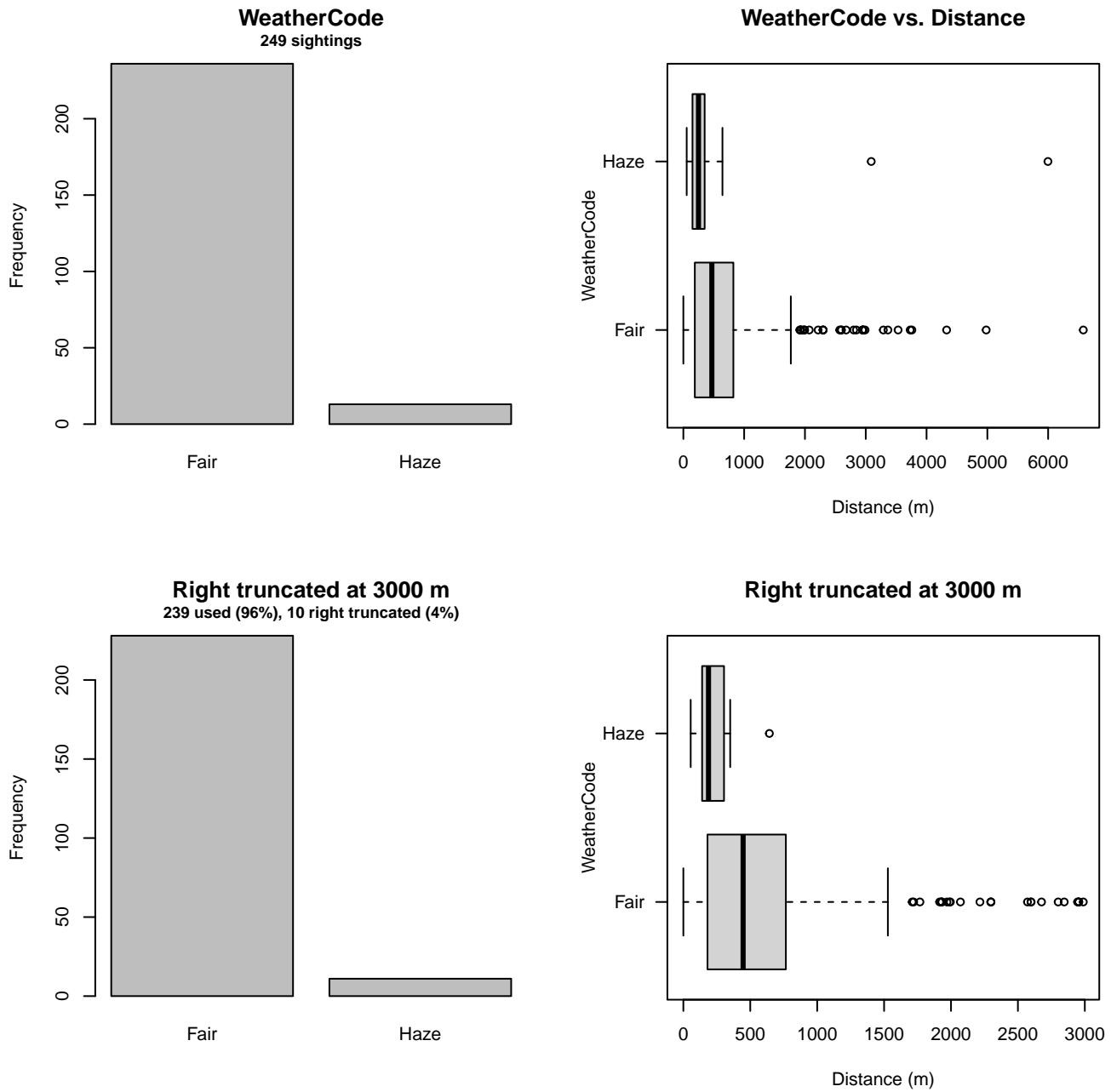


Figure 46: Distribution of the WeatherCode covariate before (top row) and after (bottom row) observations were truncated to fit the Song of the Whale detection function.

2.2 Without a Taxonomic Covariate

We fitted the detection functions in this section to pools of species with similar detectability characteristics but could not use a taxonomic identification as a covariate to account for differences between them. We usually took this approach after trying the taxonomic covariate and finding it had insufficient statistical power to be retained. We also resorted to it when the focal taxon being modeled had too few observations to be allocated its own taxonomic covariate level and was too poorly known for us to confidently determine which other taxa we could group it with.

2.2.1 Aerial Surveys

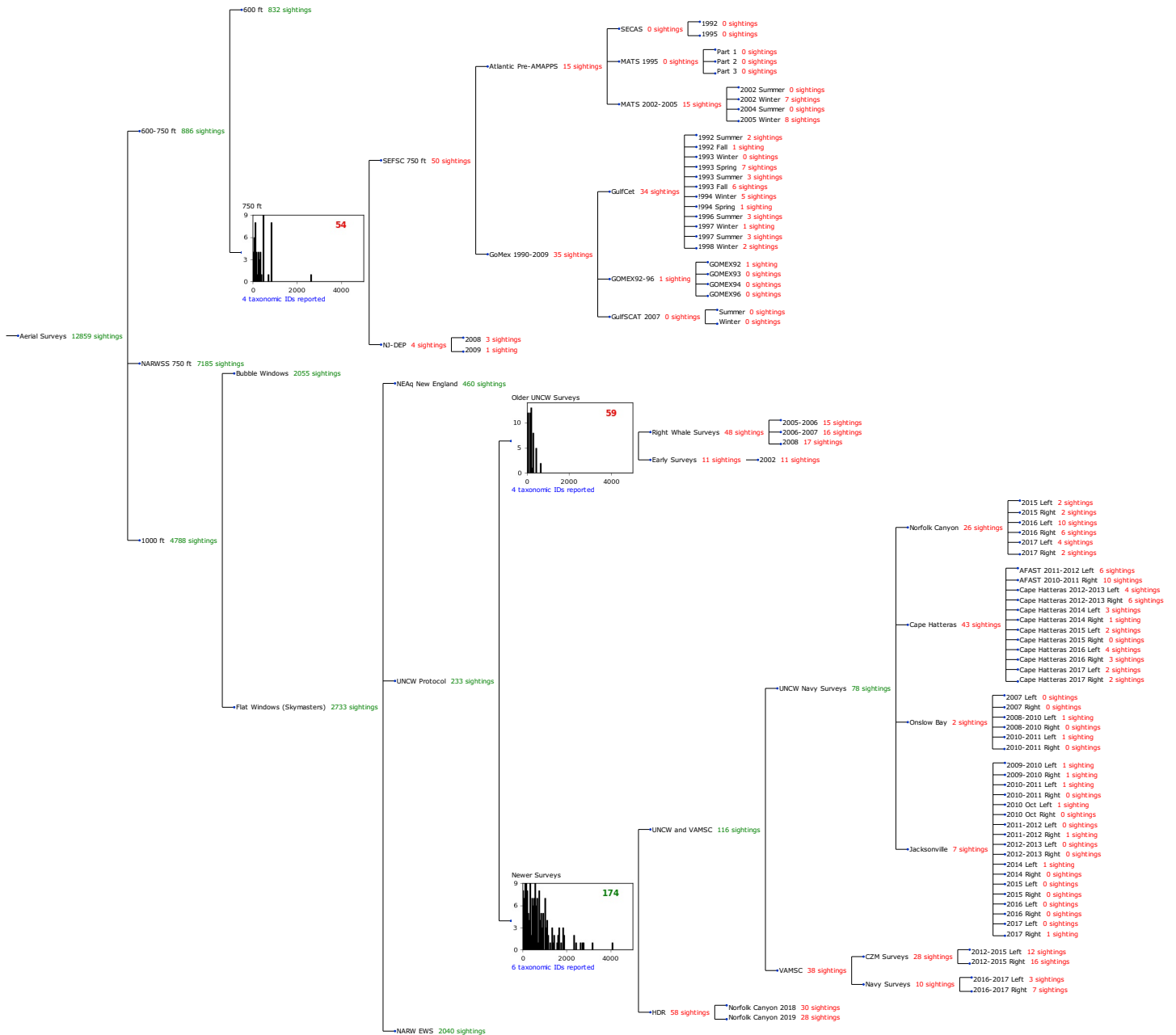


Figure 47: Detection hierarchy for aerial surveys, showing how they were pooled during detectability modeling, for detection functions that pooled multiple taxa but could not use a taxonomic covariate to account for differences between them. Each histogram represents a detection function and summarizes the perpendicular distances of observations that were pooled to fit it, prior to truncation. Observation counts, also prior to truncation, are shown in green when they met the recommendation of Buckland et al. (2001) that detection functions utilize at least 60 sightings, and red otherwise. For rare taxa, it was not always possible to meet this recommendation, yielding higher statistical uncertainty. During the spatial modeling stage of the analysis, effective strip widths were computed for each survey using the closest detection function above it in the hierarchy (i.e. moving from right to left in the figure). Surveys that do not have a detection function above them in this figure were either addressed by a detection function presented in a different section of this report, or were omitted from the analysis.

2.2.1.1 750 ft

After right-truncating observations greater than 1297 m, we fitted the detection function to the 53 observations that remained (Table 16). The selected detection function (Figure 48) used a hazard rate key function with no covariates.

Table 16: Observations used to fit the 750 ft detection function.

ScientificName	n
Balaenoptera physalus	8
Eubalaena glacialis	5
Megaptera novaeangliae	7
Physeter macrocephalus	33
Total	53

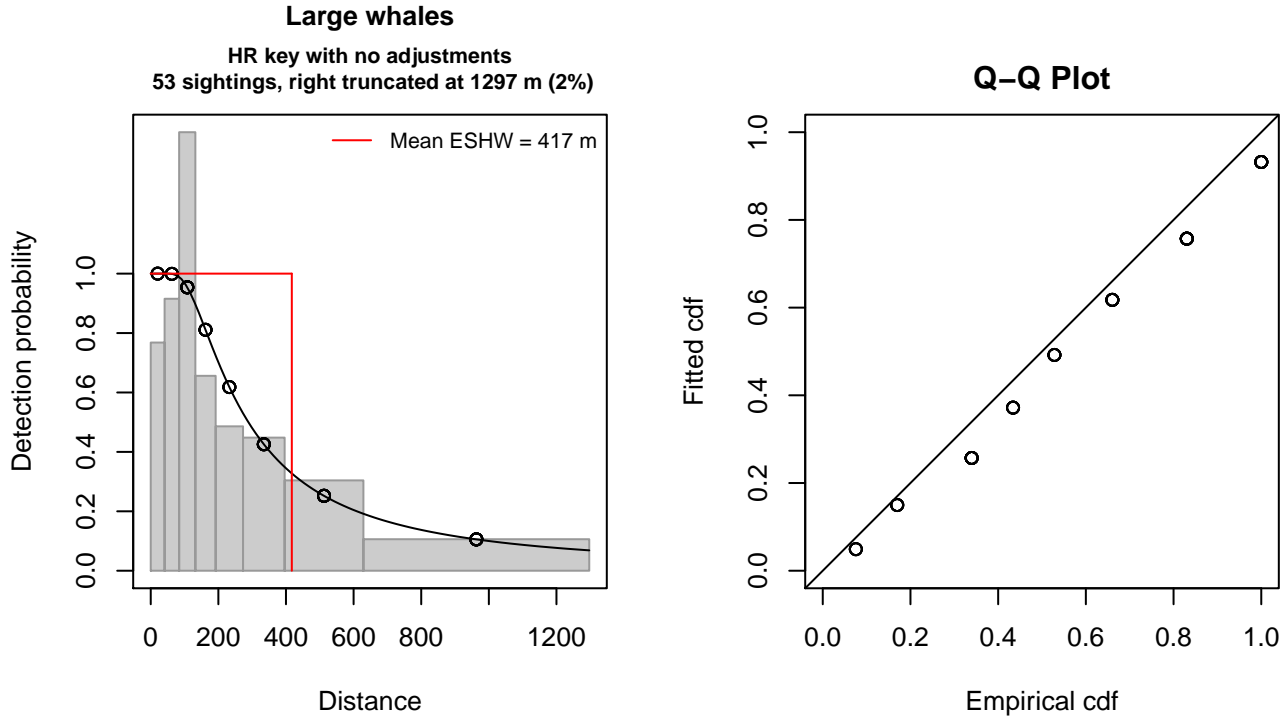


Figure 48: 750 ft detection function and Q-Q plot showing its goodness of fit.

Statistical output for this detection function:

Summary for ds object

Number of observations : 53
Distance range : 0 - 1297
AIC : 222.2921

Detection function:

Hazard-rate key function

Detection function parameters

Scale coefficient(s):

	estimate	se
(Intercept)	5.423929	0.4460729

Shape coefficient(s):

	estimate	se
(Intercept)	0.4163623	0.3128171

	Estimate	SE	CV
Average p	0.321688	0.07665669	0.2382951
N in covered region	164.755912	43.46025892	0.2637857

Distance sampling Cramer-von Mises test (unweighted)
Test statistic = 0.101698 p = 0.576612

2.2.1.2 Older UNCW Surveys

After right-truncating observations greater than 838 m, we fitted the detection function to the 59 observations that remained (Table 17). The selected detection function (Figure 49) used a hazard rate key function with Beaufort (Figure 50) as a covariate.

Table 17: Observations used to fit the Older UNCW Surveys detection function.

ScientificName	n
Balaenoptera physalus	13
Eubalaena glacialis	24
Megaptera novaeangliae	13
Physeter macrocephalus	9
Total	59

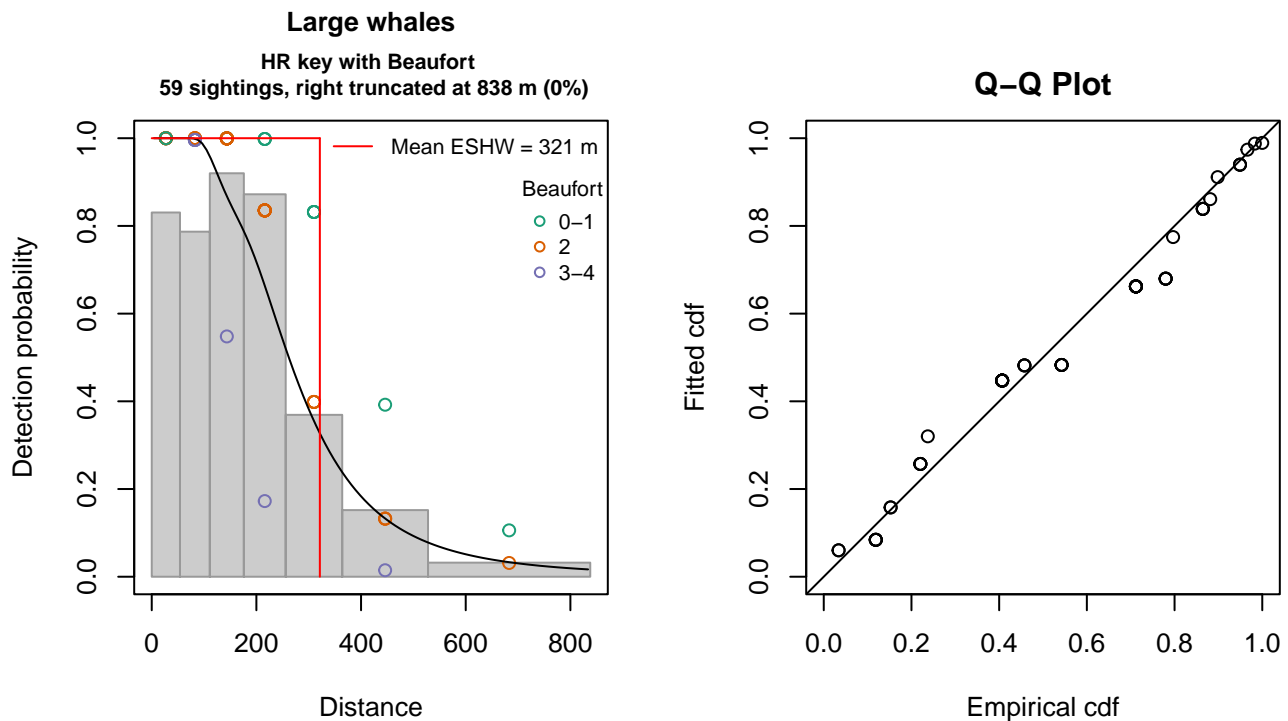


Figure 49: Older UNCW Surveys detection function and Q-Q plot showing its goodness of fit.

Statistical output for this detection function:

```
Summary for ds object
Number of observations : 59
Distance range       : 0 - 838
AIC                  : 218.1082
```

```
Detection function:
Hazard-rate key function
```

```
Detection function parameters
Scale coefficient(s):
```

	estimate	se
(Intercept)	5.9013957	0.2950158
Beaufort2	-0.3578033	0.3134356
Beaufort3-4	-1.0008354	0.3877033

Shape coefficient(s):

	estimate	se
(Intercept)	1.254247	0.2627137

	Estimate	SE	CV
Average p	0.3508662	0.04814793	0.1372259
N in covered region	168.1552636	29.31126242	0.1743107

Distance sampling Cramer-von Mises test (unweighted)
 Test statistic = 0.291522 p = 0.142842

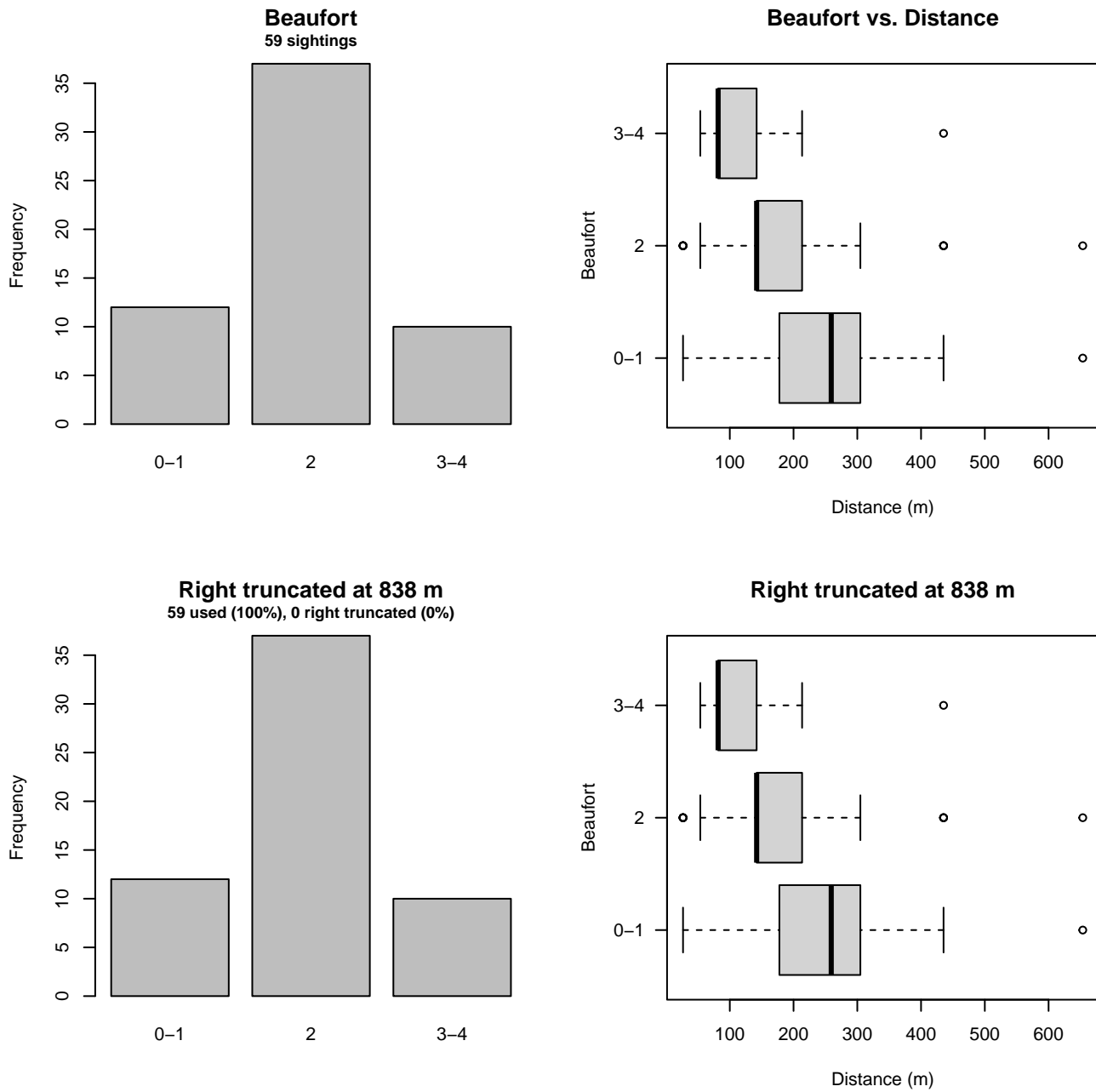


Figure 50: Distribution of the Beaufort covariate before (top row) and after (bottom row) observations were truncated to fit the Older UNCW Surveys detection function.

2.2.1.3 Newer Surveys

After right-truncating observations greater than 2000 m, we fitted the detection function to the 164 observations that remained (Table 18). The selected detection function (Figure 51) used a half normal key function with Beaufort (Figure 52) as a covariate.

Table 18: Observations used to fit the Newer Surveys detection function.

ScientificName	n
Balaenoptera borealis	3
Balaenoptera musculus	1
Balaenoptera physalus	48
Eubalaena glacialis	11
Megaptera novaeangliae	40
Physeter macrocephalus	61
Total	164

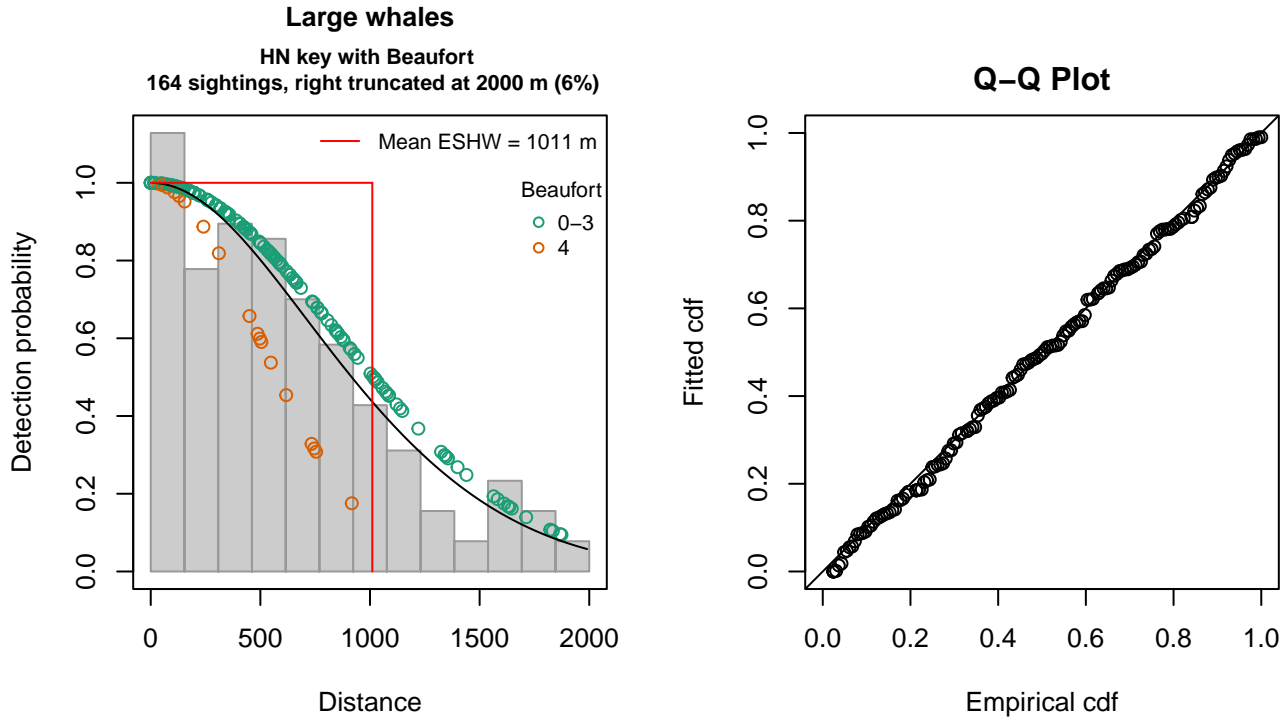


Figure 51: Newer Surveys detection function and Q-Q plot showing its goodness of fit.

Statistical output for this detection function:

Summary for ds object

Number of observations : 164
Distance range : 0 - 2000
AIC : 2414.311

Detection function:

Half-normal key function

Detection function parameters

Scale coefficient(s):

	estimate	se
(Intercept)	6.7601346	0.07305226
Beaufort4	-0.5625984	0.24677736

	Estimate	SE	CV
Average p	0.4908118	0.03341248	0.06807595
N in covered region	334.1403290	29.56205574	0.08847198

Distance sampling Cramer-von Mises test (unweighted)
 Test statistic = 0.025201 p = 0.989164

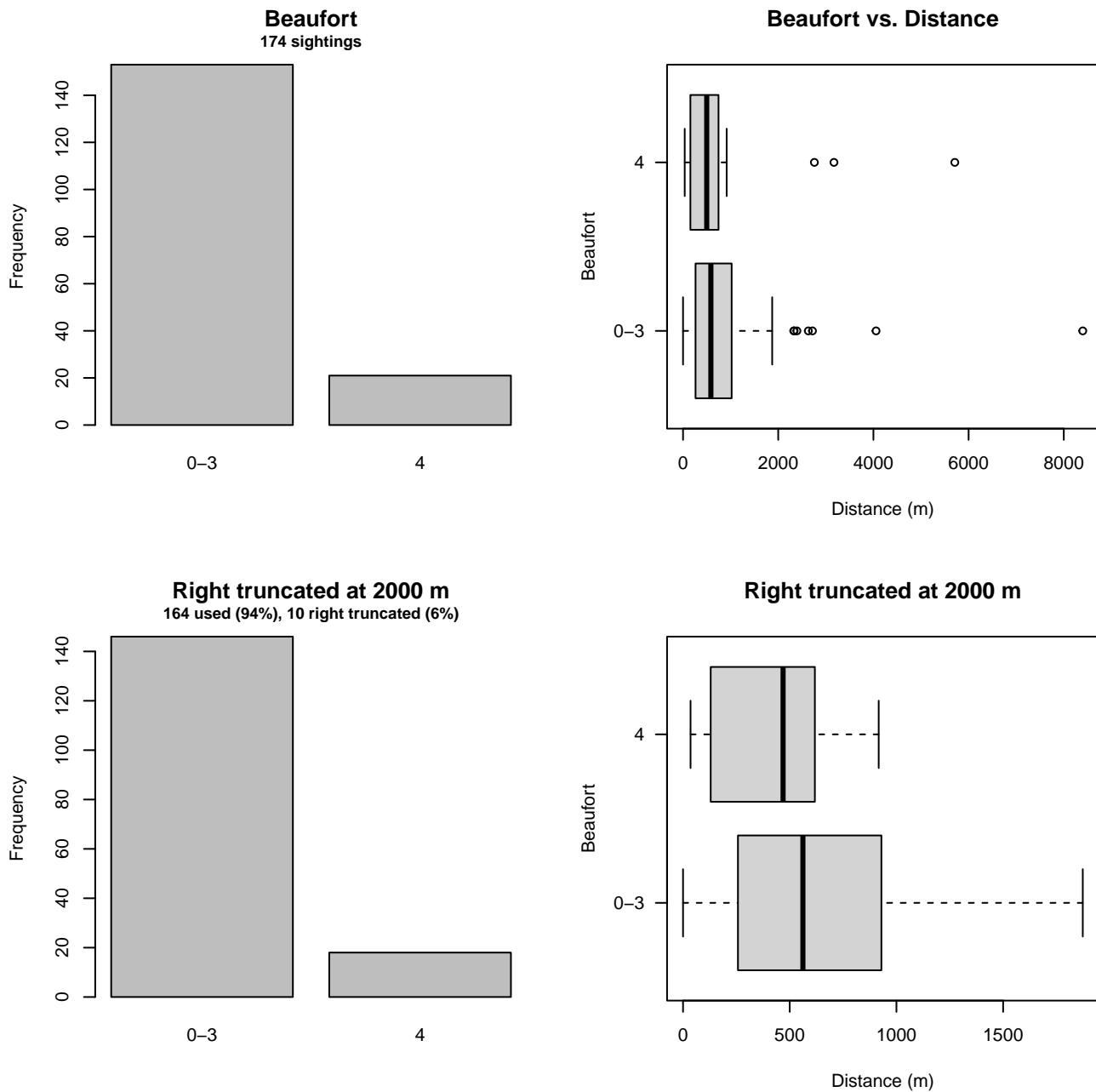


Figure 52: Distribution of the Beaufort covariate before (top row) and after (bottom row) observations were truncated to fit the Newer Surveys detection function.

3 Bias Corrections

Density surface modeling methodology uses *distance sampling* (Buckland et al. 2001) to model the probability that an observer on a line transect survey will detect an animal given the perpendicular distance to it from the transect line. Distance sampling assumes that detection probability is 1 when perpendicular distance is 0. When this assumption is not met, detection probability is biased high, leading to an underestimation of density and abundance. This is known as the $g_0 < 1$ problem, where g_0 refers to the detection probability at distance 0. Modelers often try to address this problem by estimating g_0 empirically and dividing it into estimated density or abundance, thereby correcting those estimates to account for the animals that were presumed missed.

Two important sources of bias for visual surveys are known as *availability bias*, in which an animal was present on the transect line but impossible to detect, e.g. because it was under water, and *perception bias*, in which an animal was present and available but not noticed, e.g. because of its small size or cryptic coloration or behavior (Marsh and Sinclair 1989). Modelers often estimate the influence of these two sources of bias on detection probability independently, yielding two estimates of g_0 , hereafter referred to as g_{0A} and g_{0P} , and multiply them together to obtain a final, combined estimate: $g_0 = g_{0A} \cdot g_{0P}$.

Our overall approach was to perform this correction on a per-observation basis, to have the flexibility to account for many factors such as platform type, surveyor institution, group size, group composition (e.g. singleton, mother-calf pair, or surface active group), and geographic location (e.g. feeding grounds vs. calving grounds). The level of complexity of the corrections varied by species according to the amount of information available, with North Atlantic right whale having the most elaborate corrections, derived from a substantial set of publications documenting its behavior, and various lesser known odontocetes having corrections based only on platform type (aerial or shipboard), derived from comparatively sparse information. Here we document the corrections used for blue whale.

3.1 Aerial Surveys

Palka et al. (2021) developed perception bias corrections for various marine mammal species and species guilds using two team, mark recapture distance sampling (MRDS) methodology (Burt et al. 2014) for aerial surveys conducted in 2010-2017 by NEFSC and SEFSC during the AMAPPS program. For blue whale, they prepared an estimate for NEFSC’s aerial surveys (a guild of blue, humpback, right, and northern bottlenose whales), but not SEFSC’s, presumably because SEFSC did not sight any blue whales. We applied the NEFSC estimate to all aerial sightings. All were in the northeast, with the exception of one sighting reported by HDR off Virginia (Table 1, Figure 1).

We caution that it is possible that perception bias was different on the other aerial programs, as they often used different aircraft, flew at different altitudes, and were staffed by different personnel. Of particular concern are that many programs flew Cessna 337 Skymasters, which had flat windows, while NOAA flew de Havilland Twin Otters, which had bubble windows, which likely afforded a better view of the transect line and therefore might have required less of a correction than the Skymasters. Correcting the other programs using NOAA’s estimate as we have done is likely to yield less bias than leaving them uncorrected, but we urge all programs to undertake their own efforts to estimate perception bias, as resources allow.

All of the sightings used in this analysis reported no more than one blue whale, but several of them were of multi-species feeding assemblages with other large whales. (NYS-DEC did sight a group of three blue whales during an off-effort cross-leg that was not used in the analysis.) To account for the influence of large group sizes on perception bias, we set the perception bias correction factor for sightings of 3 or more large whales to $g_{0P} = 1$, on the assumption that they would very rarely be missed, compared to a singleton or pair.

We estimated availability bias corrections using the Laake et al. (1997) estimator and dive intervals reported by Carretta et al. (2000) (Table 20). To estimate time in view, needed by the Laake estimator, we used results reported by Robertson et al. (2015), rescaled linearly for each survey program according to its target altitude and speed.

To address the influence of group size on availability bias, we applied the group availability estimator of McLellan et al. (2018) on a per-observation basis. Following Palka et al. (2021), who also used that method, we assumed that individuals in the group dived asynchronously. In the case of multi-species assemblages, we included all of the species. The resulting g_{0A} corrections ranged from about 0.4 to 0.95 (Figure 53). We caution that the assumption of asynchronous diving can lead to an underestimation of density and abundance if diving is actually synchronous; see McLellan et al. (2018) for an exploration of this effect.

Table 19: Perception bias corrections for blue whale applied to aerial surveys.

Surveys	Group Size	g_{0P}	g_{0P} Source
All	< 3	0.67	Palka et al. (2021): NEFSC
All	≥ 3	1.00	Assumed

Table 20: Surface and dive intervals for blue whale used to estimate availability bias corrections.

Surface Interval (s)	Dive Interval (s)	Source
144	234	Carretta et al. (2000)

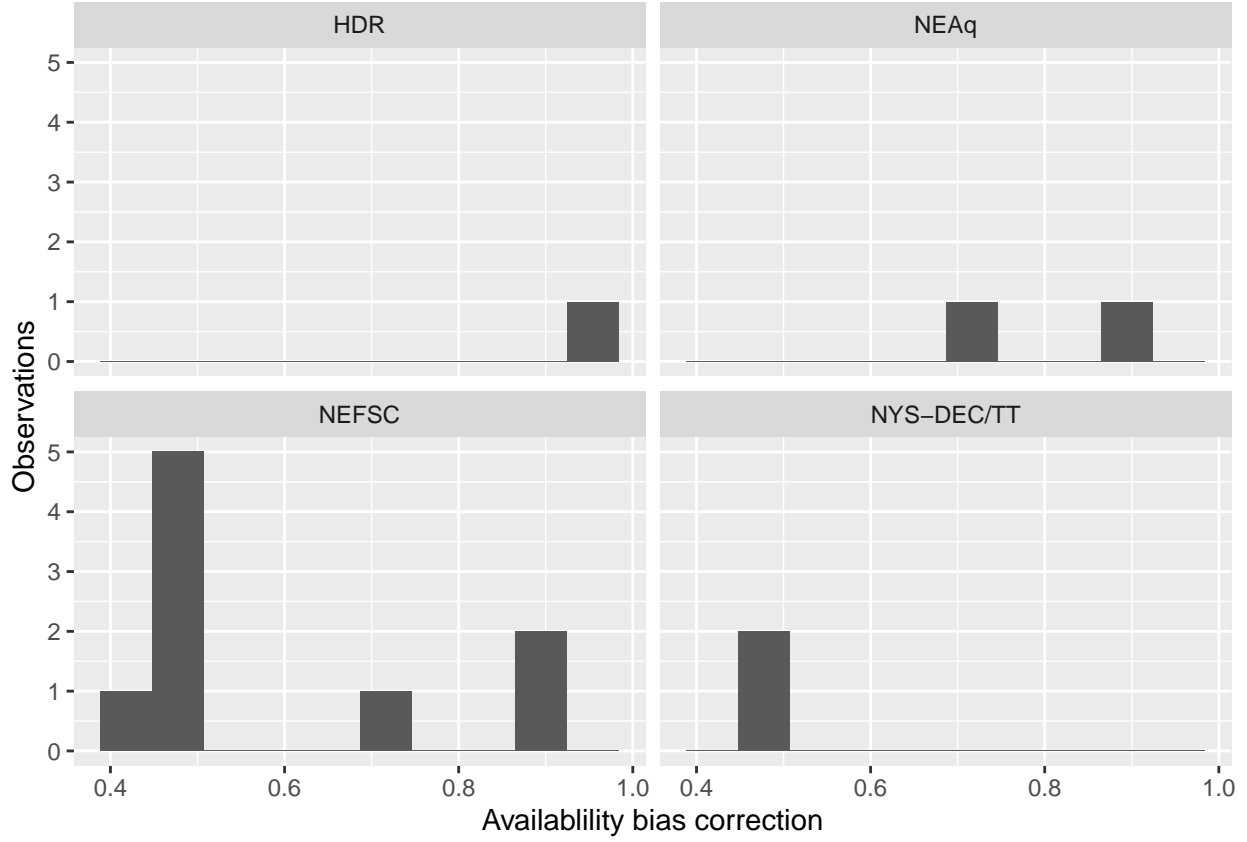


Figure 53: Availability bias corrections for blue whale for aerial surveys, by institution.

3.2 Shipboard Surveys

Most of the shipboard surveys in our analysis used high-power (25x150), pedestal-mounted binoculars. The only institution that reported sightings of blue whales during high-power binocular surveys was NOAA NEFSC. Palka et al. (2021) developed perception bias corrections using two team, MRDS methodology (Burt et al. 2014) for high-power binocular surveys conducted in 2010-2017 by NEFSC during the AMAPPS program. We applied this correction to all high-power binocular sightings (all were from NEFSC).

For naked eye surveys, the only sightings were reported by MCR, conducted on the motor sailboat R/V Song of the Whale. For this, we used the blue whale perception bias estimate from Cañadas et al. (2021) for the class of vessels that best matched the speed and platform height of R/V Song of the Whale.

Given that the dive interval of this species (Table 20) was short relative to the amount of time a given patch of water remained in view to shipboard observers using high-power binoculars, we assumed that no availability bias correction was needed ($g_{0A} = 1$) for NEFSC's surveys, following the approach taken by Palka et al. (2021) for baleen whales. For R/V Song of the Whale, we used the estimate $g_{0A} = 0.99$ from Cañadas et al. (2021).

Table 21: Perception and availability bias corrections for blue whale applied to shipboard surveys.

Surveys	Searching Method	Group Size	g_{0P}	g_{0P} Source	g_{0A}	g_{0A} Source
NEFSC	Binoculars	Any	0.48	Palka et al. (2021): NEFSC	1.00	Assumed
MCR	Naked eye	Any	0.72	Cañadas et al. (2021)	0.99	Cañadas et al. (2021)

4 Density Model

The distribution of the blue whale in the North Atlantic generally extends from the Arctic to at least mid-latitude waters (Hayes et al. 2020). In an analysis modern-day visual surveys of the central and northeast North Atlantic, Pike et al. (2009) concluded that blue whales are usually present in northern areas only during summer months. Recent passive acoustic monitoring (PAM) has detected them in fall and winter as far north as the Davis Strait, Irminger Basin, and Iceland Basin (Davis et al. 2020). In late fall and winter, American whaling logbooks records reported sightings as far south as the Cape Verde Islands and approximately at 15 °N, 40 °W near the Mid-Atlantic Ridge in the month of January (Reeves et al. 2004).

Blue whales were heavily hunted across the North Atlantic in the late 19th and early 20th centuries, and the largest summertime concentrations that remain may be in the vicinity of Iceland, with significant summer numbers also occurring in the Gulf of St. Lawrence, off eastern Canada, and off West Greenland (Pike et al. 2009). NOAA’s 2019 Stock Assessment Report (SAR) determined that the best estimate of the Gulf of St. Lawrence population was 402 (Hayes et al. 2020), the number of unique individuals photographically identified there between 1980-2008 (Ramp and Sears 2013).

Lesage et al. (2018) conducted a comprehensive analysis of blue whale habitat in eastern Canadian waters using all available data, including whaling records, photo ID studies, systematic visual surveys, acoustic detections, telemetry from tagged animals, opportunistic sightings, and presence-only modeling (the latter published by Gomez et al. (2017)). These researchers identified the continental shelf edge off Nova Scotia, including its submarine canyons, as one of four areas in the broader region important for blue whale feeding or socializing.

Subsequent PAM studies affirmed the importance of this region. Recorders deployed on the eastern half of the Scotian Shelf (east of Halifax), both mid-shelf and along the continental slope, detected blue whales year-round (Davis et al. 2020; Delarue et al. 2022; Wingfield et al. 2022). On the western half of Scotian Shelf (south and west of Halifax), acoustic detections occurred August to April, but not May to July (Davis et al. 2020).

Lesage et al. (2018) concluded that although wintering areas of blue whales in the western North Atlantic are poorly defined, the data suggest wintering habitat is relatively diffuse and includes the Scotian Shelf as well as the U.S. waters of the Mid-Atlantic Bight (MAB), and the warm and deep oceanic waters off the MAB. NOAA’s 2019 SAR characterizes the blue whale as “an occasional visitor” to waters of the U.S. Atlantic Exclusive Economic Zone (Hayes et al. 2020). Consistent with this, the systematic visual surveys available for our analysis reported only 21 sightings within our study area, all occurring north of Cape Hatteras (Figure 1) and mostly during the second half of the year (Figure 54), but collectively too few to allow confident inference of the spatiotemporal dynamics of the species’ distribution.

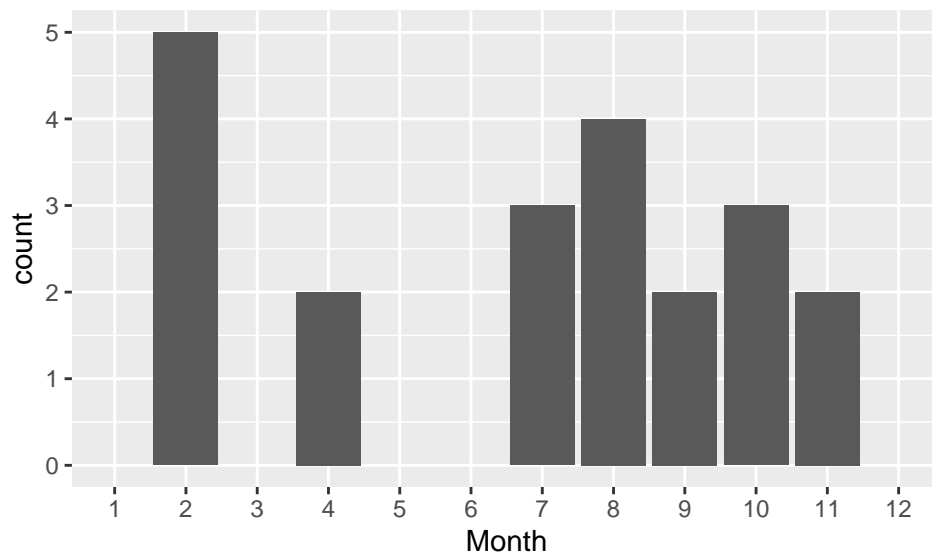


Figure 54: Counts of sightings by month from the systematic visual surveys available for our analysis.

PAM studies offer a more detailed picture. Between Cape Hatteras and the northeast tip of Georges Bank, Davis et al. (2020) reported occasional PAM detections of blue whales from August through March. Most detections occurred at recorders placed along the shelf break, but detections also occurred at recorders on the continental shelf “far more than expected”, according to the authors. At Cape Hatteras and south to Jacksonville and the Blake Spur, blue whales were detected July through March (Davis et al. 2020; Van Parijs et al. 2021; Kowarski et al. 2022). All of these detections occurred along the continental slope; from what we could discern from these publications, the shallowest detection in this area occurred off Wilmington,

North Carolina, in waters approximately 460m deep. No detections occurred in the shallower waters of the upper shelf south of Cape Hatteras.

Davis et al. (2020) cautioned that their analysis detected blue whale song, thought to be produced mainly by males (A, B, and AB phrases), but not other vocalizations. They noted that detections were sparse across their dataset from April to August, a season in which blue whales are likely to exhibit different acoustic behavior than the preceding months during which detections were much more frequent. Kowarski et al. (2022) reiterated this caution, stating that “an absence of acoustic detections, particularly in spring and summer, may reflect animals being present but not vocalizing, or producing signals more difficult to detect.”

With only 21 sightings, we lacked the data needed to fit a detailed density model. However, given the endangered status of the blue whale and the large amount of new information available, particularly from passive acoustic monitoring, we sought to improve on our previous model (Roberts et al. 2016) if at all possible. In that model, we had only 8 sightings, which was too few to fit a model with covariates, so we elected to distribute density uniformly across the study area, on the basis that the entire area was included in species range maps from scientific organizations, e.g. those from the International Whaling Commission and the International Union for Conservation of Nature. For the new model, we first assumed that the species was absent from the upper shelf (shallower than 125m) south of Cape Hatteras, on the basis that numerous years of intensive visual surveying and acoustic monitoring that targeted North Atlantic right whales but also recorded other large whales such as humpback and fin whales did not report any blue whales. We then explored a range of simple models for the area that remained, referred to in this report as “Surveyed Area (Excluding SE Shelf)” (Figure 55).

All candidate models used only one or two covariates, out of a desire for parsimony given the sparse sightings. Of the candidate models tested, the model that scored the best used distance to the 125m isobath as the only covariate and explained 8.4% of the deviance in the data. We were not surprised this model scored best, as all of the sightings were relatively close to this isobath. However, model predictions (not shown) ended up being highly concentrated at the isobath, yielding a pattern similar to a “bathtub ring” of density that extended up the mid-Atlantic, around the Gulf of Maine, and around the banks of the Scotian Shelf. We determined that this model was overfitted, and in light of the other available evidence, we discarded it.

The next best model, which we selected, included an interaction of sea surface temperature and depth (Figure 58) and explained 6.0% of the deviance in the data. For depths > 300m, corresponding to the continental slope, the model fitted a positive effect across a broad range of temperatures, with a peak at the deepest depths at 7 °C, conditions that are encountered along the slope of the Scotian Shelf. For depths < 100 m, corresponding to the upper continental shelf, a negative effect was fitted for temperatures less than about 15 °C, with the most negative values occurring in the shallowest, coldest waters, corresponding to inshore waters in winter. For intermediate depths of 100-300m, corresponding to the deeper shelf waters of the Gulf of Maine and Scotian basins, a slightly positive effect was fitted across a wide range of temperatures.

Model extrapolation diagnostics indicated univariate extrapolation along the northern inside portion of the Scotian Shelf in January through April (Figures 64a-64d). The extrapolation was small in magnitude, in terms of the NT1 statistic being close to zero, and resulted from temperatures occurring slightly below the minimum sampled value of 1.8 °C, and were therefore not a substantial cause for concern.

4.1 Final Model

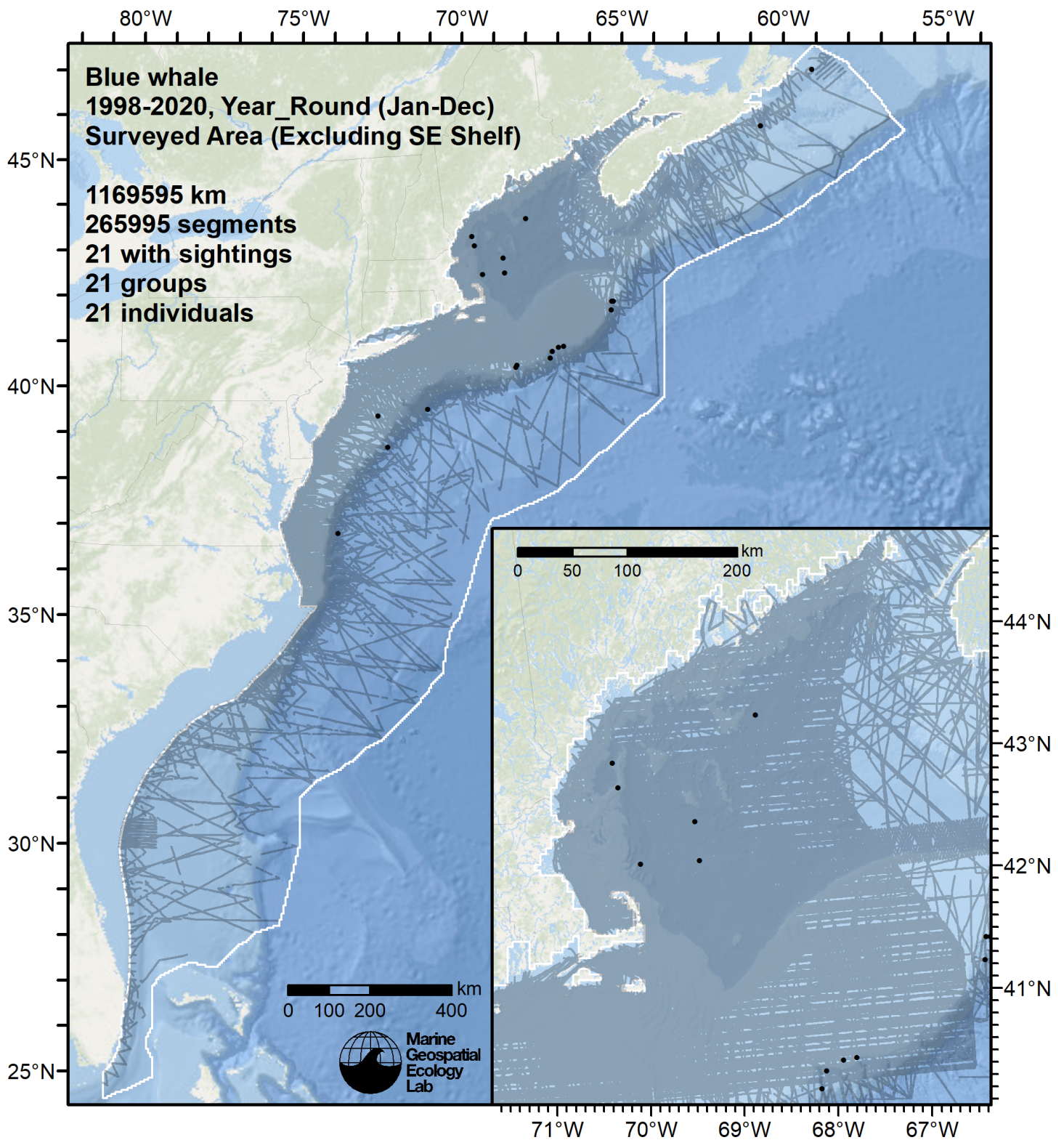


Figure 55: Survey segments used to fit the model for the region Surveyed Area (Excluding SE Shelf). Black points indicate segments with observations.

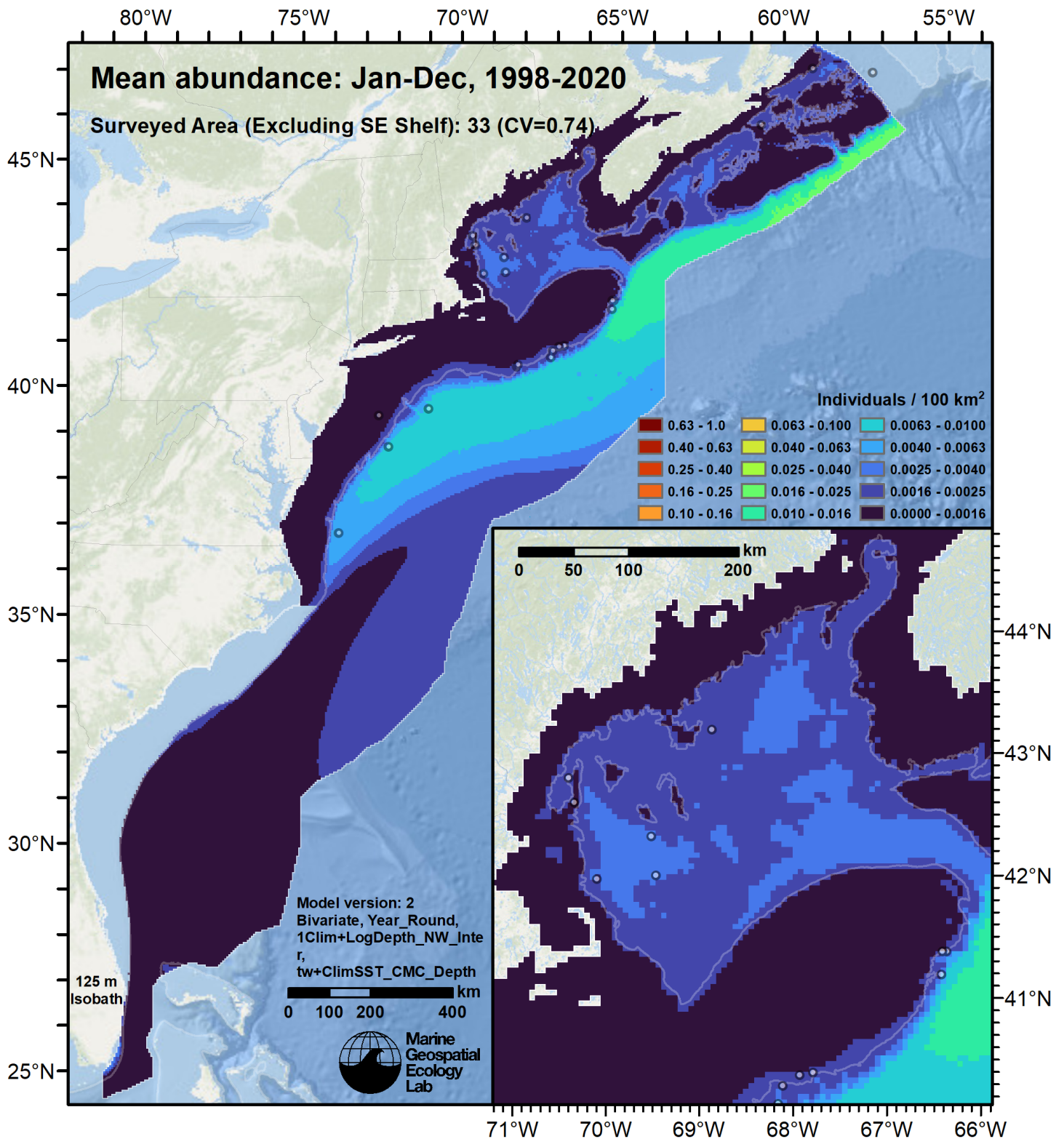


Figure 56: Blue whale mean density for the indicated period, as predicted by the model for the region Surveyed Area (Excluding SE Shelf). Open circles indicate segments with observations. Mean total abundance and its coefficient of variation (CV) are given in the subtitle. Variance was estimated with the analytic approach given by Miller et al. (2022), Appendix S1, and accounts both for uncertainty in model parameter estimates and for seasonal variability in dynamic covariates but not interannual variability in them, as these covariates were monthly climatological averages.

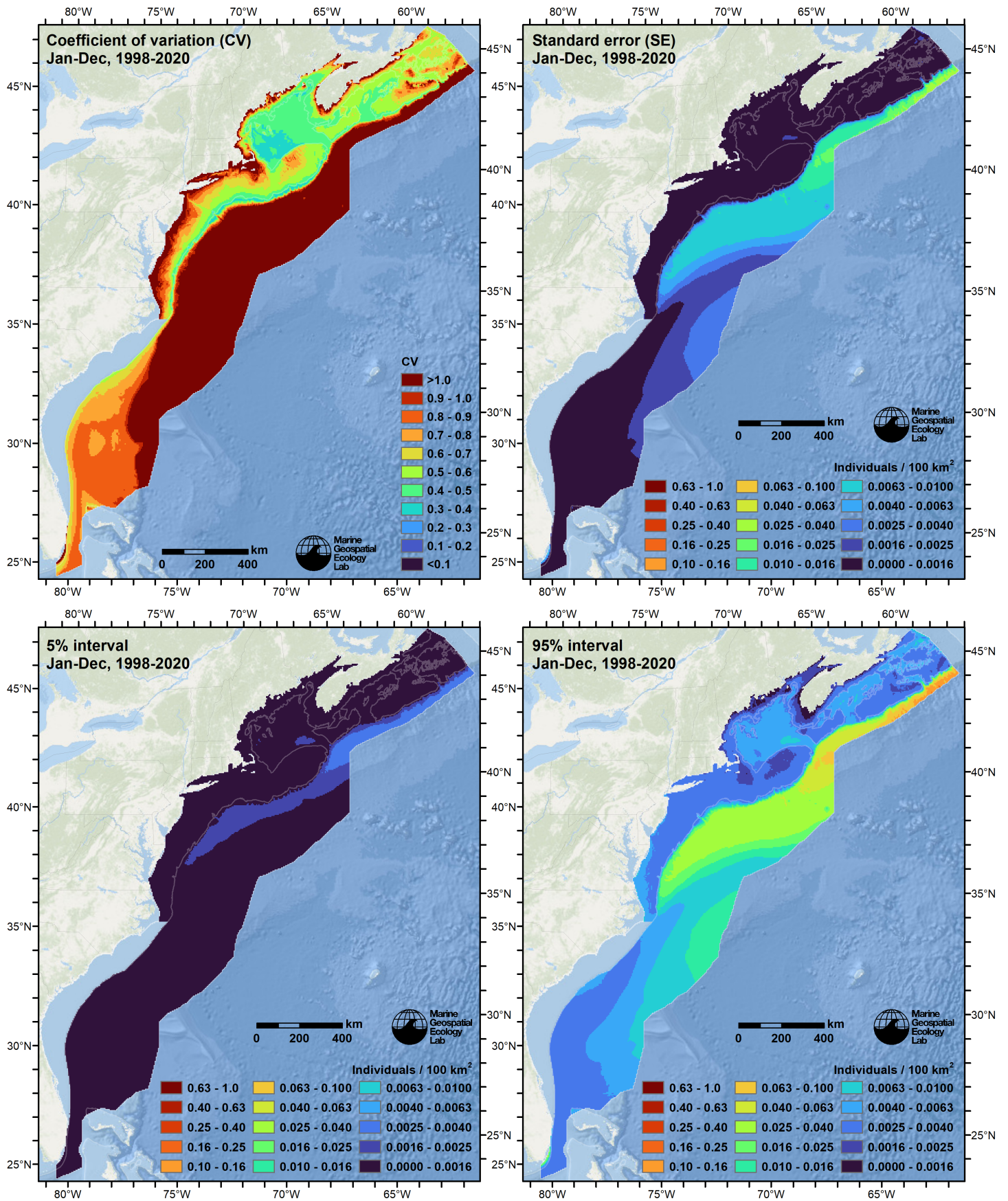


Figure 57: Uncertainty statistics for the blue whale mean density surface (Figure 56) predicted by the model for the region Surveyed Area (Excluding SE Shelf). Variance was estimated with the analytic approach given by Miller et al. (2022), Appendix S1, and accounts both for uncertainty in model parameter estimates and for seasonal variability in dynamic covariates but not interannual variability in them, as these covariates were monthly climatological averages.

Statistical output for this model:

Family: Tweedie(p=1.111)
Link function: log

Formula:

IndividualsCorrected ~ offset(log(SegmentArea)) + te(ClimSST_CMC,
log10(Depth), bs = "ts")

Parametric coefficients:

	Estimate	Std. Error	t value	Pr(> t)
(Intercept)	-25.1455	0.2756	-91.25	<2e-16 ***

Signif. codes: 0 '***' 0.001 '**' 0.01 '*' 0.05 '.' 0.1 ' ' 1

Approximate significance of smooth terms:

	edf	Ref.df	F	p-value
te(ClimSST_CMC,log10(Depth))	3.456	24	0.478	0.0057 **

Signif. codes: 0 '***' 0.001 '**' 0.01 '*' 0.05 '.' 0.1 ' ' 1

R-sq.(adj) = 7.36e-05 Deviance explained = 6.01%

-REML = 238 Scale est. = 6.4032 n = 265995

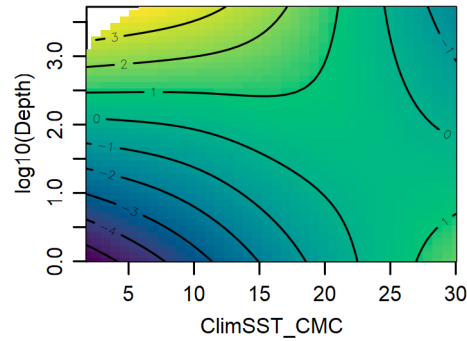


Figure 58: Functional plots for the final model for the region Surveyed Area (Excluding SE Shelf). Transforms and other treatments are indicated in axis labels. \log_{10} indicates the covariate was \log_{10} transformed. $/1000$ indicates meters were transformed to kilometers for interpretation convenience.

Table 22: Covariates used in the final model for the region Surveyed Area (Excluding SE Shelf).

Covariate	Description
ClimSST_CMC	Climatological monthly mean sea surface temperature ($^{\circ}\text{C}$) from GHRSSST Level 4 CMC0.2deg and CMC0.1deg (Brasnett (2008); Canada Meteorological Center (2012); Meissner et al. (2016); Canada Meteorological Center (2016))
Depth	Depth (m) of the seafloor, from SRTM30_PLUS (Becker et al. (2009))

4.2 Diagnostic Plots

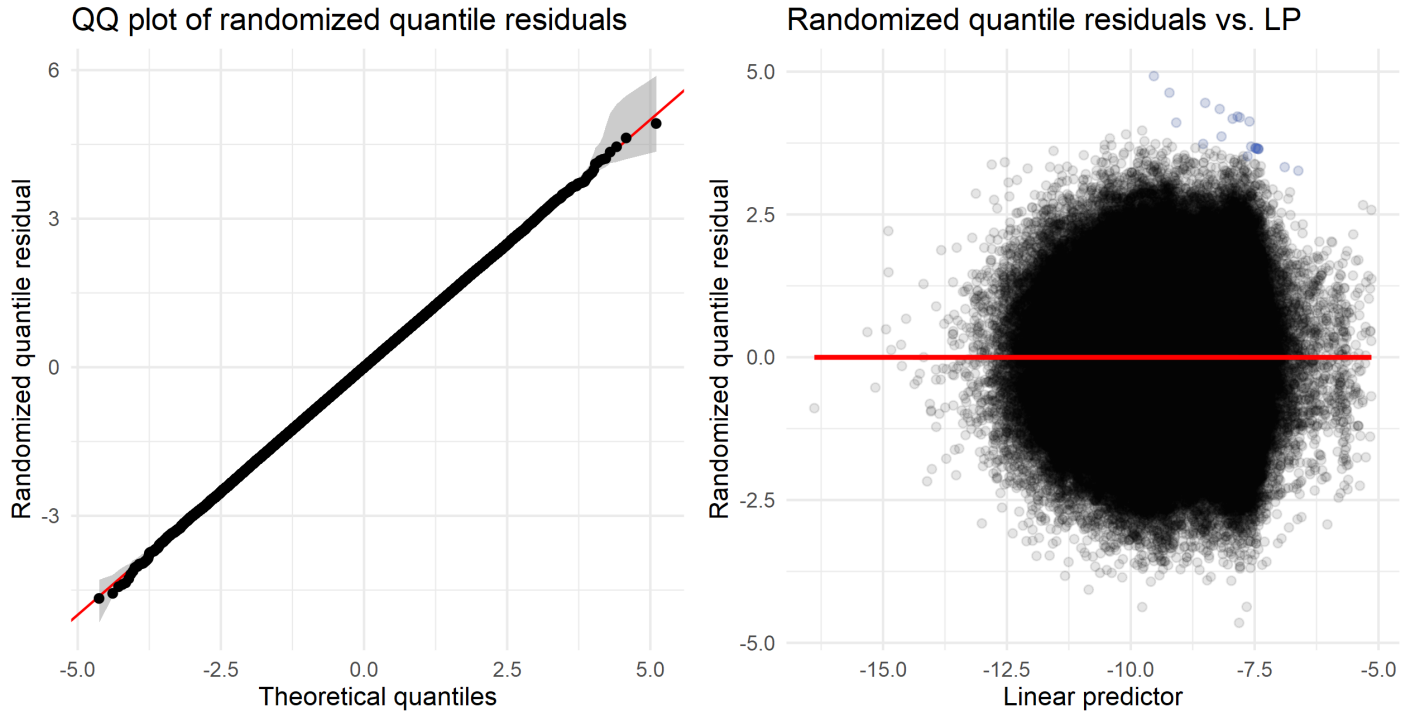


Figure 59: Residual plots for the final model for the region Surveyed Area (Excluding SE Shelf).

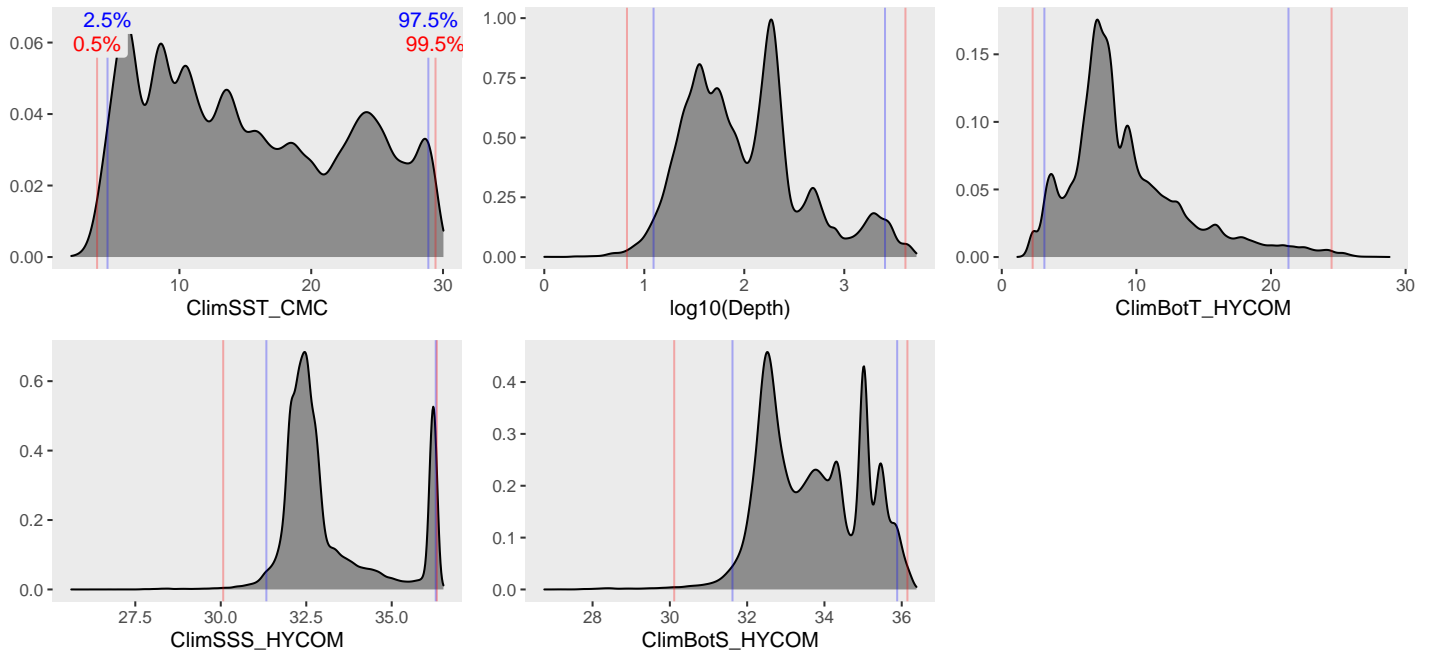


Figure 60: Density histograms showing the distributions of the covariates considered during the final model selection step. The final model may have included only a subset of the covariates shown here (see Figure 58), and additional covariates may have been considered in preceding selection steps. Red and blue lines enclose 99% and 95% of the distributions, respectively. Transforms and other treatments are indicated in axis labels. \log_{10} indicates the covariate was \log_{10} transformed. $/1000$ indicates meters were transformed to kilometers for interpretation convenience.

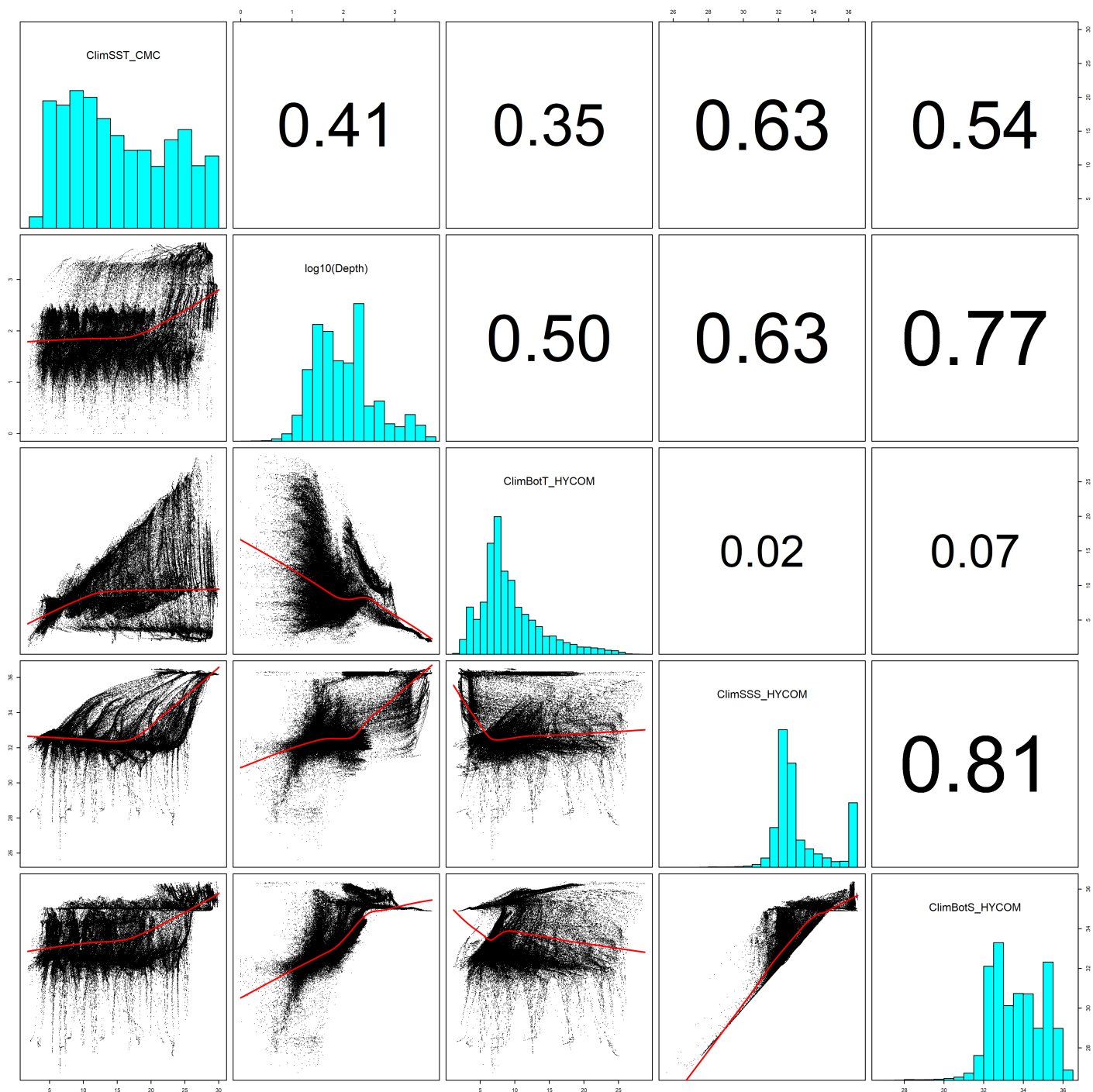


Figure 61: Scatterplot matrix of the covariates considered during the final model selection step. The final model may have included only a subset of the covariates shown here (see Figure 58), and additional covariates may have been considered in preceding selection steps. Covariates are transformed as shown in Figure 60. This plot is used to check simple correlations between covariates (via pairwise Pearson coefficients above the diagonal) and visually inspect for concurvity (via scatterplots and red lowess curves below the diagonal).

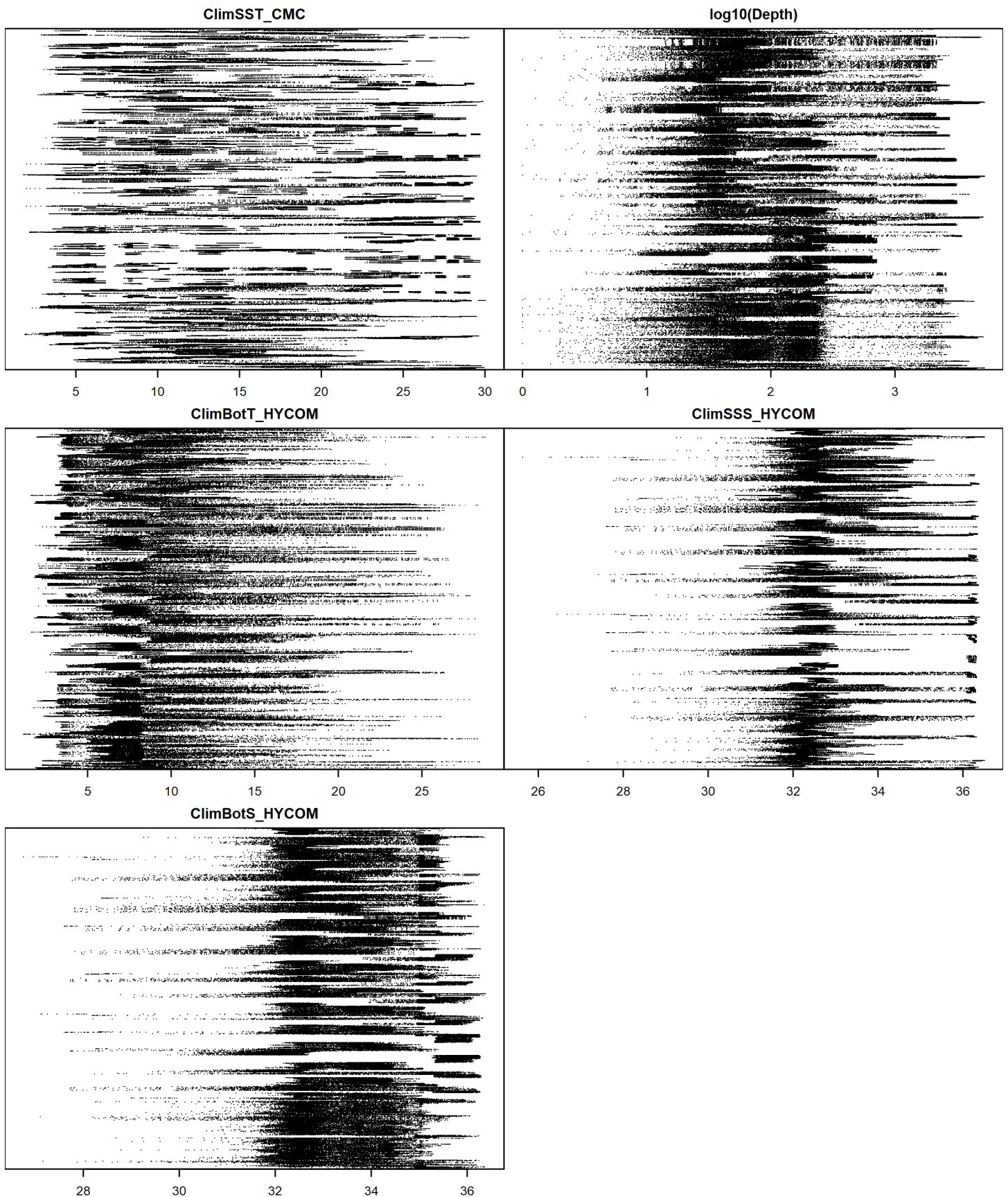


Figure 62: Dotplot of the covariates considered during the final model selection step. The final model may have included only a subset of the covariates shown here (see Figure 58), and additional covariates may have been considered in preceding selection steps. Covariates are transformed as shown in Figure 60. This plot is used to check for suspicious patterns and outliers in the data. Points are ordered vertically by segment ID, sequentially in time.

4.3 Extrapolation Diagnostics

4.3.1 Univariate Extrapolation

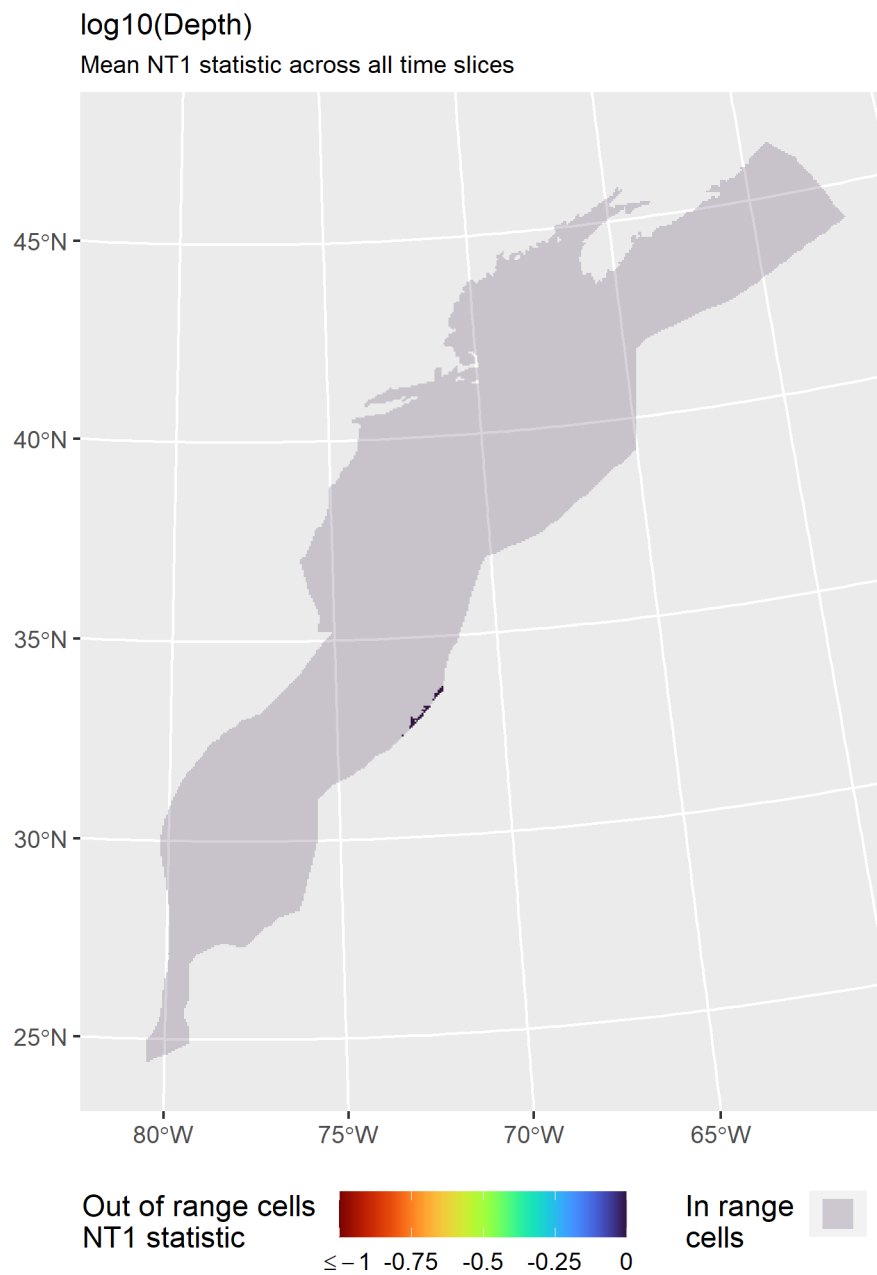


Figure 63: NT1 statistic (Mesgaran et al. (2014)) for static covariates used in the model for the region Surveyed Area (Excluding SE Shelf). Areas outside the sampled range of a covariate appear in color, indicating univariate extrapolation of that covariate occurred there. Areas within the sampled range appear in gray, indicating it did not occur.

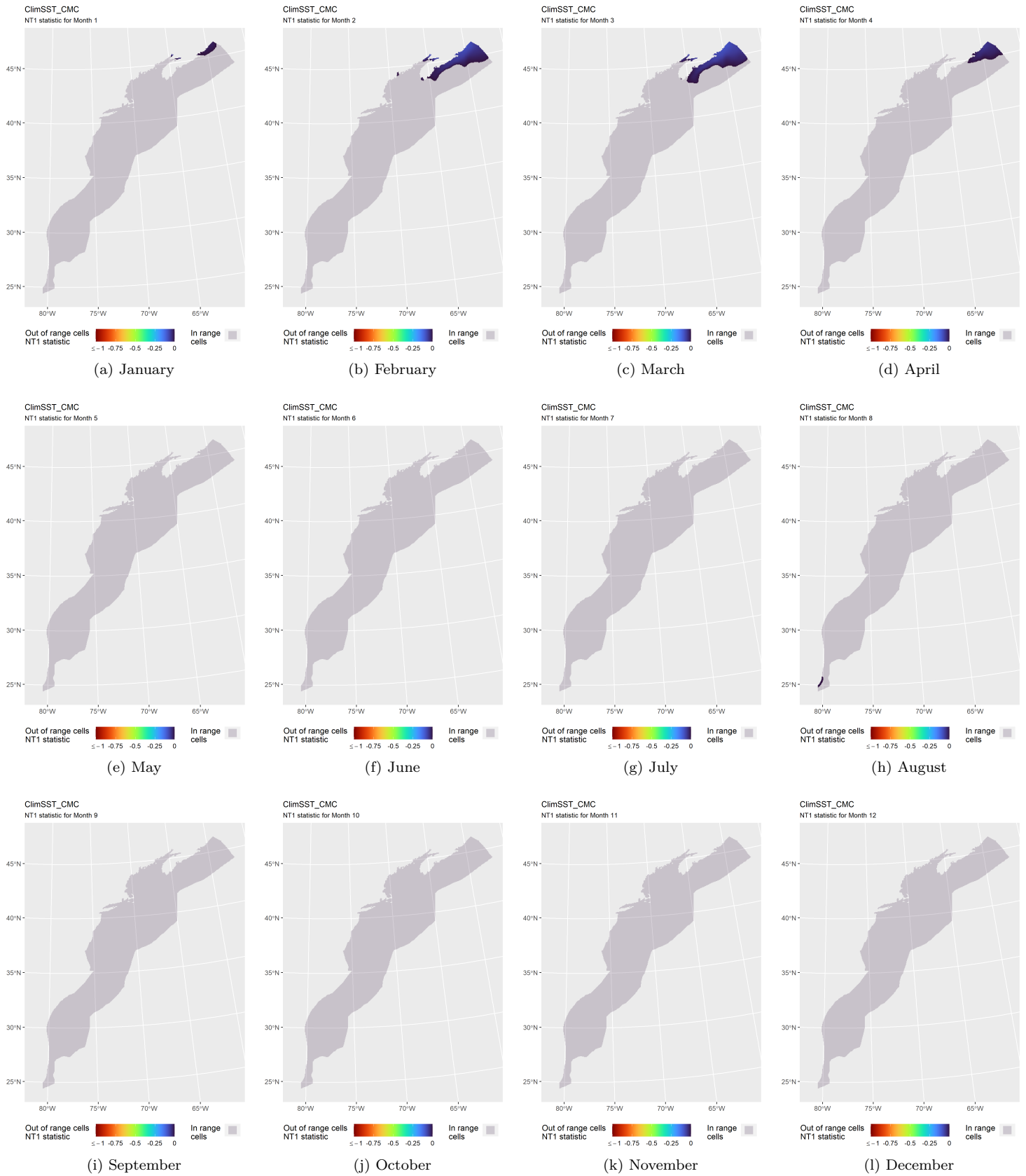


Figure 64: NT1 statistic (Mesgaran et al. (2014)) for the ClimSST_CMC covariate in the model for the region Surveyed Area (Excluding SE Shelf). Areas outside the sampled range of a covariate appear in color, indicating univariate extrapolation of that covariate occurred there during the month. Areas within the sampled range appear in gray, indicating it did not occur.

4.3.2 Multivariate Extrapolation

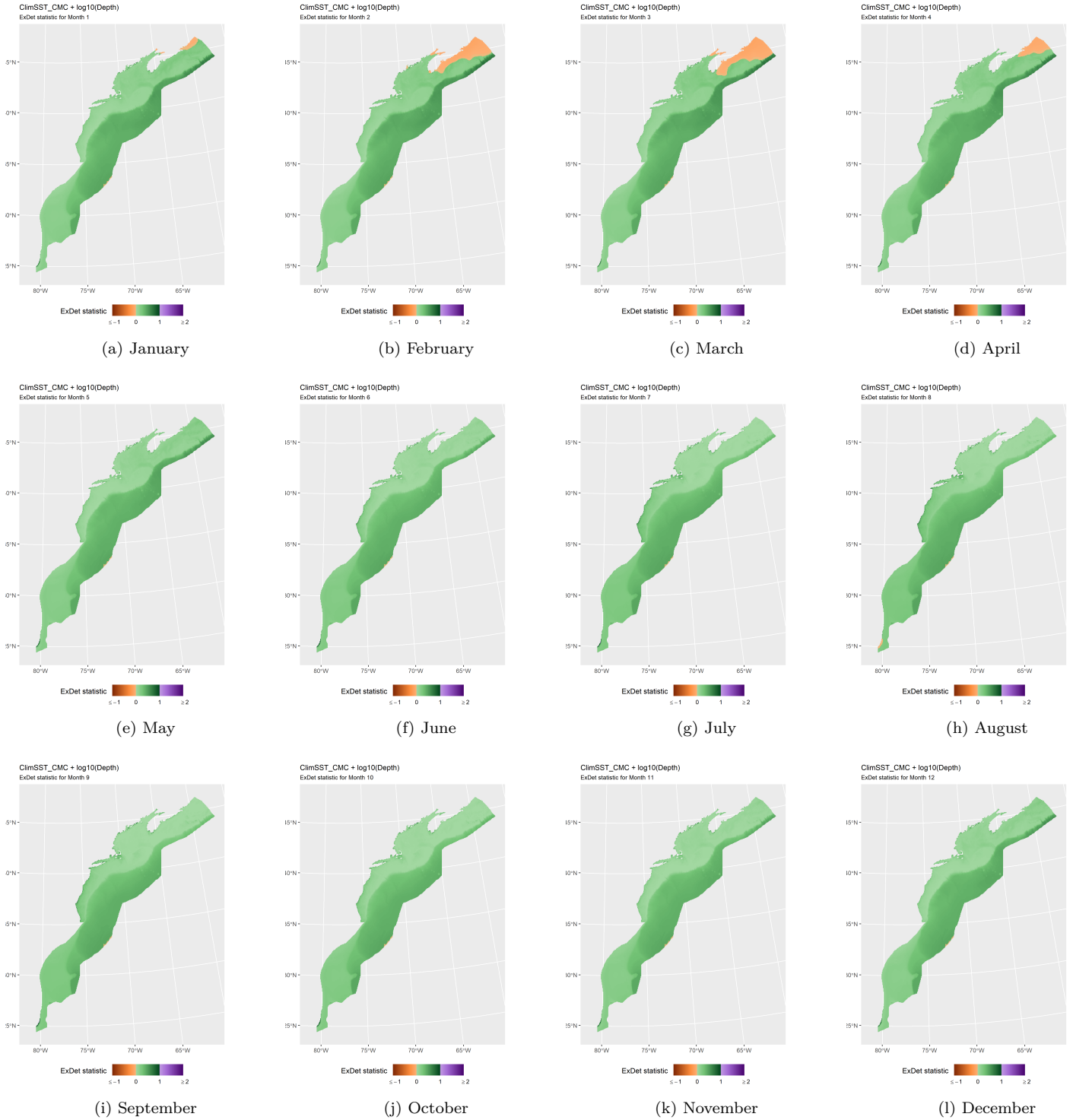


Figure 65: ExDet statistic (Mesgaran et al. (2014)) for all of the covariates used in the model for the region Surveyed Area (Excluding SE Shelf). Areas in orange ($\text{ExDet} < 0$) required univariate extrapolation of one or more covariates (see previous section). Areas in purple ($\text{ExDet} > 1$), did not require univariate extrapolation but did require multivariate extrapolation, by virtue of having novel combinations of covariates not represented in the survey data, according to the NT2 statistic (Mesgaran et al. (2014)). Areas in green ($0 \leq \text{ExDet} \leq 1$) did not require either type of extrapolation.

5 Predictions

Based on our evaluation of this model in the context of what is known of this species (see Section 6), we summarized its predictions into single, year-round climatological density and uncertainty surfaces (Figure 67). To illustrate the seasonal dynamics that result when predictions are summarized monthly instead, we included monthly mean abundances (Figure 66, Table 23), but to avoid confusion we did not include monthly maps in this report. They are available from us on request, but we recommend the year-round map be used for decision-making purposes, as discussed in Section 6.

5.1 Summarized Predictions

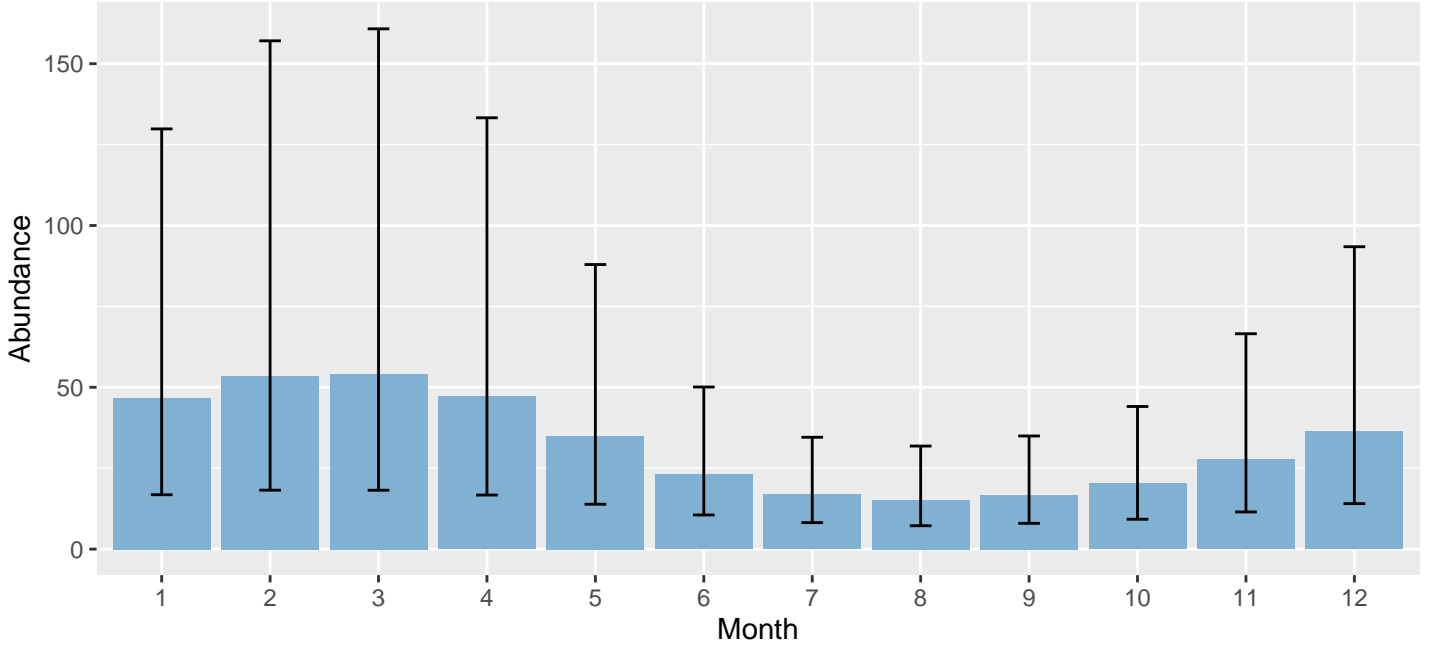


Figure 66: Mean monthly abundance for the prediction area for 1998-2020. Error bars are a 95% interval, made with a log-normal approximation using the prediction’s CV. The CV was estimated with the analytic approach given by Miller et al. (2022), Appendix S1, and accounts both for uncertainty in model parameter estimates and for temporal variability in dynamic covariates.

Table 23: Mean monthly abundance and density for the prediction area for 1998-2020. CV and intervals estimated as described for the previous figure.

Month	Abundance	CV	95% Interval	Area (km ²)	Density (individuals / 100 km ²)
1	47	0.559	17 - 130	1,273,075	0.00367
2	53	0.594	18 - 157	1,273,075	0.00420
3	54	0.602	18 - 161	1,273,075	0.00425
4	47	0.569	17 - 133	1,273,075	0.00371
5	35	0.499	14 - 88	1,273,075	0.00274
6	23	0.413	11 - 50	1,273,075	0.00181
7	17	0.380	8 - 35	1,273,075	0.00132
8	15	0.393	7 - 32	1,273,075	0.00119
9	17	0.391	8 - 35	1,273,075	0.00131
10	20	0.415	9 - 44	1,273,075	0.00158
11	28	0.472	11 - 67	1,273,075	0.00217
12	36	0.513	14 - 93	1,273,075	0.00285

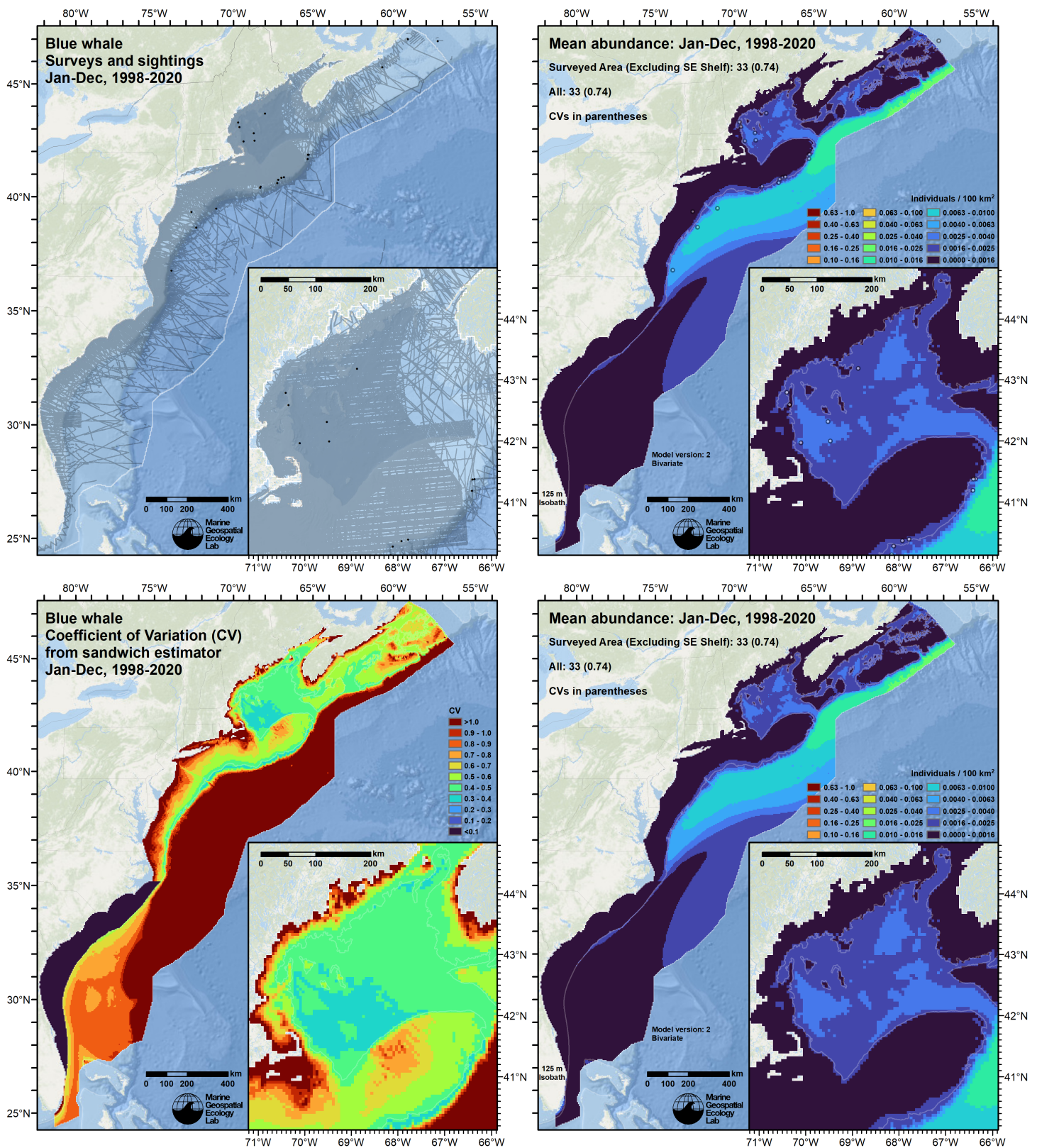


Figure 67: Survey effort and observations (top left), predicted density with observations (top right), predicted density without observations (bottom right), and coefficient of variation of predicted density (bottom left), for the given era. Variance was estimated with the analytic approach given by Miller et al. (2022), Appendix S1, and accounts both for uncertainty in model parameter estimates and for temporal variability in dynamic covariates.

5.2 Abundance Comparisons

5.2.1 NOAA Stock Assessment Report

Table 24: Comparison of regional abundance estimates from the 2019 NOAA Stock Assessment Report (SAR) (Hayes et al. (2020)) to estimates from this density model extracted from roughly comparable zones (Figure 68 below). The SAR estimates were based on a single year of surveying, while the model estimates were taken from the multi-year mean monthly density surface predicted by our model. Note that we elected to provide a single year-round mean surface to model users rather than 12 monthly surfaces (see discussion in Section 6).

2021 Stock Assessment Report			Density Model		
Month/Year	Area	N_{est}	Period	Zone	Abundance
Jun-Sep 2016	Central Virginia to lower Bay of Fundy ^a	39	Jan-Dec 1998-2020 ^b	NEFSC	17
	Florida to central Virginia ^c		Jan-Dec 1998-2020	SEFSC	8
	Bay of Fundy/Scotian Shelf ^d		Jan-Dec 1998-2020	Canada	8
Jun-Sep 2016	Total	39	Jun-Sep 1998-2020	Total	33

^a Estimate originally from Palka (2020).

^b We summarized our predictions into a single density surface that applies to all months (see Section 6).

^c The SAR did not provide an estimate for this area, presumably because no blue whales were sighted in it during SEFSC's 2016 survey.

^d The SAR did not provide an estimate for this area, presumably because none was available from Canada DFO.

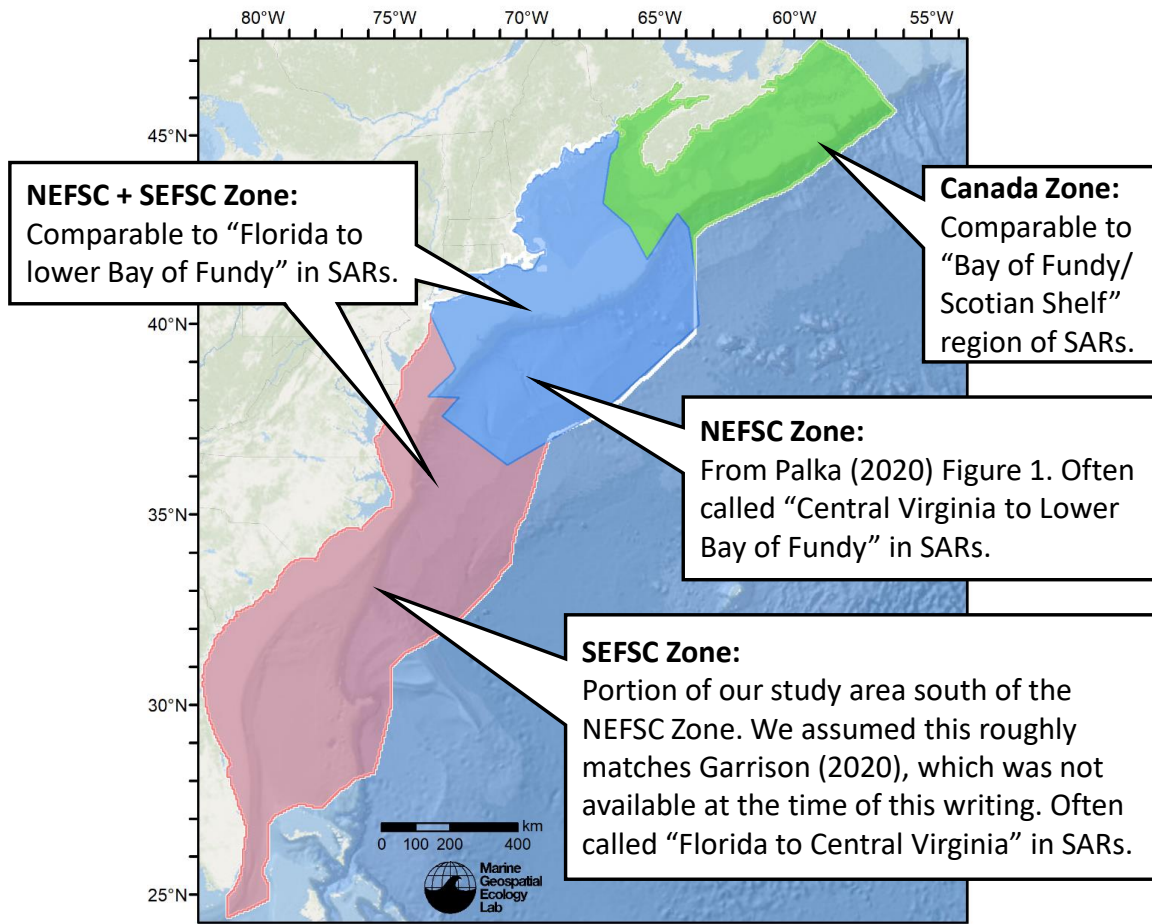


Figure 68: Zones for which we extracted abundance estimates from the density model for comparison to estimates from the NOAA Stock Assessment Report.

5.2.2 Previous Density Model

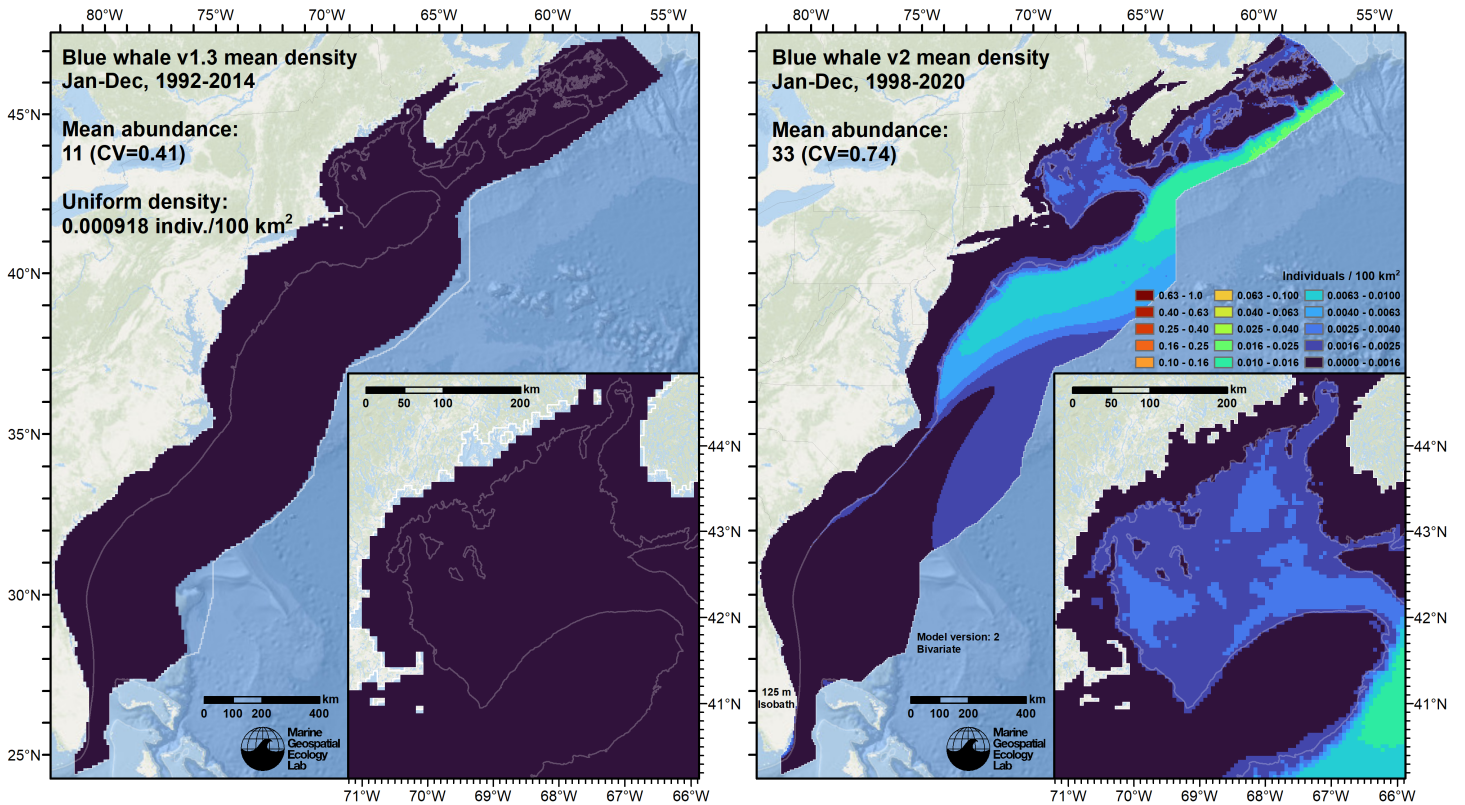


Figure 69: Comparison of the mean density predictions from the previous model (left) released by Roberts et al. (2016) to those from this model (right).

6 Discussion

The small number of sightings available to fit this model were too few to fully elucidate the seasonal dynamics of this rare species' distribution in our study area. Accordingly, we elected to summarize the model into a single, year-round mean density map (Figure 67). We recommend this be used for species management purposes rather than monthly maps derived from this model. We advise caution and strongly suggest that other data be considered when making decisions that might potentially affect blue whales. In particular, we recommend examination of passive acoustic monitoring results (e.g. Davis et al. (2020) and Delarue et al. (2022)), which may provide insight into seasonal dynamics, and indicate locations where blue whales were present but our map indicated low density. However, we also caution against over-interpreting maps of rates of acoustic detections or occurrence, as they do not depict density, and they may rely on vocalizations from only a subset of the population or fail to account for seasonal biases in vocal activity (Davis et al. 2020; Kowarski et al. 2022). Also the absence of vocalizations does not necessarily indicate the absence of animals.

When summarized across the modeled period (1998-2020), the mean density map (Figure 67) generally agreed with the overall spatial distribution pattern and habitat description of Lesage et al. (2018) (which we review in Section 4). The highest densities were predicted along the edge and slope of the Scotian Shelf. No sightings were reported in this area by the surveys used on our model, but effort was very sparse and we consider this extrapolation plausible based on Lesage et al. designating it important habitat after considering many other data, and because consistently high levels of acoustic activity were reported there (Davis et al. 2020; Delarue et al. 2022; Wingfield et al. 2022).

Our model predicted appreciable but lower densities along the outer edge of Georges Bank, south through the slope waters off the Mid-Atlantic Bight, down to Virginia. More than half of the sightings used in our model were reported in this area. Engelhaupt et al. (2020) reported that a whale sighted off Virginia in February 2019 foraging with a group of at least 15 fin whales (and included in our model) was photographically matched to a whale previously seen in the Gulf of St. Lawrence. The likely use of the offshore mid-Atlantic as a wintering ground for Gulf of St. Lawrence whales was demonstrated by Lesage et al. (2016), who tracked whales moving between the areas by satellite telemetry. Although none of our surveys reported sightings far from the shelf break, the only surveys that occurred so far offshore were in summer, when fewer whales are expected in the area. Lesage et al.'s telemetry tracks showed whales travelling beyond the shelf break throughout waters from

the Laurentian Channel to North Carolina, including the vicinity of the New England Seamounts, in the months of November through April. These periods including in behavior classified as area-restricted search, possibly indicative of feeding. The presence of whales in this area in winter, along and beyond the shelf break, including at Bear Seamount, was also confirmed by acoustic detections reported by Davis et al. (2020).

Our model predicted low density in deep waters of the Gulf of Maine, where six sightings were reported across the modeled period, but a very large amount of effort occurred, yielding a low density. This roughly accords with acoustic detections presented by Davis et al. (2020), who reported detections only at the deeper recorders in the Gulf of Maine and only in fall and winter.

Our model predicted little to no density in two areas of U.S. waters where acoustic monitoring studies reported noteworthy acoustic activity, where we strongly urge caution. The first was in the deeper waters along the continental slope south of Cape Hatteras, where multiple studies detected blue whales in July through March (Davis et al. 2020; Van Parijs et al. 2021; Kowarski et al. 2022). (Detections did not occur at the full range of months at each location.) No detections were reported in shallower waters, such as those off Jacksonville in the U.S. Navy's Undersea Warfare Training Range (USWTR), which has received extensive acoustic monitoring (see <https://www.navy-marinespeciesmonitoring.us/reporting/atlantic/>). The other area of concern was in continental shelf waters between Hudson Canyon and the Great South Channel, in which monitoring projects in the New York Bight (Muirhead et al. 2018) and south of Rhode Island and Massachusetts (Kraus et al. 2016) reported very occasional detections (these were included in the synthesis of Davis et al. (2020)). Although these detections were infrequent, they did occur in multiple years, suggesting a regular presence of blue whales.

The 2021 NOAA Stock Assessment Report (SAR) (Hayes et al. 2020) estimated an abundance of 39 whales for the period June through September 2016 and the region "Central Virginia to lower Bay of Fundy" (Table 24), corresponding to our NEFSC zone (Figure 68). Our model, when averaged across all months of the year (what we recommend for species management purposes), predicted an abundance of 17 whales in the NEFSC zone and 33 in total across the study area. The SAR estimate was made by Palka (2020) from 3 sightings collected by the 2016 NEFSC AMAPPS shipboard survey of the continental shelf break and slope. Previous NEFSC surveys of essentially the same zone reported no sightings in summer 2011, 3 sightings in summer 2013, and 1 sighting in spring 2014. (All of these data were incorporated into our model.) Although it is impossible to draw statistically-significant conclusions from so few data, the lower sighting counts in other years suggest that our lower multi-year average is not unreasonable. Overall, the match in magnitude of abundances estimated by model and by the SAR is reassuring.

Although we do not recommend that monthly summaries from our model be used for species management decisions, we note that the monthly summaries predicted highest abundances in winter and lowest in summer (Figure 66), consistent with Lesange et al.'s (2018) description of the region as winter habitat. With additional surveying it may eventually become possible to accumulate enough sightings to build a model that allows confident prediction of seasonal dynamics.

Total abundance in this new model is roughly three times that of our previous model (Figure 69). This is not surprising given the number of additional sightings that were available for the new model. In particular, none of the AMAPPS surveys mentioned above were available for use in our prior model (Roberts et al. 2016), nor the sighting from HDR (Engelhaupt et al. 2020), nor those from New England Aquarium or NYS-DEC (Redfern et al. 2021; Zoidis et al. 2021). However, the apparently large difference between the two models should not be interpreted to indicate that the population is increasing; more data are needed to draw that conclusion.

References

- Barco SG, Burt L, DePerte A, Digiovanni R Jr. (2015) Marine Mammal and Sea Turtle Sightings in the Vicinity of the Maryland Wind Energy Area July 2013-June 2015, VAQF Scientific Report #2015-06. Virginia Aquarium & Marine Science Center Foundation, Virginia Beach, VA
- Becker JJ, Sandwell DT, Smith WHF, Braud J, Binder B, Depner J, Fabre D, Factor J, Ingalls S, Kim S-H, Ladner R, Marks K, Nelson S, Pharaoh A, Trimmer R, Von Rosenberg J, Wallace G, Weatherall P (2009) Global Bathymetry and Elevation Data at 30 Arc Seconds Resolution: SRTM30_PLUS. *Marine Geodesy* 32:355–371. doi: [10.1080/01490410903297766](https://doi.org/10.1080/01490410903297766)
- Brasnett B (2008) The impact of satellite retrievals in a global sea-surface-temperature analysis. *Quarterly Journal of the Royal Meteorological Society* 134:1745–1760. doi: [10.1002/qj.319](https://doi.org/10.1002/qj.319)
- Buckland ST, Anderson DR, Burnham KP, Laake JL, Borchers DL, Thomas L (2001) *Introduction to Distance Sampling: Estimating Abundance of Biological Populations*. Oxford University Press, Oxford, UK
- Burt ML, Borchers DL, Jenkins KJ, Marques TA (2014) Using mark-recapture distance sampling methods on line transect surveys. *Methods in Ecology and Evolution* 5:1180–1191. doi: [10.1111/2041-210X.12294](https://doi.org/10.1111/2041-210X.12294)

- Canada Meteorological Center (2012) GHRSSST Level 4 CMC0.2deg Global Foundation Sea Surface Temperature Analysis Version 2.0. PODAAC, CA, USA. doi: [10.5067/GHCMC-4FM02](https://doi.org/10.5067/GHCMC-4FM02)
- Canada Meteorological Center (2016) GHRSSST Level 4 CMC0.1deg Global Foundation Sea Surface Temperature Analysis Version 3.0. PODAAC, CA, USA. doi: [10.5067/GHCMC-4FM03](https://doi.org/10.5067/GHCMC-4FM03)
- Cañadas A, Roberts JJ, Yack TM, Halpin PN (2021) Development of Exploratory Marine Species Density Models in the NAVEUR/C6F Study Area. Report prepared for Naval Facilities Engineering Command, Atlantic under Contract No. N62470-15-D-8006, Task Order 18F4048. Duke University Marine Geospatial Ecology Lab, Durham, NC
- Carretta JV, Lowry MS, Stinchcomb CE, Lynn MS, E. CR (2000) Distribution and abundance of marine mammals at San Clemente Island and surrounding offshore waters: Results from aerial and ground surveys in 1998 and 1999. NOAA Administrative Report LJ-00-02. NOAA National Marine Fisheries Service, Southwest Fisheries Center, La Jolla, CA
- Cole T, Gerrior P, Merrick RL (2007) [Methodologies of the NOAA National Marine Fisheries Service Aerial Survey Program for Right Whales \(*Eubalaena glacialis*\) in the Northeast U.S., 1998-2006](#). U.S. Department of Commerce, Woods Hole, MA
- Cotter MP (2019) Aerial Surveys for Protected Marine Species in the Norfolk Canyon Region: 2018–2019 Final Report. HDR, Inc., Virginia Beach, VA
- Davis GE, Baumgartner MF, Corkeron PJ, Bell J, Berchok C, Bonnell JM, Bort Thornton J, Brault S, Buchanan GA, Cholewiak DM, Clark CW, Delarue J, Hatch LT, Klinck H, Kraus SD, Martin B, Mellinger DK, Moors-Murphy H, Nieukirk S, Nowacek DP, Parks SE, Parry D, Pegg N, Read AJ, Rice AN, Risch D, Scott A, Soldevilla MS, Stafford KM, Stanistreet JE, Summers E, Todd S, Van Parijs SM (2020) Exploring movement patterns and changing distributions of baleen whales in the western North Atlantic using a decade of passive acoustic data. *Glob Change Biol* gcb.15191. doi: [10.1111/gcb.15191](https://doi.org/10.1111/gcb.15191)
- Delarue JJ-Y, Moors-Murphy H, Kowarski KA, Davis GE, Urazghildiiev IR, Martin SB (2022) Acoustic occurrence of baleen whales, particularly blue, fin, and humpback whales, off eastern Canada, 2015-2017. *Endang Species Res* 47:265–289. doi: [10.3354/esr01176](https://doi.org/10.3354/esr01176)
- Engelhaupt DT, Pusser T, Aschettino JM, Engelhaupt AG, Cotter MP, Richlen MF, Bell JT (2020) Blue whale (*Balaenoptera musculus*) sightings off the coast of Virginia. *Mar Biodivers Rec* 13:6. doi: [10.1186/s41200-020-00189-y](https://doi.org/10.1186/s41200-020-00189-y)
- Foley HJ, Paxton CGM, McAlarney RJ, Pabst DA, Read AJ (2019) Occurrence, Distribution, and Density of Protected Species in the Jacksonville, Florida, Atlantic Fleet Training and Testing (AFTT) Study Area. Duke University Marine Lab, Beaufort, NC
- Garrison LP, Martinez A, Maze-Foley K (2010) [Habitat and abundance of cetaceans in Atlantic Ocean continental slope waters off the eastern USA](#). *Journal of Cetacean Research and Management* 11:267–277.
- Geo-Marine, Inc. (2010) [New Jersey Department of Environmental Protection Baseline Studies Final Report Volume III: Marine Mammal and Sea Turtle Studies](#). Geo-Marine, Inc., Plano, TX
- Gomez C, Lawson J, Kouwenberg A, Moors-Murphy H, Buren A, Fuentes-Yaco C, Marotte E, Wiersma Y, Wimmer T (2017) Predicted distribution of whales at risk: Identifying priority areas to enhance cetacean monitoring in the Northwest Atlantic Ocean. *Endang Species Res* 32:437–458. doi: [10.3354/esr00823](https://doi.org/10.3354/esr00823)
- Hayes SA, Josephson E, Maze-Foley K, Rosel PE, Byrd B, Chavez-Rosales S, Cole TV, Garrison LP, Hatch J, Henry A, Horstman SC, Litz J, Lyssikatos MC, Mullin KD, Orphanides C, Pace RM, Palka DL, Powell J, Wenzel FW (2020) [US Atlantic and Gulf of Mexico Marine Mammal Stock Assessments - 2019](#). NOAA National Marine Fisheries Service, Northeast Fisheries Science Center, Woods Hole, MA
- Kowarski KA, Martin SB, Maxner EE, Lawrence CB, Delarue JJ-Y, Miksis-Olds JL (2022) Cetacean acoustic occurrence on the US Atlantic Outer Continental Shelf from 2017 to 2020. *Marine Mammal Science* mms.12962. doi: [10.1111/mms.12962](https://doi.org/10.1111/mms.12962)
- Kraus SD, Leiter S, Stone K, Wikgren B, Mayo CA, Hughes P, Kenney RD, Clark CW, Rice AN, Estabrook BJ, Tielens JT (2016) [Northeast Large Pelagic Survey Collaborative Aerial and Acoustic Surveys for Large Whales and Sea Turtles, OCS Study BOEM 2016-054](#). US Department of the Interior, Bureau of Ocean Energy Management, Sterling, Virginia
- Laake JL, Calambokidis J, Osmek SD, Rugh DJ (1997) Probability of Detecting Harbor Porpoise From Aerial Surveys: Estimating g(0). *Journal of Wildlife Management* 61:63–75. doi: [10.2307/3802415](https://doi.org/10.2307/3802415)
- Leiter S, Stone K, Thompson J, Accardo C, Wikgren B, Zani M, Cole T, Kenney R, Mayo C, Kraus S (2017) North Atlantic right whale *Eubalaena glacialis* occurrence in offshore wind energy areas near Massachusetts and Rhode Island, USA. *Endang Species Res* 34:45–59. doi: [10.3354/esr00827](https://doi.org/10.3354/esr00827)
- Lesage V, Gavrilchuk K, Andrews RD, Sears R (2016) [Wintering areas, fall movements and foraging sites of blue whales satellite-tracked in the Western North Atlantic](#). Fisheries and Oceans Canada, Mont-Joli, QC, Canada

- Lesage V, Gosselin J-F, Lawson JW, McQuinn I, Moors-Murphy H, Plourde S, Sears R, Simard Y (2018) Habitats important to blue whales (*Balaenoptera musculus*) in the western North Atlantic. Fisheries and Oceans Canada, Mont-Joli, QC, Canada
- Mallette SD, Lockhart GG, McAlarney RJ, Cummings EW, McLellan WA, Pabst DA, Barco SG (2014) Documenting Whale Migration off Virginia's Coast for Use in Marine Spatial Planning: Aerial and Vessel Surveys in the Proximity of the Virginia Wind Energy Area (VA WEA), VAQF Scientific Report 2014-08. Virginia Aquarium & Marine Science Center Foundation, Virginia Beach, VA
- Mallette SD, Lockhart GG, McAlarney RJ, Cummings EW, McLellan WA, Pabst DA, Barco SG (2015) Documenting Whale Migration off Virginia's Coast for Use in Marine Spatial Planning: Aerial Surveys in the Proximity of the Virginia Wind Energy Area (VA WEA) Survey/Reporting Period: May 2014 - December 2014, VAQF Scientific Report 2015-02. Virginia Aquarium & Marine Science Center Foundation, Virginia Beach, VA
- Mallette SD, McAlarney RJ, Lockhart GG, Cummings EW, Pabst DA, McLellan WA, Barco SG (2017) [Aerial Survey Baseline Monitoring in the Continental Shelf Region of the VACAPES OPAREA: 2016 Annual Progress Report](#). Virginia Aquarium & Marine Science Center Foundation, Virginia Beach, VA
- Marsh H, Sinclair DF (1989) Correcting for Visibility Bias in Strip Transect Aerial Surveys of Aquatic Fauna. *The Journal of Wildlife Management* 53:1017. doi: [10.2307/3809604](#)
- McAlarney R, Cummings E, McLellan W, Pabst A (2018) Aerial Surveys for Protected Marine Species in the Norfolk Canyon Region: 2017 Annual Progress Report. University of North Carolina Wilmington, Wilmington, NC
- McLellan WA, McAlarney RJ, Cummings EW, Read AJ, Paxton CGM, Bell JT, Pabst DA (2018) Distribution and abundance of beaked whales (Family Ziphiidae) Off Cape Hatteras, North Carolina, U.S.A. *Marine Mammal Science*. doi: [10.1111/mms.12500](#)
- Meissner T, Wentz FJ, Scott J, Vazquez-Cuervo J (2016) Sensitivity of Ocean Surface Salinity Measurements From Spaceborne L-Band Radiometers to Ancillary Sea Surface Temperature. *IEEE Trans Geosci Remote Sensing* 54:7105–7111. doi: [10.1109/TGRS.2016.2596100](#)
- Mesgaran MB, Cousens RD, Webber BL (2014) Here be dragons: A tool for quantifying novelty due to covariate range and correlation change when projecting species distribution models. *Diversity Distrib* 20:1147–1159. doi: [10.1111/ddi.12209](#)
- Miller DL, Becker EA, Forney KA, Roberts JJ, Cañadas A, Schick RS (2022) Estimating uncertainty in density surface models. *PeerJ* 10:e13950. doi: [10.7717/peerj.13950](#)
- Muirhead CA, Warde AM, Biedron IS, Nicole Mihnovecs A, Clark CW, Rice AN (2018) Seasonal acoustic occurrence of blue, fin, and North Atlantic right whales in the New York Bight. *Aquatic Conservation: Marine and Freshwater Ecosystems*. doi: [10.1002/aqc.2874](#)
- Mullin KD, Fulling GL (2003) [Abundance of cetaceans in the southern U.S. North Atlantic Ocean during summer 1998](#). *Fishery Bulletin* 101:603–613.
- O'Brien O, Pendleton DE, Ganley LC, McKenna KR, Kenney RD, Quintana-Rizzo E, Mayo CA, Kraus SD, Redfern JV (2022) Repatriation of a historical North Atlantic right whale habitat during an era of rapid climate change. *Sci Rep* 12:12407. doi: [10.1038/s41598-022-16200-8](#)
- Palka D (2020) [Cetacean Abundance in the US Northwestern Atlantic Ocean Summer 2016](#). *Northeast Fish Sci Cent Ref Doc. 20-05*. NOAA National Marine Fisheries Service, Northeast Fisheries Science Center, Woods Hole, MA
- Palka D, Aichinger Dias L, Broughton E, Chavez-Rosales S, Cholewiak D, Davis G, DeAngelis A, Garrison L, Haas H, Hatch J, Hyde K, Jech M, Josephson E, Mueller-Brennan L, Orphanides C, Pegg N, Sasso C, Sigourney D, Soldevilla M, Walsh H (2021) [Atlantic Marine Assessment Program for Protected Species: FY15 – FY19 \(OCS Study BOEM 2021-051\)](#). U.S. Department of the Interior, Bureau of Ocean Energy Management, Washington, DC
- Palka DL (2006) [Summer abundance estimates of cetaceans in US North Atlantic navy operating areas \(NEFSC Reference Document 06-03\)](#). U.S. Department of Commerce, Northeast Fisheries Science Center, Woods Hole, MA
- Palka DL, Chavez-Rosales S, Josephson E, Cholewiak D, Haas HL, Garrison L, Jones M, Sigourney D, Waring G, Jech M, Broughton E, Soldevilla M, Davis G, DeAngelis A, Sasso CR, Winton MV, Smolowitz RJ, Fay G, LaBrecque E, Leiness JB, Dettloff K, Warden M, Murray K, Orphanides C (2017) [Atlantic Marine Assessment Program for Protected Species: 2010-2014 \(OCS Study BOEM 2017-071\)](#). U.S. Department of the Interior, Bureau of Ocean Energy Management, Washington, DC
- Pike DG, Víkingsson GA, Gunnlaugsson T, Øien N (2009) [A note on the distribution and abundance of blue whales \(*Balaenoptera musculus*\) in the Central and Northeast North Atlantic](#). *NAMMCO Scientific Publications* 7:19–29.

- Quintana-Rizzo E, Leiter S, Cole T, Hagbloom M, Knowlton A, Nagelkirk P, O'Brien O, Khan C, Henry A, Duley P, Crowe L, Mayo C, Kraus S (2021) Residency, demographics, and movement patterns of North Atlantic right whales *Eubalaena glacialis* in an offshore wind energy development area in southern New England, USA. *Endang Species Res* 45:251–268. doi: [10.3354/esr01137](https://doi.org/10.3354/esr01137)
- Ramp C, Sears R (2013) [Distribution, densities, and annual occurrence of individual blue whales \(*Balaenoptera musculus*\) in the Gulf of St. Lawrence, Canada from 1980-2008](#). Mingan Island Cetacean Study, St. Lambert, Qc, Canada
- Read AJ, Barco S, Bell J, Borchers DL, Burt ML, Cummings EW, Dunn J, Fougères EM, Hazen L, Hodge LEW, Laura A-M, McAlarney RJ, Peter N, Pabst DA, Paxton CGM, Schneider SZ, Urian KW, Waples DM, McLellan WA (2014) [Occurrence, distribution and abundance of cetaceans in Onslow Bay, North Carolina, USA](#). *Journal of Cetacean Research and Management* 14:23–35.
- Redfern JV, Kryc KA, Weiss L, Hodge BC, O'Brien O, Kraus SD, Quintana-Rizzo E, Auster PJ (2021) Opening a Marine Monument to Commercial Fishing Compromises Species Protections. *Front Mar Sci* 8:645314. doi: [10.3389/fmars.2021.645314](https://doi.org/10.3389/fmars.2021.645314)
- Reeves RR, Smith TD, Josephson EA, Clapham PJ, Woolmer G (2004) Historical Observations of Humpback and Blue Whales in the North Atlantic Ocean: Clues to Migratory Routes and Possibly Additional Feeding Grounds. *Marine Mammal Science* 20:774–786. doi: [10.1111/j.1748-7692.2004.tb01192.x](https://doi.org/10.1111/j.1748-7692.2004.tb01192.x)
- Roberts JJ, Best BD, Mannocci L, Fujioka E, Halpin PN, Palka DL, Garrison LP, Mullin KD, Cole TVN, Khan CB, McLellan WA, Pabst DA, Lockhart GG (2016) Habitat-based cetacean density models for the U.S. Atlantic and Gulf of Mexico. *Scientific Reports* 6:22615. doi: [10.1038/srep22615](https://doi.org/10.1038/srep22615)
- Roberts JJ, Yack TM, Halpin PN (2023) Marine mammal density models for the U.S. Navy Atlantic Fleet Training and Testing (AFTT) study area for the Phase IV Navy Marine Species Density Database (NMSDD), Document Version 1.3. Duke University Marine Geospatial Ecology Lab, Durham, NC
- Robertson FC, Koski WR, Brandon JR, Thomas TA, Trites AW (2015) [Correction factors account for the availability of bowhead whales exposed to seismic operations in the Beaufort Sea](#). *Journal of Cetacean Research and Management* 15:35–44.
- Ryan C, Boisseau O, Cucknell A, Romagosa M, Moscrop A, McLanaghan R (2013) [Final report for trans-Atlantic research passages between the UK and USA via the Azores and Iceland, conducted from R/V Song of the Whale 26 March to 28 September 2012](#). Marine Conservation Research International, Essex, UK
- Stone KM, Leiter SM, Kenney RD, Wikgren BC, Thompson JL, Taylor JKD, Kraus SD (2017) Distribution and abundance of cetaceans in a wind energy development area offshore of Massachusetts and Rhode Island. *J Coast Conserv* 21:527–543. doi: [10.1007/s11852-017-0526-4](https://doi.org/10.1007/s11852-017-0526-4)
- Torres LG, McLellan WA, Meagher E, Pabst DA (2005) [Seasonal distribution and relative abundance of bottlenose dolphins, *Tursiops truncatus*, along the US mid-Atlantic coast](#). *Journal of Cetacean Research and Management* 7:153.
- Van Parijs S, Cholewiak D, Berga AS, Frasier KE, Trickey J, Ackerknecht T, Field C, Cohen R, Hildebrand JA, Baumann-Pickering S, Mueller-Brennan L, Pegg N (2021) [Analysis of Acoustic Ecology of North Atlantic Shelf Break Cetaceans and Effects of Anthropogenic Noise Impacts FY 2020 Progress Report](#). NOAA National Marine Fisheries Service, Northeast Fisheries Science Center, Woods Hole, MA
- Whitt AD, Powell JA, Richardson AG, Bosyk JR (2015) [Abundance and distribution of marine mammals in nearshore waters off New Jersey, USA](#). *Journal of Cetacean Research and Management* 15:45–59.
- Wingfield J, Rubin B, Xu J, Stanistreet J, Moors-Murphy H (2022) Annual, seasonal, and diel patterns in blue whale call occurrence off eastern Canada. *Endang Species Res* 49:71–86. doi: [10.3354/esr01204](https://doi.org/10.3354/esr01204)
- Zoidis AM, Lomac-MacNair KS, Ireland DS, Rickard ME, McKown KA, Schlesinger MD (2021) Distribution and density of six large whale species in the New York Bight from monthly aerial surveys 2017 to 2020. *Continental Shelf Research* 230:104572. doi: [10.1016/j.csr.2021.104572](https://doi.org/10.1016/j.csr.2021.104572)